3YP Report

Saving Oneself

Theo W. Costain

Thomas Hayden

Desa Markovic

Nihaar Shah

Michaelmas 2016

Trinity 2017

Contents

1 Introduction

T. HAYDEN

In 2015 a team of engineers from Harvard revealed the cumulation of their last six years of work; a complete neural reconstruction of a section of mouse brain[1]. To be precise, a volume of 1500 μm^3 of mouse brain. This volume was painstakingly labeled manually. However, it was noted that such a task could be automised a great deal by machine learning. Applying machine learning to connectomics has become a popular area of research. Competition has been fierce and progress rapid.

The brain is the least understood organ in the Human body and by far the most important one. Understanding how the brain works is a task that has puzzled humans for centuries. Even now, the inner workings of the brain remain largely a mystery. Finding a reconstruction of even a small section of the human brain will help to further our understanding a great deal. However, a complete map of the connectome will essentially allow for a snapshot of a person's mind to be captured. Our thoughts and feelings are entirely contained within our brain and by recording the state of the brain, it may even be possible to record enough information to allow for the complete reconstruction of the brain after death.

This report explores the feasibility of such a project and attempts to overcome some

of the many hurdles that stand in the way of progress. The report describes the Brain to Disk Connectomics Protocol (BDCP) which details the entire process from brain removal to generating and storing the full neuronal circuit. Costings and timings for the full projects are estimated based on the best currently available technology.

It is important to note the difficulty of the task ahead. One of the main issues of this project is the sheer enormity and complexity of the human brain. The average volume of a healthy adult human brain is 1510cm^3 for men and 1320cm^3 for women[2]. That is around 1×10^{12} times larger than the section of mouse brain collected in 2015. If a complete reconstruction is required then all of this data must be collected with no lost material. Clearly this will be a monumental task.

2 Outline of the Brain to Disk Connectomics Protocol

T. HAYDEN

The Brain to Disc Connectomics Protocol (BDCP) is a complete end to end pipeline detailing the procedures required to collect enough information to attempt to recreate the brain after death. The main section of the BDCP can be broadly spilt into four distinct stages; chemical processing, sectioning, imaging and data processing. These are described in detail in section 3. Chemical processing involves fixing, staining and embedding the brain and is necessary to preserve the brain and to enable it to be sectioned and imaged without loss of ultrastructure. After chemical processing, the brain is then sectioned. The sectioning process reduces the embedded brain into thin sections to allow the imaging techniques to capture all relevant neuronal detail. After imaging, the data collected must be processed and stored. This will eventually result in a complete map of all neuronal connections as well as the strength of their synaptic connections. A timeline for the BDCP is outlined in figure 1. After the BDCP, reanimation is considered in section 4.

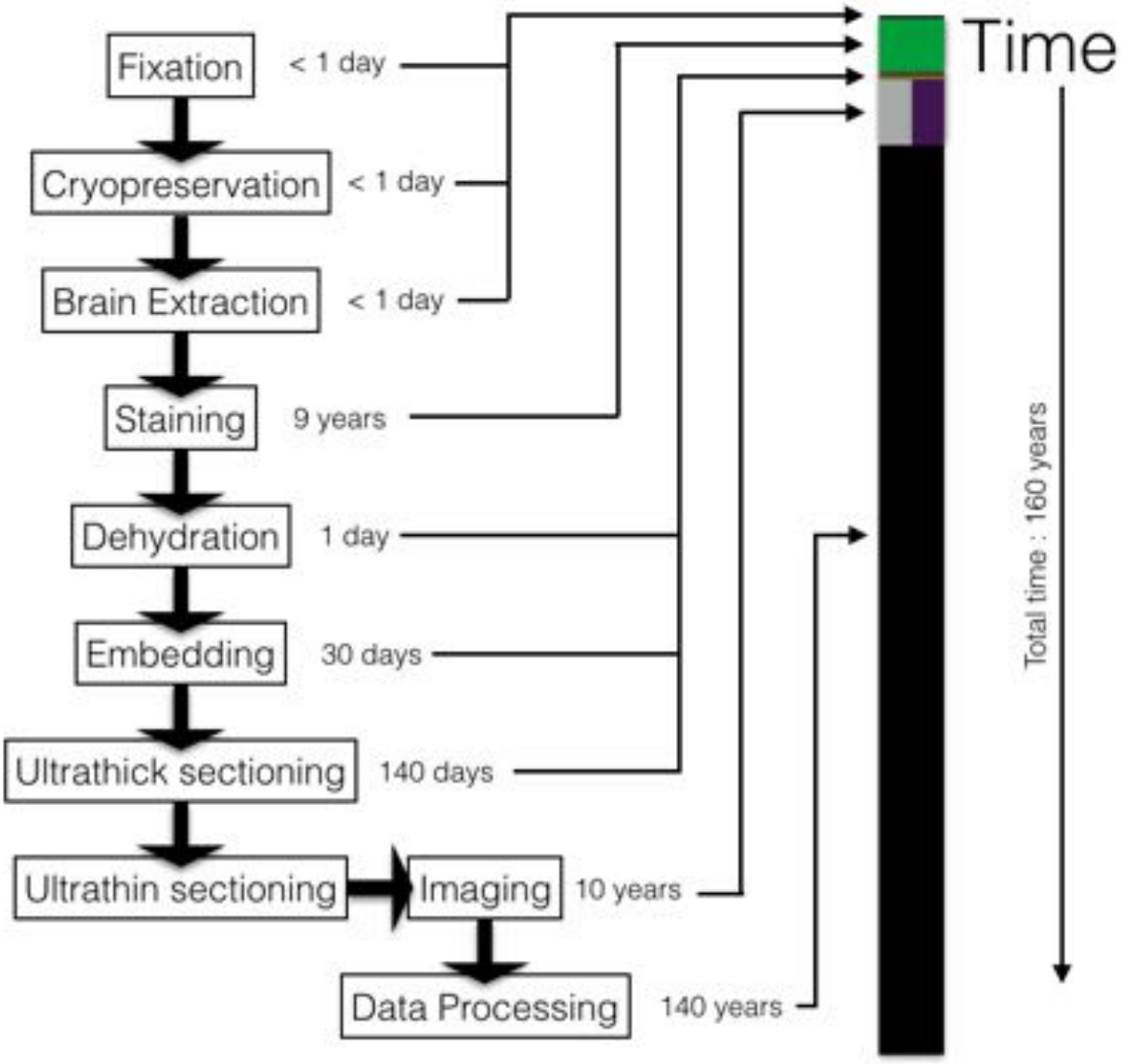

Figure 1: A timeline of the entire BDCP.

3 Brain to Disk Connectomics Protocol

3.1 Chemical Processing

DESANKA MARKOVIC

In order to consistently trace the connectome, the brain must be processed in a way that allows for reliable storage, sectioning and imaging of the tissue. Chemical pre-processing of the brain has 3 key aims - to prevent the decay of tissue, to make the tissue more robust and to enable imaging of tissue. It is vitally important that each step of the processing is completed perfectly or the specimen preserved will ultimately be unusable.

Preservation of the brain's structure successfully over extended periods of time is essen-

tial to our protocol. Sectioning and imaging the brain is a lengthy process, and some brains will need to be stored while this process is completed on other specimens. However, while storage at cool temperatures slows the process somewhat, tissue begins to decompose very soon after death. As blood oxygen levels drop, acidic compounds accumulate and trigger autolysis - the self-digestion of cells as a result of the release of enzymes from within the cell itself[3]. This, along with the action of bacteria found in the body, rapidly destroys the delicate ultrastructure of the brain tissue. In order to halt this decomposition, the brain must undergo a process known as fixation. Fixation stabilises proteins and lipids[4] and arrests metabolic processes, preventing immediate degeneration of the tissue. Long term brain storage is then achieved by cryopreservation (cooling the brain to sub-zero temperatures).

Chemically processing the brain also makes the tissue tougher and more robust. This enables the brain to undergo procedures that would cause unacceptable levels of damage and deformation otherwise - for example perfusion with toxic chemicals that produce increased osmotic pressure in the tissue[5]. As already mentioned, fixation stabilises proteins and lipids in the brain - as well as preventing decomposition this makes the tissue tougher, allowing the brain to be extracted without tissue damage. In order to reduce tissue loss and distortion when sectioning the tissue[6] however, we must make it even more rigid - this is achieved by resin-embed the brain.

Finally, we require high resolution imaging and have chosen electron microscopy (EM) as our imaging technique. Tissue samples for EM must be processed in a very particular way. As noted, embedding the brain makes it stiffer and tougher - this allows us to take very thin tissue slices (on the order of µm) and obtain a high z resolution in our image volume. Embedding the brain also makes the samples electron beam-stable[6]. In addition to this, tissue samples are imaged in a vacuum and the brain must also be dehydrated to prevent damage during imaging as a consequence of vaporising water molecules[7]. As well as Embedding and dehydration are is only part of the preparation needed, the brain must also be selectively stained with heavy metal dyes. This makes the tissue visible to the electron beam and increases contrast between features, such as cell membranes and vesicles, improving the success rate of synapse detection algorithms. This is achieved by selectively staining the tissue with heavy metal dyes.

On a final note, the best structural preservation will result from optimal conditions - that is, on-site anaesthesia and euthanasia and pre-death perfusion. However, there is anecdotal evidence to suggest that the procedure may be successfully completed even if begun some time after death[8], particularly if the patient is kept at a cool temperature.

3.1.1 The Overall Design

Broadly, our procedure for processing the fresh brain can be summarised in 5 key steps.

Figure 2: Summary of Chemical Processing Procedure

Having completed the steps as outlined above (see the relevant sections for further details), we should have 168 blocks of fully fixed, stained and resin embedded brain ready for ultra-thin and semi-thin sectioning (please see Section 2: Cutting, for further details).

3.1.2 Chemical Distribution

Solutions and other reagents can be introduced to the brain tissue via two methods - immersion and perfusion.

3.1.2.1 Immersion

Immersion involves submerging the tissue in solution to allow penetration via diffusion. However, diffusion is a slow process - glutaraldehyde, for example, penetrates tissue at a rate of 0.75 mm/h[9] and requires extended incubation periods for large sections of tissue. Removal from the cranium and sectioning of the brain prior to fixation is also not a viable option, as handling the soft unfixed brain results in unacceptable levels of damage and tissue loss, and biodegradation may occur in the time taken to complete the process. As a result, we will only use immersion for procedures where speed is not vital and the tissue has been stabilised somewhat - staining, dehydration and embedding.

3.1.2.2 Perfusion

An alternative to immersing the brain is perfusion, which uses the brain's own vascular structure to distribute solutions quickly and efficiently. This is particularly important for the washout and fixation procedures, where it is vital to halt decomposition and metabolic processes across the brain as quickly as possible. However it is not well suited to the introduction of highly viscous solutions (such as resin). As a result, we will be using perfusion to introduce washout, fixative and cryoprotectant solutions.

3.1.2.3 Perfusion Apparatus

Two pieces of perfusion equipment, both based on those described in[5] (with solution reservoirs and pump pressures modified for human patients), are used in the Fixation and Cryopreservation steps of our protocol.

3.1.2.4 The Washout Cart

The first piece of equipment used is the mobile washout cart (see figure 3), this is used to perform the washout, initial fixation and cool the brain. The cart consists of a 15L washout solution reservoir connected in series with a T junction, a Millipore 0.2 µm peristaltic filter and a heat exchanger. A Y-connector joins the cart to two cannulas placed in the patient. A thermocouple inserted in the tubing monitors the temperature of the solution as it enters the cannulas.

Because the cart is mobile, perfusion can continue to happen while the patient is transferred from the operating theatre, ensuring a smooth transfer to the computer-controlled perfusion machine. This minimises periods of ischemia while the brain tissue is still unfixed and allows washout perfusion to begin

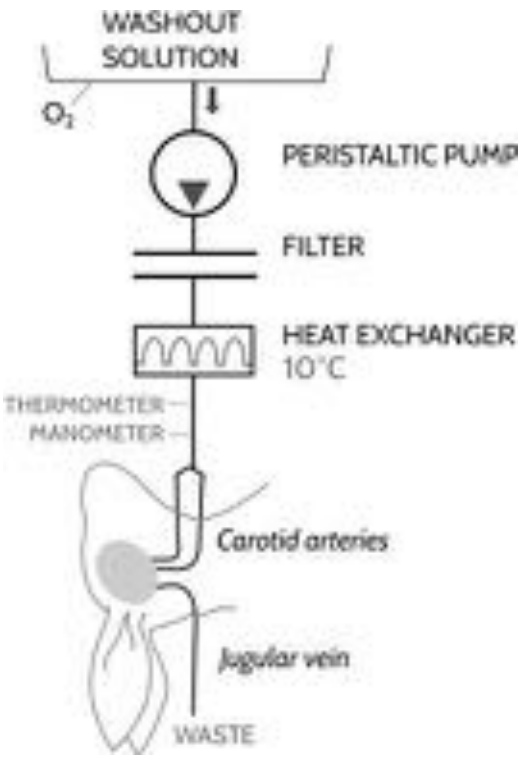

Figure 3: Washout Cart[5]

outside of the operating theatre, should a patient die unexpectedly.

3.1.2.5 The Computer Controlled Perfusion Machine

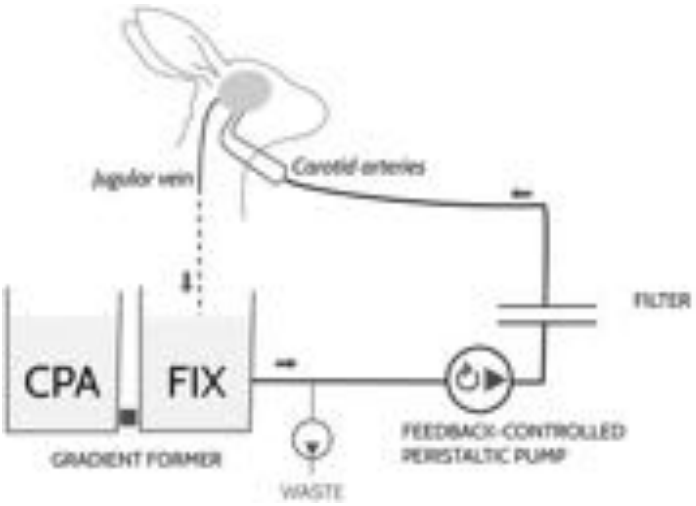

Figure 4: Computer Controlled Perfusion Circuit[5]

A computer-controlled perfusion machine (see figure 4) is used to introduce fixative and cryoprotectant solution to the brain and allows for greater automation of the process. A concentration gradient generator - essentially two connected reservoirs, one containing cryoprotectant solution and the other containing fixative solution outputs solutions - is connected in series to two pumps and a 0.2 m peristaltic filter. The first pump lowers the level of the gradient generator, creating a gradient. The second pump is feedback controlled to maintain a constant perfusion pressure.

3.1.3 Anaesthesia

In order to minimise tissue degradation as much as possible, the procedure must begin before the patient is dead - as a result, the patient must be placed under general anaesthesia and euthanized onsite. The dosages given below are based on a male of average weight, 83.6 kg[10], below the age of 55. However, the exact dose will be adjusted dependent on the patients weight and age. A trained anaesthetist must be present at all times to ensure the patient is properly anaesthetised throughout the procedure. General anaesthesia can be divided into two stages, induction and maintenance.

Induction of anaesthesia is achieved via an intravenous injection of propofol and fentanyl (although other anaesthesia protocols may be recommended in certain cases). Propofol and fentanyl work together to provide a smooth induction for the patient[11]. The recommended

dose of propofol for induction (assuming the described patient) is 2.5 mg/kg, administered at a rate of 20-40 mg every 10 seconds - amounting to a total dose of 209 mg[12]. The recommended dose of fentanyl to enhance anaesthesia while retaining spontaneous respiration is about 0.1 mg, although this should be adjusted according to patient response[12].

Once anaesthesia has been induced it must be correctly maintained to ensure the patient remains totally unconscious throughout the procedure. This is achieved by administering a volatile agent, isoflurane, via inhalation[11]. A typical maintenance dose of isoflurane for an adult is around 2.5% in oxygen, although this may be increased if the patient begins to appear responsive[12]. The volume of oxygen-isoflurane should be 3 times that of the minute volume of the patient[13] - for a typical adult this is around 21 L/min[14]. For half an hour of anaesthesia 1.59 L of isoflurane and 61.5 L of oxygen should be sufficient.

3.1.4 Washout

Once anaesthetised, a bilateral carotid cannula is performed on the patient and the washout solution administered[5]. The washout solution (see Table 3) should be the same pH as blood, 7.40, and can be adjusted using hydrochloric acid. To prevent hypoxia, the washout solution should also be oxygenated by bubbling oxygen through it at least 1 hour prior to perfusion.

Table 1: Washout Solution[5]

Chemical	**Concentration**
PBS 10 Concentrate	100 mL/L
Ketamine	5.40 mL/L
Sodium Heparin	0.50 mL/L
Euthasol	0.35 mL/L

3.1.4.1 Washout Procedure[5]

1. An incision is made in the neck and the surrounding tissue dissected to expose the carotid artery.

2. Ligatures are looped around the two common carotid arteries.

3. Insert the low-flow cannula in the right carotid and begin perfusion of the washout solution at a pressure of 100 mmHg[15]. Keep the other carotid clamped.

4. Within 30 s sever the right jugular vein.

5. Release the clamp on the left carotid and repeat the process, severing the other jugular vein also.

6. The entire cannulation procedure should take around 2 minutes to complete. Once complete, perfuse the brain with washout solution for a further 20min at 10C before proceeding to fixation.

7. Surgically separate the head from the body and transfer the head and apparatus to the fume cupboard.

Ischemia (insufficient flow to the brain) is avoided by ensuring the washout solution flow rate is around that of normal cerebral blood flow. Average blood flow rate per 100g through a human brain is 54 ml/min - assuming an average brain weight of 1350g, this gives a blood flow rate of 730 ml/min[16]. The volume of solution required can then be calculated using Volume(ml) = Flow Rate(ml/min) $\times$ Time(min). To perfuse the brain for 20mins at a flow rate of 730 ml/min around 15L of washout solution is required.

3.1.5 Fixation

As already mentioned, it is important to arrest the bodys natural metabolic processes as soon as possible, and having washed out the brain, we quickly move onto perfusing the brain with fixative solution. Chemical fixation kills and stabilises the cells, preventing the progression of decomposition processes. Fixing agents can be coagulant (those that precipitate proteins) or non-coagulant[17]. As we aim to preserve as much of the brains natural state and morphology as possible, we will use the latter, namely aldehyde fixatives.

Aldehyde fixatives work by creating crosslinks between proteins, preserving their relative positioning in the tissue. Once fixed, the brain is significantly more robust to temperature, osmolality, pH and mechanical damage[9] - and importantly, able to withstand cryoprotectant perfusion. We will be using glutaraldehyde over formaldehyde, another comon fixative, because its contains two aldehyde groups and thus forms cross links faster[18].

Aldehyde fixation also introduces morphological artefacts that allow for improved differentiation between excitatory and inhibitory synapses. Aldehyde treated excitatory synapses show spherical vesicles, while the vesicles in inhibitory synapses develop flattened shapes[19].

3.1.5.1 Fixative Solution Additives

The addition of membrane impermeable salts $Na_2HPO_4 \cdot 2\ H_2O$ and $NaH_2PO_4 \cdot 2\ H_2O$ to the solution prevents osmotic imbalance, helpng to preserve extra cellular space[20]. This improves the preservation of tissue morphology and aids later staining and post fixation steps. Another additive is sodium azide, a poison that rapidly inactivates mitochondria, preventing mitochondrial swelling artefacts[8]. Finally Sodium Dodecyl Sulfate (SDS), a surfectant, is added to the fixative solution to temporarily permeabilise the blood-brain barrier[5]. This allows solutions to pass from blood vessels to the tissue unhindered, preventing the typical shrinkage caused by the blood-brain barrier[9].

3.1.5.2 Fixative Solution

Table 2: Fixative Solution[5]

Chemical	**Concentration**
$Na_2HPO_4 \cdot 2\ H_2O$	14.65 g/L
$NaH_2PO_4 \cdot 2\ H_2O$	2.76 g/L
Glutaraldehyde	3% w/v

Table 3: Fixative Additives[5]

Chemical	**Concentration**
Sodium Dodecyl Sulfate	0.01 % w/v
Sodium Azide	0.1 % w/v

3.1.5.3 Fixation Procedure[5]

1. Transfer the head and washout cart to a fume hood.
2. Attach a 15L reservoir of fixative solution with additives (see tables 2 and 3) to the T junction of the washout cart.
3. Perfuse fixative solution at room temperature with a pressure of 100 mmHg for 20min.
4. Attach the computer contolled pump to the same connections as the peristaltic pump (see figure 3). Simultaneously decrease the speed of the carts pump and increase the

speed of the computer controlled pump, maintaining a pressure of 100mmHg.

5. Disengage the peristaltic pump once it's speed drops to 0.

6. Having completed transfer to computer control, engage the gradient generator (see figure 4) and perfuse with fixative solution (minus additives) for a further 45 min.

The volume of fixative required can be calculated in a similar manner to the washout solution - 32.9 L will be required.

3.1.6 Cryopreservation

Merely fixing the brain with aldehydes and storing in cool conditions is not enough to prevent tissue degeneration during long term storage - firstly, the fixed brain is still chemically active at 4C, and some breakdown of proteins may occur over time[9]. Secondly, and more importantly, lipids are not stabilised by aldehyde fixation and over time can migrate across the tissue, causing mechanical damage. But, in order to process multiple brains at once, extended brain storage it will almost certainly be necessary.

Freezing the fixed brain also produces unsatisfactory results with the development of ice crystals causing tissue dehydration and ultrastructural damage[21]. Instead, we intend to vitrify the brain - cool the tissue in such a way that it solidifies to a glass-like state, avoiding the formation of damaging ice crystals.

In order to successfully vitrify the brain, it must be perfused with cryoprotectants, essentially antifreeze. As the brain cools, instead of freezing, the water-cryoprotectant solution become more and more viscous until it eventually solidifies. Once vitrified, the progression of time is effectively halted, allowing the brain to be stored for extended periods of time[21]. To progress with the remainder of our processing steps, we simply rewarm the brain and remove of the cryoprotectant.

In addition to providing reliable long term storage, vitrification also affords us flexibility with respect to the rest of our processing protocol. Provided any new techniques are compatible with aldehyde fixed tissue, it should be theoretically possible to change our protocol entirely from this point forward if improved staining protocols, embedding media etc. are developed.

3.1.6.1 Cryprotectants (CPAs)

As discussed cryoprotectants allow the brain to vitrify, protecting the tissue from freeze damage. However, cryoprotectants themselves can be damaging to tissue and it is important to introduce cryoprotectants slowly to limit toxicity[22] and osmotic imbalance[5]. This is achieved by steadily and linearly increasing the concentration of CPA in the perfusate over a period of time using a gradient generator (see figure 4).

Of the available cryoprotectants we have chosen ethylene glycol was chosen specifically because, based on permeability studies, it penetrates the brain better than other popular cryoprotectants[5]. Again, as with the fixative solution, membrane impermeable salts, $Na_2HPO_4 \cdot 2\ H_2O$ and $NaH_2PO_4 \cdot 2\ H_2O$ are added to reduce osmotic imbalance.

Table 4: Cryoprotectant Solution[5]

Chemical	**Concentration**
$Na_2HPO_4 \cdot 2\ H_2O$	14.65 g/L
$NaH_2PO_4 \cdot 2\ H_2O$	2.76 g/L
Glutaraldehyde	3% w/v
Ethylene Glycol	65% w/v

3.1.6.2 CPA Perfusion Procedure[5]

Having perfused the brain with fixative solution for 45 minutes

1. Engage the gradient generator
2. Linearly increased the concentration of CPA over the course of 4 hours, maintaining a pressure of 100mmHg. The fixative reservoir should be stirred continuously with a magnetic stir bar.
3. Recirculate CPA solution at full strength for an hour, then disconnect the head from the perfusion machine.

The volume of solution required was found by scaling up from other animal brains according to volume. Mouse brains require 3 L of solutions in total (1.5 L of CPA and Fixative each) and pigs, whose brains are 7.5 times smaller than human brains[23] require 8L. By extension

a human brain will need around 60 L of solution altogether (30L of CPA and fixative each) and for the final re-circulation 3L of CPA should be used.

3.1.6.3 Vitrification Procedure

Once the brain has been perfused, re-immerse the head in CPA to avoid water from the air condensing on it[9]. The brain should then be placed in a 21st Century Medicine, Inc. Controllable Isothermal Vapor Storage (CIVS) device and cooled to -135C[5]. At this point the brain can be stored almost indefinitely (although conservative estimates are around 100 years).

3.1.6.4 Warming and CPA Removal

To continue processing, warm the head to room temperature and remove CPA from the tissue. CPA removal can be accomplished in exactly the same way as introduction, but in reverse - linearly decrease the concentration of CPA for 4 hours, then circulate with fresh fixative solution for an hour. 33L of fixative solution and 30L of CPA should be used respectively

3.1.7 Brain Extraction

Thus far we have kept the brain inside the cranium both as a protective measure and to allow perfusion. However, the next steps of our protocol involve immersing the brain in solutions and consequently we must extract the brain from the cranium before proceeding any further.

3.1.7.1 Extraction Procedure[24]

1. Make an incision in the coronal plane from behind one ear to the other.
2. Pull the front flap of skin down towards the eyebrows and the back flap towards the occipital protuberance.
3. Using a circular saw, cut through the skull along its circumference - horizontally across the forehead then over the posterior superior surface. Care should be taken to only cut the bone and not penetrate the brain.

4. Remove the scull cap and sever the optic nerves, carotid arteries and pituitary stalk.

5. Finally raise the frontal lobes and cut the tentorium and spinal cord, before lifting the brain out of the skull.

3.1.8 Staining and Post Fixation

In order to trace the connectome reliably, we require very high resolution images. Currently, this can only be achieved using electron microscopy, a technique that involves firing an electron beam at a sample in order to produce images. Electron deflection depends on the atomic number of the atoms in the beams path, however, biological tissue has both a low and similar electron density throughout[25]. Samples must therefore be impregnated with heavy metal stains such as osmium tetroxide, uranyl acetate or lead citrate[26] whose high atomic number allows them to scatter the electron beam more effectively, providing greater contrast between tissue features.

In addition to improving contrast in EM images, some stains also behave as post fixatives. Our fixative procedure so far only works to bind proteins - once warmed, lipids may again be susceptible to movement within the tissue. Additionally, lipids are a key component of membranes. As synapses are always found at membranes, enhancing membrane contrast should improve synapse detection. Consequently, stains capable of stabilising and staining lipids are desirable.

There are many potential staining and post fixative protocols, we have chosen BROPA (over OTO, ROTO and wbPATCO to name a few). As already mentioned, we aim to preserve as much neuronal information as possible. Accordingly, mechanical damage and artefact formation should be minimised - our chosen protocol consistently stains the whole brain, allowing us to section post embedding when the tissue has been made more robust to cutting losses.

3.1.8.1 Osmium Tetroxide (OsO4)

Osmium tetroxide is a heavy metal stain and post fixative that binds particularly well to lipids[26], forming a black reduction compound by addition with the double carbon to carbon bond in lipids[27].

3.1.8.2 Uranyl Acetate

Uranyl acetate is another popular heavy metal stain. However, while our goal is primarily to enhance membrane contrast, uranyl acetate is a relatively non-specific stain[28]. It is also most useful as a post-embedding stain[29], whereas we plan to stain beforehand. This, coupled with the fact that uranyl acetate is sensitive to light and precipitates with age[29], has lead us to avoid using it.

3.1.8.3 Osmium Stain Amplification

High stain density is required in order to identify the smallest neuronal processes accurately - consequently stain amplification is a vital part of our protocol. Stain amplifiers are reducing agents that react with osmium tetroxide, attaching themselves to osmium deposits already present in the sample. The amplifier then acts as a bridge, allowing further osmium to deposit[28].

TCH (Thiocarbohydrazide) is a common amplifier and is used in the OTO, ROTO and wbPATCO protocols. However, when applied to large samples, TCH amplification results in the formation of nitrogen bubbles, causing mechanical damage and deformation[20].

An alternative amplification compound is Pyrogallol (trihydroxybenzene). Amplification with pyrogallol provides superior performance to TCH with better membrane contrast, stain uniformity and penetration, improved preservation of extracellular space and decreased mechanical damage[20].

3.1.8.4 BROPA

We have chosen to implement the BROPA (Brain-wide Reduced Osmium staining with Pyrogallol-mediated Amplification) protocol. The whole brain is immersed in a series of osmium tetroxide and pyrogallol steps in order to stain and post fix the brain. The use of osmium tetroxide and pyrogallol results in excellent membrane contrast and ultrastructure preservation good enough to identify synapses and trace the thinnest neurites[20].

A key advantage of BROPA, over other protocols, is its ability to consistently stain larger samples. The addition of formamide in the initial reduced osmium step prevents barrier

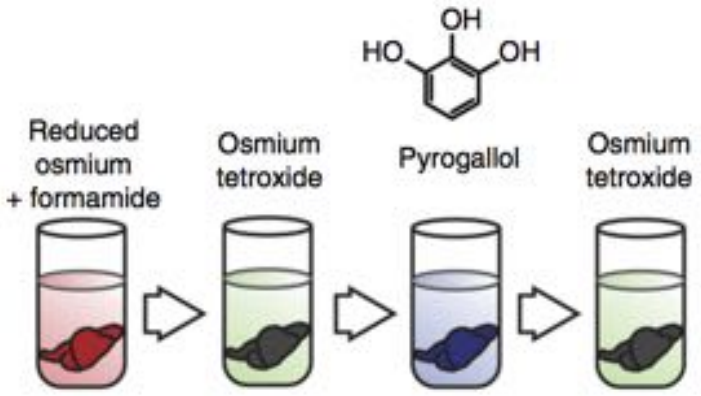

Figure 5: BROPA Staining Protocol[20]

formation and allows uniform staining of the whole brain. This may be because it allows the highly charged species $Fe(CN)_6^{-4}$ to cross cell membranes[20].

3.1.8.5 Alternative Protocols

wbPATCO (Whole Brain Periodic Acid Thiocarbohydrazide Osmium Tetroxide) is an alternative staining protocol that involves the use of periodic acid for the first incubation step and TCH to amplify the staining. While the technique is capable of staining the whole brain, it only stains myelinated axons well enough for reliable tracing and provides only moderate ultrastructural preservation[30].

Another alternative is ROTO (Reduced Osmium Thiocarbohydrazide Osmium) stains the sample using osmium tetroxide and uranyl acetate and lead aspartate steps along with TCH amplification again. The technique produces good membrane contrast and subcellular ultrastructure preservation[31], however, it is only suitable for small samples. Reactions between osmium tetroxide and ferrocyanide result in the formation of dark bands of precipitation and poor staining beyond depths of 200 µm[32] [20].

3.1.8.6 Staining Procedure[20]

1. Immerse the brain in an aqueous solution of OsO_4 (40mM), Cacodylate Buffer (100nM), $K_4Fe(CN)_6$ (35mM) and Formamide (2.5M) for 862 days.

2. Without rinsing, transfer the brain to an aqueous solution of OsO_4 (40mM) and Cacodylate Buffer (100nM) for 646 days.

3. Replace this solution with an aqueous solution of Cacodylate Buffer (100mM) for 36 days.

4. Next, transfer the brain to an unbuffered aqueous solution of Pyrogallol for 646 days.

5. Replace this solution with an aqueous solution of Cacodylate Buffer (100mM) for 36 days.

6. Finally, transfer the brain to an unbuffered solution of OsO4 (40mM) for 862 days.

Around 0.115 ml of each solution is required per cm^3 of brain tissue - assuming negligible brain shrinkage due to fixation as a conservative measure (i.e. a brain volume of 0.014m3), around 1.5L of solution is required at each step.

Timings have been calculated under the assumption that we can approximate the brain as a sphere and that diffusion of solutions through the brain can be modeled by the Einstein-stokes approximation, Time $= R^2/6D$ where (D = the diffusion constant for each solution, R = the brain radius).

3.1.9 Dehydration

Electron microscopes use a high energy beam of electrons to image the sample. In order to prevent these electrons from being deflected by air particles, imaging must be completed in a vacuum. However, the resulting drop in pressure will cause water molecules present in the sample to vaporise, damaging the sample and resulting in a poor image[7]. Additionally, any water content remaining may interfere with later embedding of the sample[26]. Therefore, before the electron microscope can be used, the sample must be thoroughly dehydrated. Although shrinkage is to be expected with any dehydration method, it must be minimised in order to best preserve the sample structure.

3.1.9.1 Air Drying

Drying samples by exposure relies on the removal of water from via evaporation. However, as water changes state, the effects of surface tension result in deformation of the cells and an unacceptable degree of tissue shrinkage[33], making the tracing of neuronal processes unreliable.

3.1.9.2 Lyophilisation

Lyophilisation, or Freeze Drying, is a technique frequently used to preserve foodstuffs, although it has seen use in pharmaceutical products. The sample is frozen before reducing the surrounding pressure in order to sublimate the water content. However, studies of lyophilised samples have shown shrinkage to 51% of fixed and stained volumes along with ultrastructural damage as a result of ice crystal formation[34]. Again, this significant shrinkage and damage introduces morphological and ultrastructural artefacts, resulting in poor synapse detection.

3.1.9.3 Critical Point Drying

Critical Point Dehydration (CPD) relies on the fact that, at a materials critical point, the physical characteristics of the liquid state and gaseous state are identical, allowing for a transition from one state to the other without the damaging effects of surface tension. The critical point of water is too high to allow for dehydration without destruction of the sample so water in the sample must be replaced by liquid carbon dioxide. While on average providing better surface structure results than those of freeze dried samples, multiple studies have shown greater shrinkage of CPD samples - around 38% of the fixed volume in comparison[34] [35].

3.1.9.4 Solvent Dehydration

Solvent dehydration involves replacing the water content with another solvent more readily miscible with embedding media[26]. In order to minimise large changes in osmotic pressure, and the resulting cell distortion, the concentration of solvent should be increased slowly via a series of gradual steps, and should be kept low initially.

3.1.9.5 Dehydration Procedure[36]

There are a number of suitable dehydration agents available - for example Dioxane, Acetone and Dimethyl Sulfoxide[37] [38]. We have chosen use ethanol due its widespread usage, relative safety and consistency[26]. To ensure complete dehydration, 10 m^3 of dehydrating fluid are required for every 1m^3 of tissue volume[39] - assuming a brain of 0.0014m^3, 0.014 m^3 of

solution will be used at each step.

1. Rinse the brain with distilled water for 3 hours.
2. Submerge in 30% and then 50% solutions of ethanol for 30 minutes each.
3. Next place the brain in 70%, 90%, and 95% ethanol solutions for 1 hour at a time.
4. Finally submerge the brain in a 100% ethanol solution for an hour, twice.

At each ethanol infiltration progressively lower the solution temperature to cool the brain to 4 °C. Care must be taken to avoid air drying of the brain after dehydration or damage to the sample may occur[33], and embedding of the brain should follow immediately.

3.1.10 Embedding

Embedding is the process of impregnating a sample with resin (or wax) to increase tissue rigidity and strength. This allows it to withstand bombardment with high energy electrons during imaging and decreases imaging artefacts. The increased rigidity also reduces tissue loss at cut planes and cutting artefacts[6]. In particular, although traditionally SEM samples do not have to be as thin as TEM samples, we require a very high z resolution in order to trace neuronal processes accurately between brain slices (please see the Cutting and Imaging sections for further details). Consequently, our resin of choice must be hard enough to allow clean sectioning of the brain without crumbling or extensive deformation at very thin thicknesses.

Broadly, embedding resins can be split into two groups. Epoxies, for example Epon, Spurr's and Durcupan, and acrylics such as LR White, Lowicryl and Unicryl. Ideally, the chosen resin should give uniform results, be miscible with the dehydration media used and result in minimal image granularity. Most importantly however, as we will be embedding such large volumes, our chosen resin should have as low a viscosity as possible[26] while still providing the rigidity required. The greater the viscosity - anything above 150 cP is considered high[26] - the longer the incubation period required and the increased likelihood of premature resin polymerization and incomplete infiltration. The resulting resin free areas will then form cracks[20] impacting our ability to accurately trace neuronal processes across the brain.

While the embedding medium is in its liquid monomer form, the brain is immersed and left for a time to allow the resin to totally infiltrate the tissue. Having fully penetrated the brain, the embedding medium is then polymerized[40] into a hard block of plastic suitable for sectioning. Cooling the sample slowly after curing should minimise crack formation[20] - regardless, if some clean cracks do occur, it should be possible to trace even the smaller neuronal processes across[40].

3.1.10.1 Epoxy Resins

Epoxy resins have several advantages - they cause little to no shrinkage, section well and show few imaging artefacts[41]. However, one big problem with epoxy resins is their relatively high viscosity. As already noted, infiltration is a very slow process - embedding an entire human brain with epoxy resin would take an extraordinarily long time. Moreover even Spurr resin, one of the least viscous of the epoxies with a viscosity of about 60cP, has a pot-life of only 3-4 days before polymerization causes it to become too viscous to penetrate the tissue effectively[42]. As a result, epoxy resins are incapable of fully infiltrating a volume as large as the human brain and the brain would have to be sectioned into volumes on the order of mm while still unembedded, resulting in unacceptable levels of tissue loss. They are also extremely hydrophobic and anything less than perfect dehydration will result in poorly embedded tissue[41].

3.1.10.2 Acrylic Resins

A key benefit of acrylic resins in comparison to Epoxies is their low viscosity - this makes for relatively short infiltration cycles, an essential quality for the embedding of large sections. They are also very versatile and provide excellent results with both fully dehydrated tissue and partially dehydrated tissue[41]. Although we intend to fully dehydrate the brain, this quality reduces the likelihood of poorly embedded regions within the volume if dehydration is less than perfect. Although there are a number of available acrylic resins with suitable qualities - LR white, for example - we have chosen Unicryl for the reasons outlined below.

3.1.10.3 Unicryl

Unicryl is an acrylic resin that produces electron beam stable blocks with excellent ultra-structure preservation. It retains a low viscosity even down to temperatures as low as -50 °C and remains unpolymerized for around 12 months at 4 °C, and even longer at lower temperatures[43]. This is more than enough time to fully infiltrate the brain before the resin becomes too viscous to penetrate the tissue. In addition to this, because all the components of Unicryl have similar atomic weights, Unicryl penetrates tissue evenly and has excellent cutting properties both for semi-thin and ultra-thin sectioning[43].

Unicryl can be polymerized using either heat or UV. Although polymerization at a low temperature with UV decreases the potential for structural damage in the tissue, our volume will be too large for UV to fully penetrate and there will be regions of soft un-polymerized resin. Furthermore, the brain tissue will have already undergone various fixation and staining procedures. Firstly, these make the tissue less sensitive to degradation at high temperatures. More importantly however, heavily stained areas (such as membranes) will absorb UV light more readily than the surrounding tissue, which may result in an unevenly polymerized sample[44].

Polymerization of Unicryl is controlled by the rate of release of free radicals in the resin, which terminate the growing polymer chains. The rate of free radical release in turn is proportional to the heat or UV intensity applied to the sample. As a result, the properties of the block depend on the curing conditions - high heat results in brittle blocks that are difficult to cut[43] as well as gaps in sections as a result of bubbles formation[44]. It is also worth noting that the polymerization reaction is exothermic - this is a particular issue with large blocks due to the quantity of resin being polymerized[44]. Consequently the temperature of the block should be carefully monitored throughout the procedure and we will be polymerizing for a long time at the lower end of possible temperatures, 50 °C, to maintain a slow rate of polymerization.

3.1.10.4 Ininital Embedding Procedure[44]

1. place the brain in a 95mm x 150mm x 170mm[16] polyethylene mould and infiltrate in 100% resin for at least 27 hours, agitating regularly. Drain the resin and repeat this

step.

2. Drain the resin and infiltrate in 100% resin for 27 days one final time, again, agitating regularly.

3. Finally, place the infiltrated brain in a temperature controlled oven and polymerize at 50 °C for 6 days.

The dehydrated brain will be at 4 °C, this temperature should be maintained throughout the infiltration procedure until the final curing step.

The amount of resin used must be 100 times the volume of tissue being infiltrated - 0.1ml for every 1 mm^3 of tissue[44]. For a brain of 0.0014 m^3, 140 L of Unicryl will be required for each infiltration. It is important to keep agitating the resin immersed brain while infiltrating to promote proper penetration[44]. Automation can help make the process significantly less labour intensive, however, the volumes of resin required for each infiltration are huge and prohibit the use of standard overhead shakers. We could commission custom built solution shakers but a simpler solution is to borrow technology from industrial mixers designed for cement and other materials.

The Einstein-Stokes approximation only provides a good estimation for solutes moving in solution. Instead, we can approximate the brain as a sphere again and scale from the times required for 0.1mm sections[45] using the more general Fick's Law, where
Diffusion Rate α (Surface Area)/Distance - note that distance is the radius of the brain, in this case. In total, infiltration and polymerization of the block should take around 35.25 days.

3.1.10.5 Re-Embedding Procedure[43]

The embedded brain is cut into 8400 sections and these sections are then secured into stacks of 50 separated by an epon spacer[46] (please see the Cutting Section) before being re-embedded in Unicryl. For each stack:

1. Infiltrate with 100% resin for 1 hour, twice while agitating gently with a tissue shaker.

2. Infiltrate with fresh resin for 8 hours.

3. Polymerise for 3 days at 50 °C.

The same volume of resin should be used again, 0.83 ml per stack for each infiltration. In this case, the volumes of tissue being processed are far smaller - as a result automated tissue processors can be used to parallelise the process and automate the infiltration protocol. The Leica TP1020 Semi-enclosed Benchtop Tissue Processor, for example, can process 100 stacks at a time, giving a total embedding time of 20 hours. The stacks can then all be polymerized together.

3.1.11 Costing and Timings

Table 5: Significant Equipment and Material Quantities and Costs (per person)

Procedure	**Material**	**Amount**	**Price per unit**	**Cost**
Anaesthesia	Propofol (0.5%)	209 mg	0.22 $/ml	$7.27
	Fentanyl (0.05 mg/ml)	0.1 mg	$0.3/ml	$0.6
	Oxygen	61.5 L	0.014 $/L	$0.86
	Isoflurane	1.6 L	0.14 $/ml	$224
Washout	Washout Solution	7.3 L	$0.50 /L	$3.65
Fixation	Fixative Solution	47 L	13.40 $/L	$629.80
	Fixative Additives	15 L	$0.25 /L	$3.75
Vitrification	Fixative Solution	30 L	13.40 $/L	$402
	CPA Solution	33 L	$45.90 /L	$1514
Warming & CPA removal	Fixative Solution	33 L	13.40 $/L	$442.20
	CPA Solution	30 L	$45.90 /L	$1377
Staining & Post Fixation	Osmium Tetroxide (4%)	160L	2.65 $/ml	$1272000
	Cacodylate buffer (0.2M)	80L	0.08 $/L	$25600
	$K_4Fe(CN)_6$	2370 g	0.2246 $/g	$531
	Formamide (25.09 M)	16 L	0.7021 $/ml	$11230
	Pyrogallol	6460	0.3976 $/g	$2570
Dehydration	Distilled Water	22.4 L	0.84 $/L	$18.8
	Ethanol	61.6 L	81.95 $/L	$3911.60
Embedding	Unicryl	840L	1.26 $/ml	$1058400
	Tissue Processor [1]	1	N/A	$39995
Total Cost				$2,462,531

Table 6: Processing Time Scale

Procedure	**Step**	**Time Required**
Patient Preparation	Cannulation & Washout Perfusion	30 min
Fixation	Initial Fixative Perfusion	20 min
	Computer Controlled Fixative Perfusion	45 min
Cryopreservation	Cryoprotectant Perfusion	5h
	Vitrification	N/A
Staining & Post-Fixation	Reduced Osmium & Formamide	862 days
	Osmium Tetroxide (buffered)	646 days
	Cacodylate Buffer Solution	36 days
	Pyrogallol	646 days
	Cacodylate Buffer Solution	36 days
	Osmium Tetroxide (unbuffered)	862 days
Dehydration	Ethanol Series	8.5 h
Embedding	Infiltration	29.25 days
	Polymerisation	6 days
Re-embedding (in total)	Infiltration	20 h
	Polymerisation	3 h
Total Time Required		8.56 years

3.1.12 Summary

To summarise, our procedure can be simplified to the following steps. At each stage it is vitally important that the brain is fully penetrated by the relevant solutions, as failure to do at any stage will ultimately result in low quality sections containing holes and other artefacts.

1. Anaesthetise and cannulate patient.

2. Perfuse the brain with washout solution pre-death.

[1]Note, the cost of a tissue processor is only incurred for our first brain

3. Euthanize the patient and remove the head from the body.
4. Perfuse the brain with fixative solution.
5. Perfuse the brain with cryoprotectant solution.
6. Vitrify.
7. Warm to room temperature and remove cryoprotectants.
8. Extract the brain from the skull.
9. Stain using the BROPA protocol.
10. Take the brain through an Ethanol Dehydration series.
11. Embed the whole brain in Unicryl.
12. Re-embed stacks of sections in Unicryl again.

3.2 Sectioning

T. HAYDEN

The sectioning stage aims to section the brain into smaller pieces for the imaging process whilst maintaining tissue ultrastructure. In particular, it is desirable to create sections with a thickness of 29 nm (see section 3.3). Sectioning also increases the degree of parallelisation available at all stages of the BDCP. The average volume of a healthy adult human brain is 1510 cm^3 for men and 1320 cm^3 for women[2]. If this volume were to be sectioned at 29 nm then the total area imaged will be 52 100 m^2. This is over seven football fields imaged at 3.5×3.5 nm resolution. It should be noted that the ultramicrotomy community has found sectioning on this large a scale to be challenging[47]. Some progress has been made in recent years[46]. However, the methods used may not scale up to the sizes required for a human brain and in the BDCP we propose a novel approach.

3.2.1 Outline of the sectioning procedure

The sectioning process of the BDCP can be summarised by the two stages. The first stage is to perform ultrathick serial sectioning on the whole brain using a long sapphire knife (see

section 3.2.2). After ultrathick sectioning, the brain will be reduced to around seventy 5 mm thick blocks of embedded tissue. The next stage is to perform ultrathin sectioning (see section 3.2.3). the ultrathin sectioning procedure will reduce the embedded blocks to 29 nm thick strips. These strips collected and stored on kapton tape ready for the imaging process of the BDCP.

In total, the sectioning process is expected to cost around $25 million and add around 140 days to the total time required for the BDCP.

3.2.2 Ultrathick sectioning

Ultrathick sectioning is the first sectioning process after embedding the brain. Ultrathick sectioning involves reducing the brain from a single embedded block to relatively thick sections around 1 mm thick. This is done to increase the the amount of parallelisation available as well as to limit the use of the longer sapphire knives (see section 3.2.4.2). In addition, the ATUM (see section 3.2.3.2) used in ultrathin sectioning can only section samples a few mm wide.

3.2.2.1 Overview of the Ultrathick Sectioning Process

Figure (6) shows an outline of the ultrathick sectioning process. The ultrathick sectioning process will use a modified ultramicrotome (see section 3.2.2.2) to perform all of the sectioning. The embedded brain is mounted onto the modified ultramicrotome. The sample is moved over the long sapphire knife (see section 3.2.4.2) and sections float in the water bath. The knife is placed under special conditions to improve section quality (see section 3.2.4.7). The sections are carefully collected using a collection grid and stored before being placed into the section stacking apparatus (see section 3.2.2.4 and figure (12a)) where they are rembedded into larger blocks. The stacked sections are then trimmed and are now in $5 \times 160 \times 140$ mm embedded pieces ready for ultrathin sectioning. A Typical human brain would produce around 70 of these stacked sections.

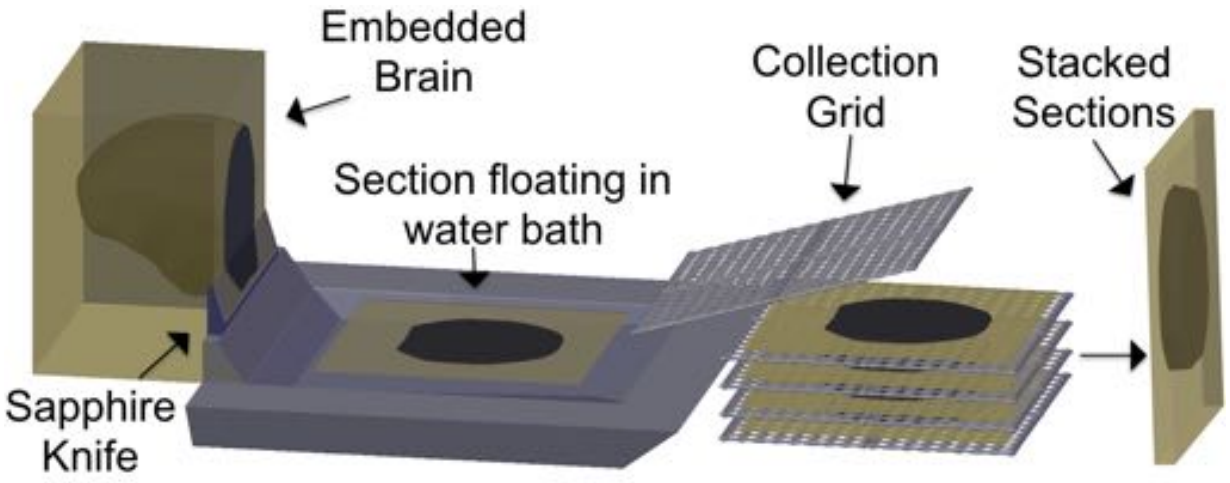

Figure 6: An outline of the ultrathick sectioning procedure.

3.2.2.2 Ultramicrotomes

All of the sectioning of embedded sections will be done using ultramicrotomes. These are widely used by the ultramicrotomy community for sectioning. Conventional microtomes used for light microscopy are not able to section finely enough our purposes. In addition, conventional microtomes can cause excessive surface damage[48] which is unacceptable for our purposes. Ultramicrotomes will give the best chance of sectioning the embedded brain with minimal damage. There are some novel alternatives (see section 3.2.2.5) but for the BDCP we will try to use well established technologies.

Figure (8a) shows a simplified diagram of a typical ultramicrotome. In the diagram, the sample, S, is mounted on the holder, H. The arm, A, moves the sample on path P. The sample is repeatedly brought forward a set distance and moved over the knife producing a thin section which floats on a liquid in the trough T. The arm then retracts and repeats the process[49]. The sections are manually collected from the trough. Figure (7) shows section retrival methods. In the BDCP we will collect sections using large grids and store them temporarily. The sections will then be grouped together in the section stacking process (see section 3.2.2.4).

Figure (8b) shows the Lecia EM UC7[50], a popular modern Ultramicrotome. For the BDCP, a specially designed ultramicrotome will have to be designed which allows for the use of longer knives and the mounting of larger samples.

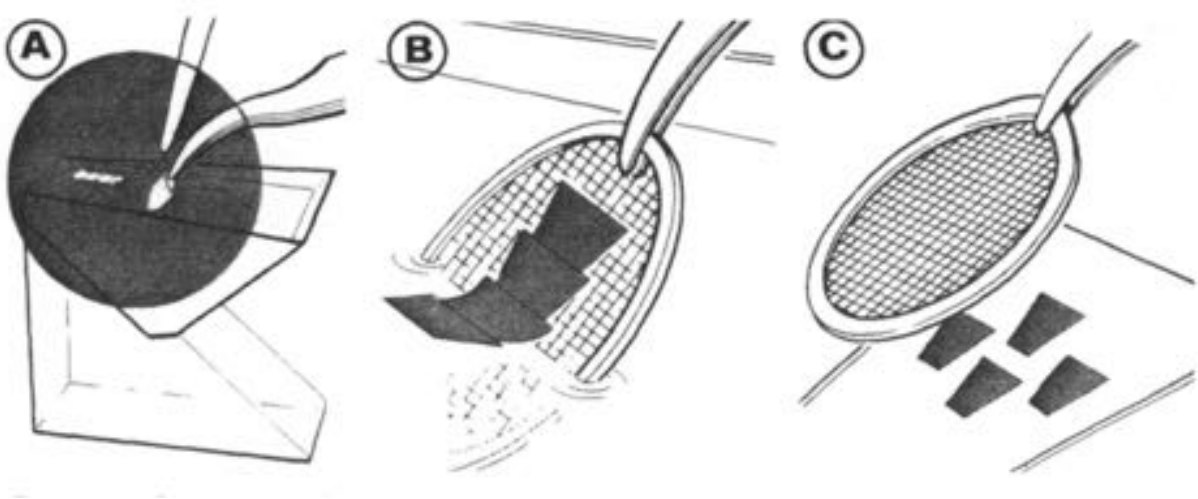

Figure 7: Section retrieval procedure. A) shows a glass fibre tool being used to move the section into place. B) shows the TEM grid lifting the section out of the trough. C) shows an alternative to B) where the TEM grid is placed on top of the section causing the section to stick to the grid[49].

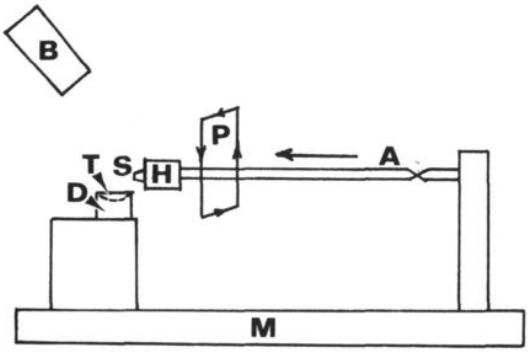

(a) A diagram of the basic components and operation of a typical modern ultramicrotome[49].

(b) The Lecia Em UC7 ultramicrotome[50].

Figure 8

3.2.2.3 Using a Longer Knife

The shortest dimension of the average human brain is 97 mm[51]. Since we are using an ultramicrotome for sectioning, a knife at least this long is required for the ultrathick sectioning method proposed. In practice, a knife slightly longer than this is required to allow for a margin of error when mounting the knife. In this report, we will consider the practicality of making and using longer diamond and sapphire knives. Section 3.2.4 has more details on the characteristics of ultramicrotomy knives made from a variety of materials.

It would be preferable to use a long diamond knife for ultrathick sectioning in the BDCP.

However, due to the impracticalities involved in fabricating such a knife, we recommend that a long sapphire knife is used instead. We take the conservative approach that the knife will be replaced after every 10 cuts. This will mean that we will need approximately 840 knives. Such a conservative approach is used as it is impractical to check the knife for damage after each section is cut. We have suggested a preliminary cutting speed of $0.1\text{mm}\,\text{s}^{-1}$. This will result in the serial sectioning process taking around 135 days.

Diamond and Sapphire Knife production Both sapphire and diamond knives are produced in a similar fashion. The standard process to create diamond knives is to first take a gem grade diamond and cleave it along one of its planes to create a flat surface. The edge of the resulting diamond is then ground to the desired edge angle using fine diamond powder and a smooth iron disk[52]. Since diamond is anisotropic, care must be taken that the grinding is done along the correct direction. Failure to do this will result in significant subsurface damage which will shorten the life of the knife. To obtain the particularly sharp and smooth edge required, the edge is polished using ultrafine diamond powder, with an average particle size of 1-5 nm, with a diamond knife polishing machine[53].

Diamond knives produced in this fashion are commercially available from several manufacturers. However this method is limited by the size of the diamond and the longest commercially available diamond knife at the time of writing is only 6mm long[54]. Longer knives could be produced using this method by using larger diamonds[55]. However this has not been researched in detail due to the prohibitively high cost of these larger diamonds.

The production of sapphire knives is similar to the production of diamond knives. The knives are made by cleaving or fracturing a single crystal of synthetic corundum and polishing the resulting edge to the desired dimensions[56]. Care must be taken to ensure that only the highest quality sapphire is used with no defects such as air bubbles or inclusions. These defects will result in a degraded knife edge as well as lowering the durability of the knife.

Diamond Synthesis This section will outline the two main techniques used to produce synthetic diamonds. However it should be noted that diamond synthesis is a rapidly growing field and it is likely that there will be new developments in the near future.

Currently, the most popular technique for diamond synthesis is chemical vapor deposition

(CVD)[57]. In this process a mixture of methane and hydrogen is passed over a diamond substrate at high temperatures and low pressures. The carbon from the methane bonds to the diamond substrate in either a graphite or tetrahedral diamond configuration. The hydrogen removes both of these newly formed structures but removes graphite at a much faster rate. Thus the substrate grows with minimal graphite formation. There are many different types of CVD processes, two of which are shown in figure (21). Using CVD it is theoretically possible to create single crystal diamonds or arbitrary size[58]. In practice, diamonds created using CVD are likely to have defects such as vacancy clusters and dislocations. The larger the diamond, the more likely it is that these defects will weaken the structure to such a degree that the diamond will not be useable for our purposes.

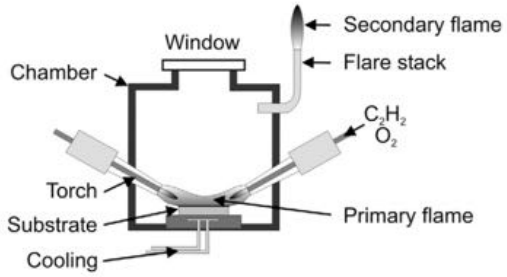

(a) Apparatus for a thermally induced CVD process.

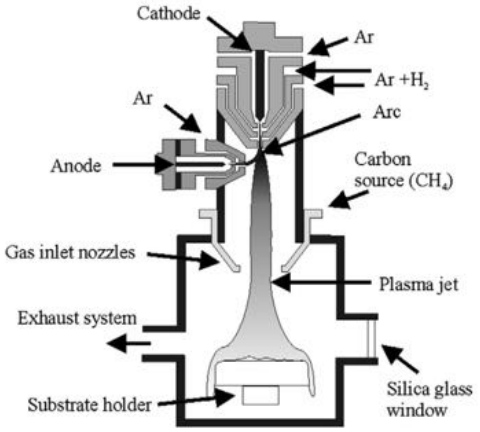

(b) Apparatus for a direct current plasma discharge CVD process.

Figure 9: Two different chemical vapor deposition (CVD) processes[57].

The second widely used technique for synthetic diamond synthesis uses a high temperature high pressure (HTHP) approach. In this process, diamond crystals are grown from a diamond seed at high temperatures and pressures[59]. Examples of HTHP apparatus can be seen in figure (10). Figure (10a) shows a typical HTHP setup. Pressure is applied using two diamond anvils. The carbon source can be high-purity graphite or diamond powder.

Whilst HTHP diamonds can then be used to make diamond knives using standard cleaving an polishing techniques, it is also possible to make HTHP diamond knives directly. Figure 10b shows a drawing from a patent concerned with creating diamond knives for ultramicrotomy using a HTHP method. Extremely fine diamond powder (7) is forced into a diamond mold (3) by a diamond anvil (6). The resulting crystal is a knife suitable for ultramicrotomy.

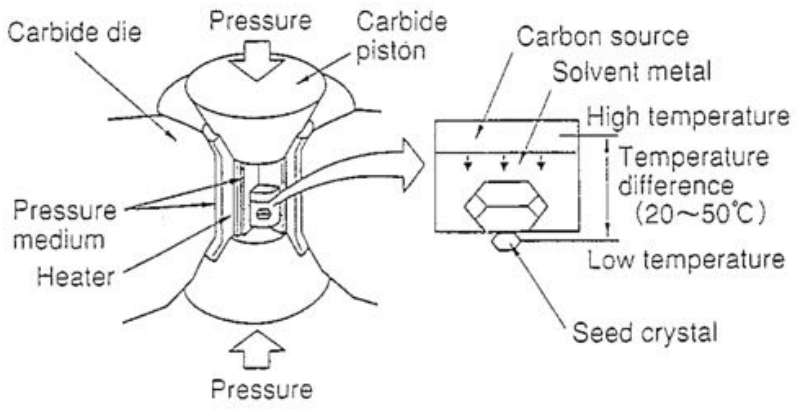

(a) The apparatus for diamond growth using a high pressure, temperature gradient approach[59].

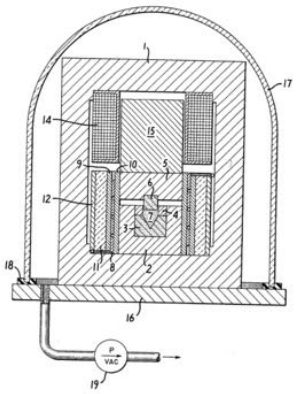

(b) A schematic from US patent US4084942 used to create arbitrarily size diamond knives[55].

Figure 10: Two different uses of high temperature high pressure methods to synthesis diamonds.

Using this setup, it is theoretically possible to create diamond knives of arbitrary lengths[55]. However in practice it is difficult to create large diamonds using HTHP as defects tend to form. The larger the diamond is, the more likely it is that there will be flaws present. Adding nitrogen or certain metals can both increase the growth rate of the diamond and increase the stability of the process, reducing flaws. However this also creates a lower quality diamond which will be more prone to damage. It should also also be noted that HTHP methods themselves need large diamonds to be used as anvils.

Some consideration should also be made into purchasing an existing natural diamond. At the time of writing the largest suitable diamond available is the Lesedi La Rona[60] which has a longest dimension of 65mm. Unfortunately this is not long enough for our purposes. It is possible that a larger diamond will be unearthed. However such a diamond will most likely be extraordinarily expensive. In addition given that no diamonds of sufficient size for the BDCP have ever been unearthed, it is unlikely that a suitable diamond will be found in the near future.

Sapphire Synthesis There are a variety of methods used to produce single crystal synthetic sapphire. However to achieve the largest size with the quality required, the Kyropoulos technique[61](see figure (11a)) should be used. In this process aluminium oxide is loaded into a crucible inside a chamber filled with inert gas. The aluminium oxide is then

melted and a sapphire seed is inserted into the crucible and slowly drawn out. This process is repeated to slowly build up a single crystal of synthetic sapphire. Using this process, single crystal sapphires with a weight of 300kg and a diameter of 500mm have been produced routinely[62] (see figure (11b)). This will allow for the production of knives long enough for our purposes. Note that the crystals produced using the Kyropoulos technique are generally of extremely high quality with minimal defects[63].

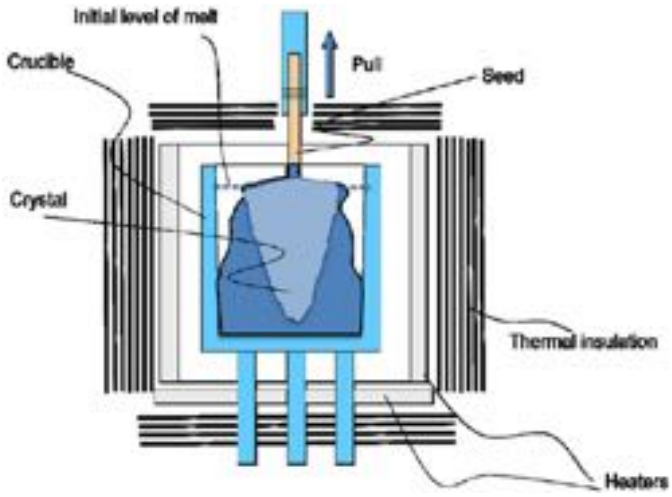

(a) The main features of the Kyropoulos process[61].

(b) Three large single crystal synthetic sapphire blocks made using the Kyropoulos process[62].

Figure 11: Using the Kyropoulos process to create large single synthetic sapphire crystals.

3.2.2.4 Section Stacking

After sections have been collected using the long knife setup, it will be possible to start the section stacking process. This step is included to reduce the number of ATUMs required (see section 3.2.3). Without section stacking, ultrathick sectioning will result in around 8400 20 µm thick sections. However, since the diamond knives used in the ultrathin process can be up to several mm long, it is inefficient to cut only one section at a time. Using the method outlined below, it is possible to stack several sections into one embedded block. This will allow for several sections to be cut on the same ATUM which will reduce the number of ATUMs required by a factor of up to 125.

After sections have been collected using the long sapphire knife they are transfered into the section stacking holder which is shown in figure (12a). The holder consists of an open box with four guides for the sections. Sections are individually placed into the holder and

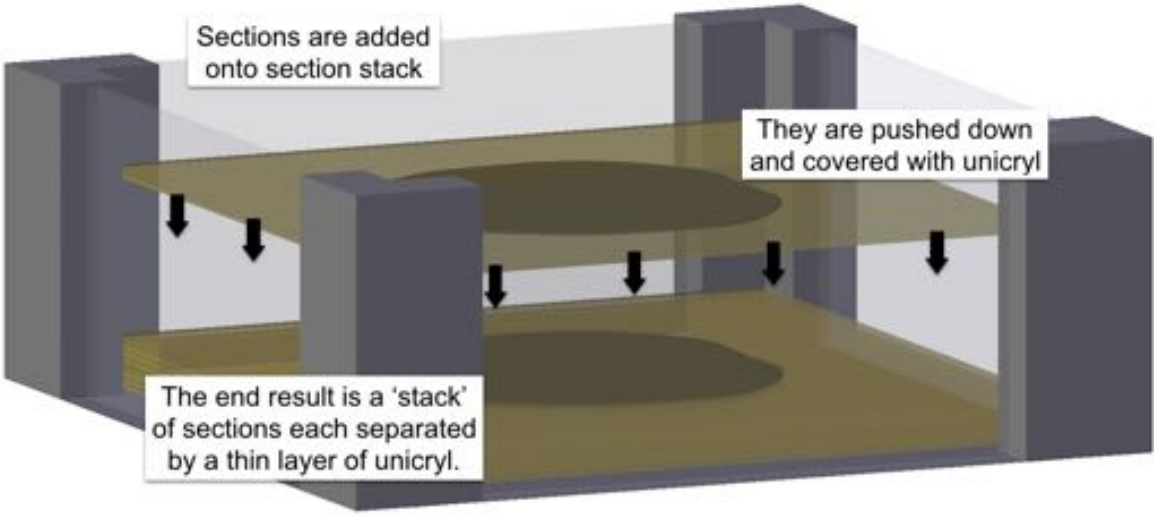

(a)

Figure 12: Apparatus used to carry out the section stacking procedure.

covered with unicryl resin. Additional sections are added to build up a stack of sections each seperated by a small layer of resin. After the stack is around 5 mm tall, the resin is cured and trimmed resulting in a fully embedded block of material containing around 125 slices of brain tissue.

3.2.2.5 Furrows method

An alternative ultrathick sectioning method was proposed by K. J. Hayworth in 2012[64]. Figure (14) shows an outline of the process. The process starts with the same fully fixed, stained and emeded brain as required for the ultrathick sectioning outlined in section 3.2.2.1. The brain is mounted in the apparatus shown in figure (14a) where heated and oil lubricated diamond knives are used to create a series of furrows on the surface of the embedded block at 3 mm intervals(see figure (14b)). Each furrow is just over 20 µm deep. After the furrowing, collection tape is adhered to the material between the furrows and a second diamond knife is used to seperate the strip of material (see figures 14c and 14d). This knife is also heated and oil lubricated. This material is then collected using the adhered tape and stored on reels. This process is repeated until

Figure 13: The redesigned diamond furrowing knife required for the furrows sectioning process.

the brain is sectioned into 250,000 strips of brain 3 mm wide, 20 µm deep and 180 mm long stored on reels of tape.

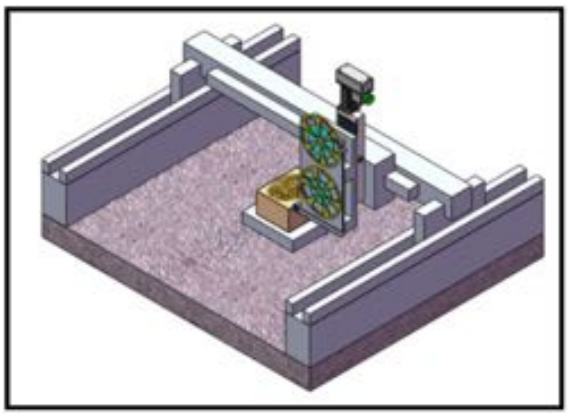

(a) Embedded brain mounted on the Thick-Strip Sectioning and Tape Collection Machine.

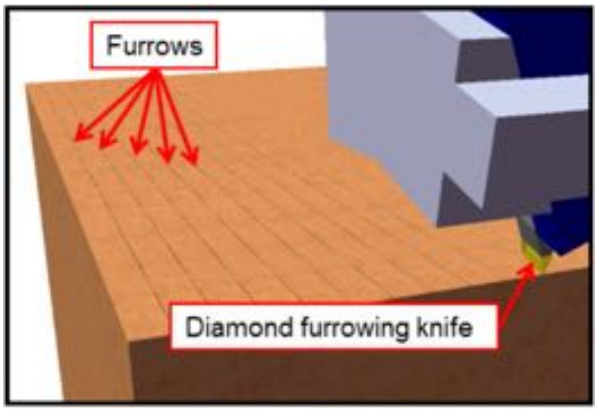

(b) The surface of the embedded block is furrowed using a heated and oil lubricated diamond furrowing knife.

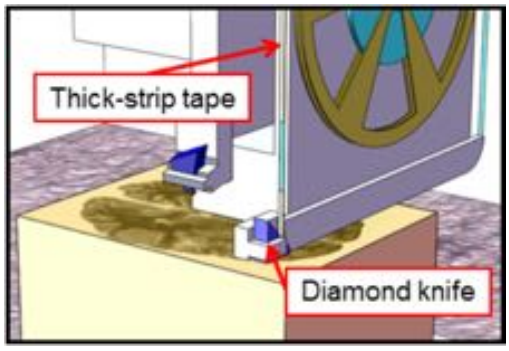

(c) Tape is adhered between the furrows and a diamond collection knife is used to create a thin strip of material.

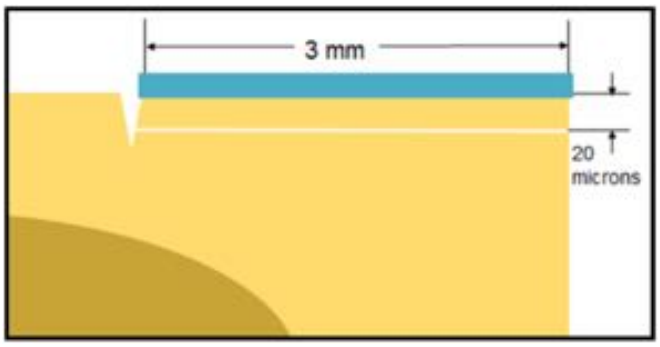

(d) The dimensions of the collected strips of material.

Figure 14: Whole brain ultrathick sectioning process using furrowing knife technique.[64].

It is important to note that the the apparatus described has not been tested. There are several parts which may not work in practice. In particular, the furrowing knife would have to be a re-designed diamond knife. Standard utramicrotomy diamond knives only have an edge on one side. The furrowing knife would have to have to have an edge on the front, bottom and back of the knife (see figure (13)). If these extra edges were not present than the cut surfaces would be damaged as they pass over the back of the knife. The knife would also have to be exceptionally thin in order to not displace too much material. It is unclear if a diamond knife could support such an edge. The edge as described would be extremely susceptible to damage.

The collection knife has less strict requirements, but it must be located precisely as must

be both flush with the surface and not extend past the furrow.

However if furrowing method was developed, the resulting tape strips of tape could be 'stacked' on top of each other and embedded in a process similar to section 3.2.2.4. The embedded blocks would then be well suited to be used with the ultrathin sectioning methods discussed in section 3.2.3. Alternatively, if the depth of the furrows could be increased to 1 mm then it would be possible to start ultrathin sectioning immediately after the furrows method. However due to untested nature as well as the complex knife requirements, we will not rely on the furrowing method as our main ultrathick sectioning technique.

The estimated cost for the development and implementation of the furrows method is around $10 million[64]. If 20 µm furrows are used then the total time for ultrathick sectioing will be around 3 years. However, if it is possible to use 1 mm deep furrows then this time can be reduced to around one month.

3.2.2.6 Sectioning the unembedded brain

As discussed in section 3.1.10, the brain will be fully embedded with unicryl before any sectioning takes place. However it should be noted that embedding such a large volume of tissue for EM has not been attempted and as such there may be unforeseen problems with this approach. If it proves that a method relying on the full embedding of the brain is unfeasible, then the brain must first be sectioned before embedding to enable complete infiltration of resin.

The standard practice[51] to section unembedded brains is to use a long stainless steel knife and simply slice across the brain. This is shown in figure (15b). A typical knife used for this purpose will have a thickness of about 1.5mm. Clearly this will cause large damage to the cut tissue.

Sectioning of unembedded tissue can also be done using a vibratome[67] or a compresstome[68]. Both of these machines can be automated and have the advantage of producing sections of more consistant thickness and quality. However there will still be significant material damage and ultrastructural damage will be unavoidable[46] [69]. In addition, both the vibratome as well as the compresstome have maximum thicknesses that they can section of atound 1mm.

(a) A vibratome being used to take sections of rat brain. Image via Wikimedia Commons[65].

(b) Professor S. Gentleman uses a long stainless steel knife to section an unembedded brain. Image via Welcome Collection[66].

Figure 15: Two different methods used to section unembedded brains.

If unembedded sectioning proves necessary then sectioning using a compresstome would give the best results[68]. 1 mm sections would be taken and embedded. After this sectioning would continue with ultrathin sectioning (see section 3.2.3). However sectioning the unembedded brain is fraught with difficulties and is avoided by the ultra-microscopy community[49]. As such to achieve the goals of the BDCP, unembedded sectioning will be avoided.

3.2.2.7 Costings for the ultrathick sectioning process.

Table 7 details the costs of ultrathick sectioning of a single embedded brain using long sapphire knives and section stacking. The ultrathick sectioning process will take around 140 days sectioning at $0.1\,\mathrm{mm\,s^{-1}}$.

Item	Item Cost ($)	Quantity	Total Cost ($)
Modified Ultramicrotome	300,000	1	300,000
Sapphire knives	4,000	840	3.4 million
Unicryl	$1.26/ml	20 L	25,200
Total Cost ($):			3.7 million

Table 7: Estimated costings for the ultrathick sectioning process in the BDCP.

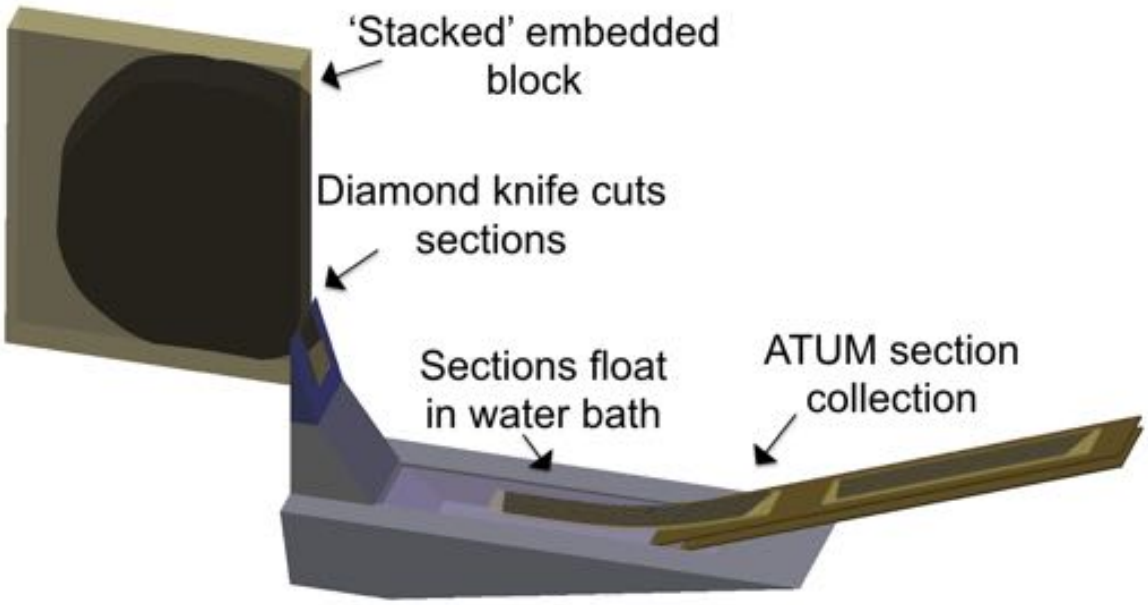

Figure 16

Figure 17: An overview of the ultrathin sectioning process. Embedded tissue blocks are serially sectioned using a modified ATUM.

3.2.3 Ultrathin sectioning

After the ultrathick sectioning process, the embedded brain will have been spilt into around 70 blocks each with dimensions of around $5 \times 160 \times 140$ mm. The next stage will be to reduce these blocks to a point where they can be imaged (see section 3.3). This will mean reducing sections of brain to a thickness of 29 nm. This will be done at a rate equal to the rate of image acquisition (see section 3.3).

3.2.3.1 Overview of ultrathin sectioning process

Figure (16) shows an overview of the ultrathin sectioning process. First an embedded block produced using the section stacking method is mounted onto a modified ATUM (see section 3.2.3.2) for serial sectioning. The ATUM must be modified to allow for the sectioning of larger sections. After sectioning with the ATUM, the sections are stored on reels of kapton tape ready for imaging using the MultiSEM (see section 3.3.2.3). The entire process will take place in parallel on around 70 ATUMs.

3.2.3.2 Automated Tape Collecting Ultra Microtome

In a typical ultramicrotome, after the process described in figure (8a) the thin section is left floating in the trough where it is collected, by pushing it onto a TEM grid using a fine tool, as described in figure (7). This process is challenging to perform consistently without damaging the samples[49]. Clearly for the scale of the BDCP an alternative is required.

The Automated Tape Collecting Ultramicrotome (ATUM)[47] is a recent development which allows for the automation of the section collection process. A labeled picture of the ATUM can be seen in figure (18b). The ATUM consists of a supply wheel which continuously feeds kapton tape through a conveyer belt device. The sample is cut using the standard procedure outlined in figure (8a) and the thin sections produced are collected by the tape as shown in figure (18a). The end result is a reel of tape containing the samples sequentially. This reel can then be stored on wafers or be used for SEM immediately. Note that the ATUM can only be used as an immediate precursor to SEM or wafer storage. This means that after using the ATUM, further sectioning is impossible as the sections are already fixed to tape. As a consequence, the ATUM is not suitable for ultrathick sectioning.

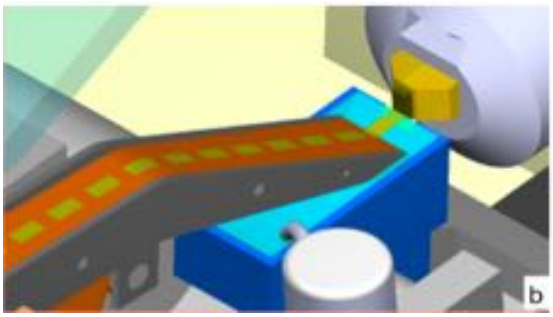

(a) Section collection using the ATUM.

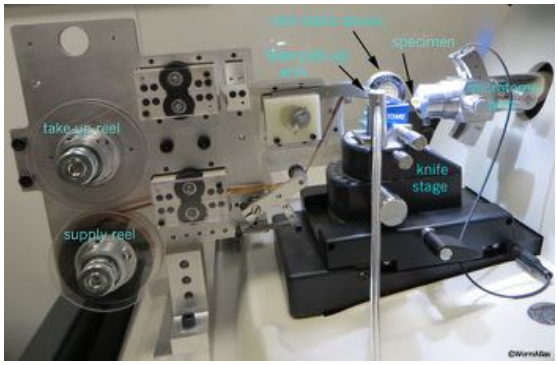

(b) The Automated tape collecting ultramicrotome.

Figure 18: The Automated tape collecting ultramicrotome(ATUM)[47].

3.2.3.3 Costings for ultrathin sectioning

Table 8 shows the main costs for the ultrathin sectioning process. Since this step is almost entirely automated, labour costs are expected to be low. The ultrathin sectioning process will take 10 years. However, since the process is completed in parallel with the imaging process, the impact on the total time required for the BDCP is low.

Item	Item Cost ($)	Quantity	Total Cost (million $)
ATUM	125,000	70	8.75
Ultramicrotomes	100,000	70	7
Diamond knives	3,670	1400	5.14
Total Cost ($):			20.9

Table 8: Estimated costings for the ultrathin sectioning process in the BDCP.

3.2.4 Other Considerations

3.2.4.1 Knives

In modern ultramicrotomy, almost all sectioning is done using diamond knives[48] [49]. Glass knives are often used for the initial trimming but the vast majority of sectioning is done using diamond knives. Sapphire (synthetic corrundum) knives have seen some use in the 1980s but have since fallen out of favour.

A good knife for ultramicrotomy should have a small blade radius, a small blade angle (see section 3.2.4.3) and be resistant to damage. In the following sections, usage of different materials will be explored.

Steel knives The first ultramicrotomes used steel blades to section their samples[48]. However this this early approach proved to have many difficulties[70]. The blades had to be ground to such a sharp angle that they lost much of their structural integrity. On top of this, the blades had to be resharpened after every use. It is also difficult to create an even cutting edge at fine scales due to the uneven grain structure of the steel. The effect of wear on a steel blade can be seen in figure (19)[71], which shows the effect that cutting card stacks has on a steel blade. Note that figure (19a) shows the blade tip radius of the steel edge before cutting to be about 1-3µm.

There is a fundamental limit to how small you can make the blade tip radius on a steel knife. A single crystal of steel is too soft to be useful as a cutting edge. On the other hand, if you use steel with smaller crystals any edge you try to make will not be consistent along its length due to the grain boundaries. For these reasons, using steel knives is not appropriate for sectioning embedded brain samples. The damage to the brain sections will be too great

and ultrastructure detail will be lost.

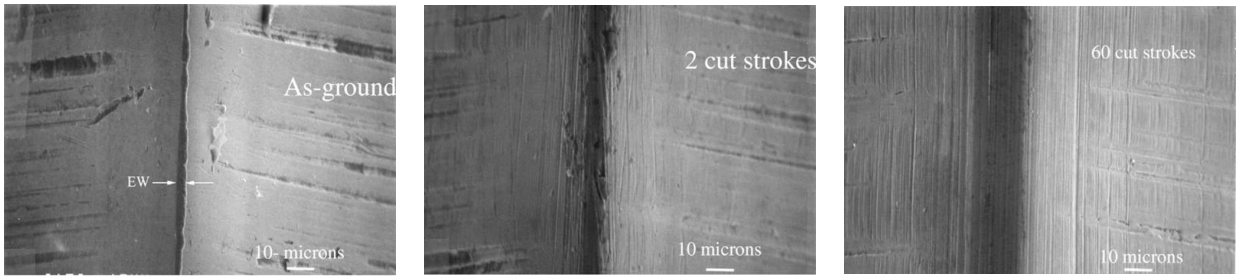

(a) A steel knife immediately after grinding and buffing.

(b) A steel knife after 2 cut strokes.

(c) A steel knife after 60 cut strokes.

Figure 19: Three SEM micrographs of steel knives showing the effect of cutting stacks of card on the blade edge[71].

Glass knives Latta-Hartmann glass knives are a good alternative to steel knives. These knives are created by scoring a square of glass then applying pressure to cause the glass to beak along the score[72]. The knives have been shown to have blade tip radius of around 4nm[73] whilst having a consistent blade edge. This is much sharper than can be achieved with a steel edge.

While the initial blade tip radius is vey small, glass knives lose their edge very quickly[56]. Sections cut using glass knives are also rougher than those cut using diamond knives[74]. figure (20a) shows a section of embedded rat liver cut with a glass knife and shadowed with chromium in the direction indicated on by the arrow. The chromium shadowing is used to reveal surface roughness. When compared with figure (20c), which shows the same tissue but cut with a standard diamond knife, the section cut with the glass knife is significantly rougher.

This increased roughness often leads to loss of ultra structural detail. For this reason, most of the modern ultramicrotomy community no longer use glass knives for sectioning. Glass knives can be improved by coating the cutting edge with tungsten[75]. This both increases the usable life of the glass knife and improves the section quality. However the section quality when using a tungsten coated knife is still inferior to using a diamond knife. Obsidian knives have also seen some use but appear to have similar properties to standard glass knives[76]. Glass knives are still widely used in sample trimming to remove excess resin before sectioning takes place.

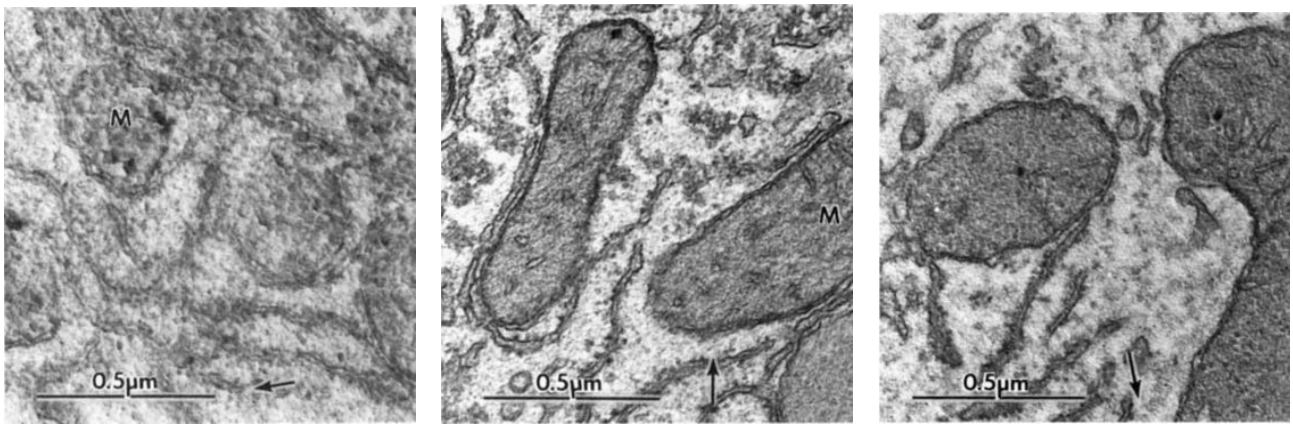

(a) Section as cut with a Glass knife prepared using the balanced break technique[72].

(b) Section as cut with a sapphire knife.

(c) Section as cut with a Diamond knife.

Figure 20: Three 70nm sections of expoxy-embedded rat liver cut using different knives and shadowed with chromium[74].

Diamond knives Diamond knives are by far the most popular knives used for sectioning in ultramicrotomy. Like glass knives, diamond knives have a small blade radius of about 4nm but with the added benefit of being exceptionally durable[73] [77]. Diamond is exceptionally hard being the hardest naturally occurring substance found on earth with a hardness of 10 on the Mohs scale.

Sections taken using good quality diamond knives are free from cutting artifacts and can be exceptionally thin. A single diamond knife typically lasts around six months of continuous use before it has to be resharpened.

3.2.4.2 Sapphire knives

The final blade material that will be considered is synthetic corundum (synthetic sapphire). Sapphire is a variety of the mineral corundum (Al_2O_3). It has a hardness of 9 on the Mohs scale which is only slightly less hard than diamond. It can also support an extremely fine edge. This makes it a good choice for making knives for ultramicrotomy. Note that 'sapphire' is generally used to refer to all varieties of corundum by the ultramicrotomy community. Sapphire has seen some use by the ultramicrotomy community in the 1980s but has since been largely replaced by the diamond knife[49].

The quality of sections cut using synthetic corundum knives has been shown to be similar to sections cut with diamond knives[74] [56] but diamond knives have proven to be much more

durable. Figure (20b) shows that sapphire knives can have similar section quality to diamond knives. However since use of sapphire knives has fallen out of use, there has been a lack of research into the characteristics of these knives. Since these sapphire knives have the potential to be much longer than diamond knives, a thorough investigation into whether sapphire knives are suitable for the BDCP process is recommended.

3.2.4.3 Cutting mechanism

For the case of brain tissue, the choice of embedding agent will dominate the cutting mechanism. The exact cutting mechanism will likely be dominated by either shear sectioning (figure (21a)) or crack sectioning (figure (21b)). However, due to the small scale and the awkward mounting requirements for SEM, the exact cutting mechanism is not known[49].

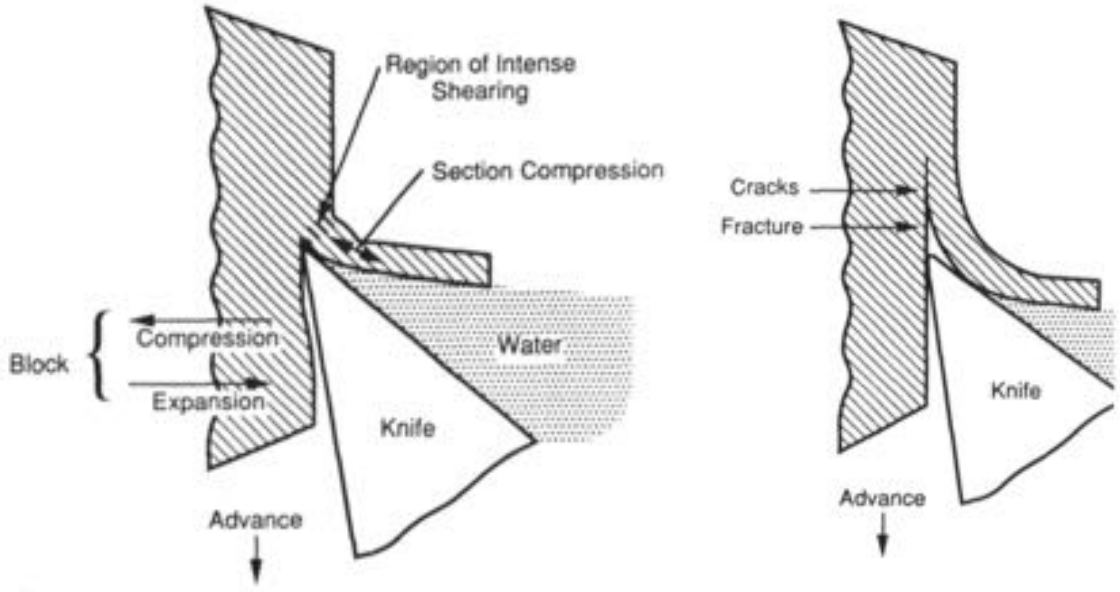

(a) Shear sectioning mechanism.

(b) Fracture mechanism.

Figure 21: Schematic diagrams showing the two main sectioning mechanisms present in ultramicrotomy[49].

3.2.4.4 Compression

One of the major artifacts present after performing ultramicrotomy are compression artifacts. In early ultra-microscopy, it was noted that there was a compression in sections of after being cut in a direction parallel to that of the cutting direction[78]. This was due to the wrinkling or fine scale folding of the section as was forced over the knife. This compression is especially

undesirable for the BDCP as it is advantageous for there to be zero compression to make the volume stitching simpler (see section 3.3).

It has been shown that reducing the blade angle helps to reduce compression[79]. While using a knife with a small blade angle will help to reduce compression, the low blade angle significantly shortens the useful life of the blade. This has limited development of small blade angle knives. The standard "low blade angle" used in ultra-microtomy is 35°, however commercially available 25° knives used for cryo-microtomy are available. We suggest that for the BDCP 35° knives are tested and used provided they are satisfactory.

It has also been shown that compression is reduced when heating the sample either during[46] or immediately after cutting[78]. The heating softens the resin and allows it to expand back to its original dimensions. Note that the heating must be done before the sample is fixed onto a SEM grid. After the sample has been loaded onto a SEM grid it is fixed in place and cannot expand. The heating is performed whilst the samples are floating in the water bath (item T in figure (8a)) immediately after cutting[78]. In some studies, sections were heated for up to an hour before being fixed onto the SEM grid. It would be challenging to implement such a system with the ATUM as it would necessitate many slices to be floating in the water bath without interacting with each other.

An alternative to this is to heat the knife itself[46]. In addition, using a knife mounted on a low voltage piezoelectric translator to cause the knife to oscillate has been shown to reduce compression[80].

3.2.4.5 Chatter

Figure (22) shows an EM image of epon-embedded submucosa tissue cut with a standard microtome. Notice that there are vertical bands across the length of the image. These are caused by vibrations from a source outside the ultramicrotome. The effects of chatter can be reduced by performing utltramicrotomy in a low vibration environment such as on vibration-damping ultramicrotome table[81]. Use of an oscillating ultramicrotome can also help to reduce the effects of chatter.

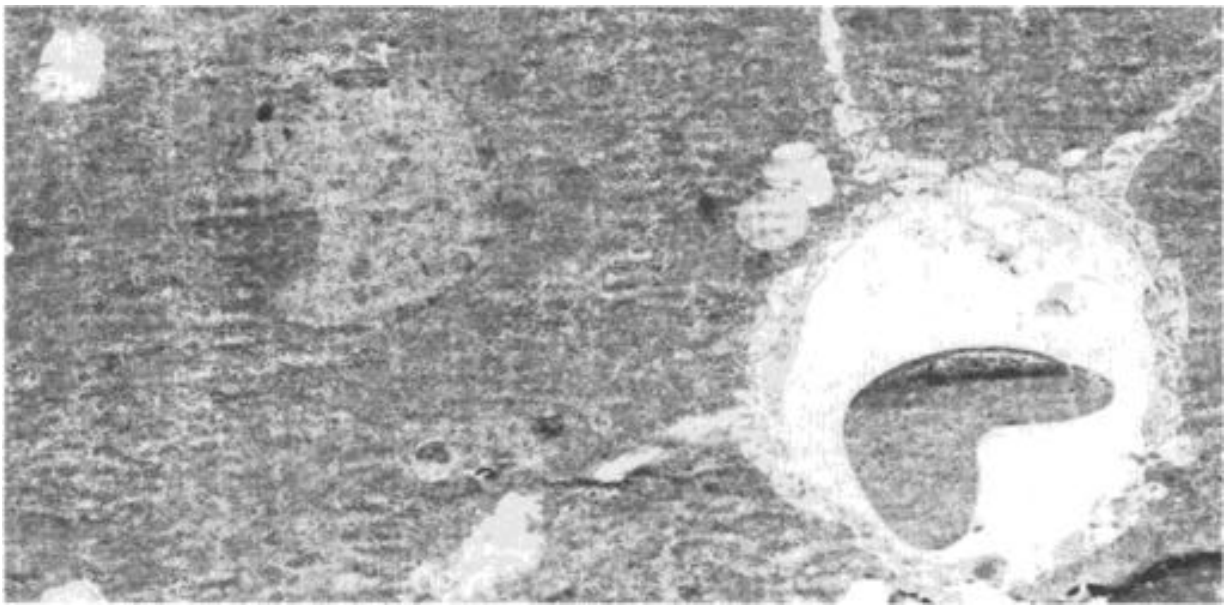

Figure 22: An EM image of submucosa tissue demonstrating effect of chatter[81].

3.2.4.6 Streaking

Another cutting artifact often seen in ultramicrotomy is streaking. This is caused by defects in the blade edge and causes bands to form in a direction parallel to that of the cutting direction. The appearance is similar to that of chatter.

The effects of streaking can be reduced by ensuring that knives are kept in good condition. Use of an oscillating microtome will cause a damaged blade to produce streaking with very wide bands and should be avoided at all costs.

3.2.4.7 Hot-knife protocol

In order to reduce sectioning artifacts, the BDCP will elect to use the 'hot-knife' protocol developed by K. J. Hayworth in 2015[46]. Knives used for sectioning the brain will be heated to around 70 °C and lubricated with low viscosity cutting oil. In addition a piezoelectric translator will provide ultrasonic oscillations for the knife. These conditions should help to improve section quality.

3.2.4.8 Sectioning for alternative microscopy techniques

Much of the sectioning discussion so far has been concerned with sectioning for standard SEM. This section will consider the sectioning requirements for other techniques. Specifi-

cally, sectioning for focused ion beam scanning electron microscopy (FIB-SEM), serial block-facing scanning electron microscopy (SBF-SEM) and transmission electron microscopy (TEM) will be considered.

Sectioning for Transmission Electron Microscopy (TEM) As discussed in section 3.3.2.1, TEM works by passing a high-energy electron beam through a thin sample. Unfortunately this means that it is not possible to use the ATUM with TEM. Instead samples will have to be sectioned using a standard ultramicrotome. The samples will be individually loaded onto TEM grids (see figure (7)) manually. This is problematic for the BDCP as around 2.6×10^{10} sections will need to be collected. It would be prohibitively expensive to hire enough staff to deal with this enormous quantity of sections. In addition, section collection can be difficult for even practiced technicians[49] and even a small error rate would result in the loss of an large number of sections.

Sectioning for Serial Block Facing Scanning Electron Microscopy (SBF-SEM) A SBF-SEM[82] works by repeatedly scraping away the top of a block of embedded material using a diamond knife. After a slice of the material has been has removed a SEM is used to image the revealed surface. The process is repeated to build up a serial set of images. Figure (23) shows the SBF-SEM process. The SBF-SEM has been commercialised as the Gatan 3-view[83] and has seen wide use in the ultramicrotomy community.

Using the SBF-SEM, it is possible to remove 50 nm sections at a time. Charging effects from the SEM prevent thinner sections from being taken. As discussed in section 3.3, for the BDCP we need sections of at most 30 nm to resolve the finest neuronal detail. This means that without further improvement SBF-SEM will not be useful for the BDCP.

Sectioning for Focused Ion Beam Scanning Electron Microscopy FIB-SEM uses a focused ion beam to repeatedly mill away layers of material and uses a SEM to image the revealed surface[85]. Gallium ions are preferred for use in the FIB as Gallium has a low melting point, low vapour pressure and low volatility all of which promote the emission of ions[86]. A diagram showing the outline of the FIB-SEM procedure is shown in figure (24).

FIB-SEM has very specific requirements as to the size of the milled surface[46] [64]. The surface should not be longer than around 20 µm in the direction parallel to the FIB to avoid

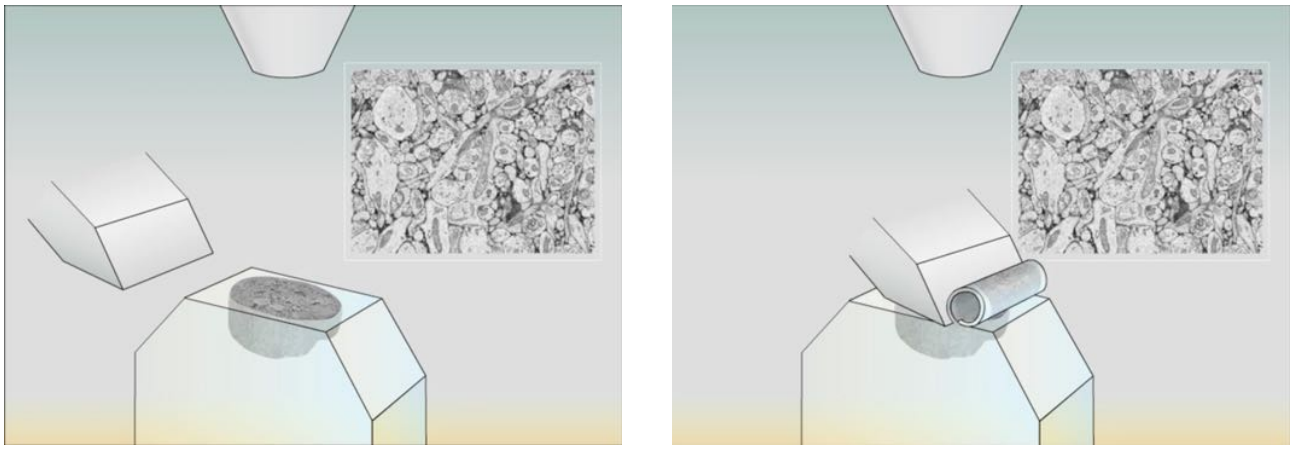

(a) The SEM images the surface of the tissue block.

(b) A diamond knife is then used to scrape of the top layer to reveal a new surface for the SEM to image.

Figure 23: Procedure for SBF-SEM sectioning and imaging a volume of tissue[83].

ion polishing artifacts. However the sections collected during the ultrathick sectioning procedure are around 20 µm thick already. Using FIB-SEM would eleminate the need for ultrathin sectioning as sections could be loaded into the FIB-SEM immediately after performing ultrathick sectioning.

However FIB-SEM has a major drawback when when compared with standard SEM. FIB-SEM is an inherently slow process. FIB-SEM machines are also relatively expensive when compared with other EM machines. It would take one FIB-SEM around 140 million years to scan the entire human brain. To buy enough FIB-SEM machines to scan the entire volume of the human brain in 10 years, it would cost around $30 trillion. This makes FIB-SEM prohibitively expensive for the BDCP.

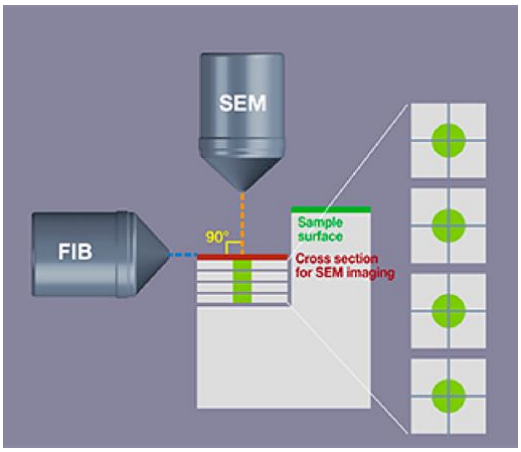

Figure 24: An outline of the FIB-SEM procedure[84].

3.2.5 Summary of the sectioning procedure

Sectioning for the BDCP consists of two stages: ultrathick sectioning and ultrathin sectioning. Whilst the ultrathin sectioning procedure builds on well tested technologies such as the ATUM, the ultrathick sectioning procedure relies on the development of new technologies. Single crystal sapphire knives that are longer than a few mm have never been build before.

However the recent developments in the Kyropoulos technique by Monocrystal Inc. should allow for the development of the long sapphire knife and could even enable the ultramicrotomy community to have a competitive alternative to the expensive diamond knives currently in use.

3.3 Imaging

THEO COSTAIN

Given the brain is such an incredibly complex organ it is hard to tell what information is needed to accurately reproduce it. Here, we take the stance, as others have as well[1], that human behaviour is determined by the complete graph of the connectome, *i.e.* the interconnections between neurons.

It is believed that there are several aspects of neuronal structure that are important[87]. However the main set appears to be: synaptic connections, synaptic strength, and connection type (*i.e.* excitatory or inhibitory). The difficulty lies in the size of these features. The smallest axonal and dendritic processes can shrink as small as $\approx 40\text{nm}$[88], and membranes under ROTO (a staining protocol similar to BROPA (**??**)) are $6\text{-}8\text{nm}$[1]. This second smaller dimension requires a spatial resolution of $3\text{-}4\text{nm}$ to meet the Nyquist sampling criteria, for accurate imaging. As we are primarily concerned with membranes and synapses, which lie on membranes, we *have* to be able to accurately resolve membranes.

Figure 25: A Zeiss MultiSEM

As a result, we aim to take images at an xy resolution no greater than 4nm and to image a whole brain in no more than 10 years. To this end we examined several technologies, both light based, and electron based, and found a clear answer, in the form of a particular model of electron microscope, specifically, the Zeiss MultiSEM. It has an xy resolution of 3nm, sufficient for our needs. Further it is extremely

fast, being able to image 1cm^2 in less than three hours, making it the fastest of the options considered, that meet our resolution requirements, whilst also providing cost efficiencies, compared to multiple SEM machines (the precursor technology). To meet our ten year goal we would need 16,500 machines with a maximum retail cost of $100Bn. It is hoped that bulk purchases, or IP acquisition, would significantly reduce this cost.

In this section, we aim to cover some of the differing approaches to imaging that are available, covering their benefits, and drawbacks, and showing how we came to our decision.

3.3.1 Light Based Methods

Visible light has wavelength roughly in the range $390\,\text{nm} - 700\,\text{nm}$. Simple calculations regarding Nyquist criteria shows that the maximum resolution theoretically possible is $\approx 780\text{nm}$. This is nowhere near our goal of 3nm. This is not able to resolve the smallest axons or dendrites. There are several methods that attempt to overcome this problem, either by reducing the wavelength of the light so that it is able to resolve the tissues at sufficient resolution, or by altering the sample such that visible light methods are able to examine the salient features more easily.

3.3.1.1 f-MRI

Functional magnetic resonance imaging is mentioned here, because of its heavy use in the study of the human brian, despite the many shortcomings it possesses with regard to our aims. It works by gaining contrast from the paramagnetism of deoxyheamoglobin. As a result, where the brain is working (stimulated) more than in other areas, contrast occurs due increased uptake of oxygen by the cells.

However the resolution of this technique is incredibly poor. At it can only be used to trace the largest of the axons present in the brain, as the resolution is in the range $3\,\text{mm} - 4\,\text{mm}$[89]. As a result developing a neural map from this is not possible, as the resolution is not sufficient to even trace most of the smaller neuronal processes.

3.3.1.2 Expansion Microscopy

Expansion microscopy[90][91][92] allows the resolution of ordinary light microscopy to be increased 40 times. Expanding fluorescent gels are attached to RNA in the cells and then amplified using HCR[93].

HCR[93] is similar to PCR, an extremely common DNA amplification technique, however unlike PCR it gives linear growth and not exponential. In short it works by supplying DNA 'hairpins' that cause a chain reaction. However the reaction can only continue so long as there is a supply of hairpins. Once the amplification has occurred the sample can then be expanded, using a swellable polyelectrolyte gel to increase the size of the sample up to 20x[94] . By targeting RNA specific regions of interest within the cell can be targeted and studied easily. For example using anti-Homer1 (red) and anti-Basson (blue)[90] we can easily identify synapses in the tissue (see Figure(26c)).

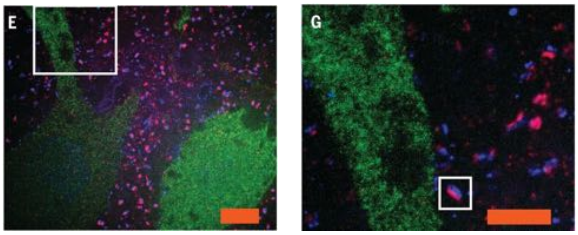

(a) An image taken after expansion

(b) Zoomed in version of (a)

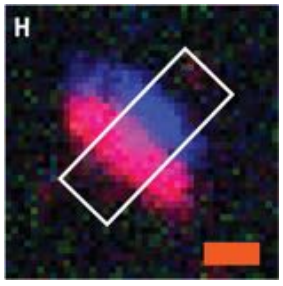

(c) An individual synapse shown in (a) and (b). Note the lack of visible membrane boundary

Figure 26: Florescence image of mouse brain

However, this process has several downsides that make it unsuitable for our purposes. The main problem is a previously mentioned problem regarding the number of samples that would need to be imaged; The human brain is roughly 1400cm at 20x linear expansion this becomes around 28 litres (roughly an eighth of an oil barrel). In order to perform sectioning on this brain in a reasonable time, we would need to section it before expansion. However, we need to embed the brain first, in order to achieve the required quality of cut, but once embedded we can no longer use the expansion protocol. As well, it is noted by others[95] that the process does not reveal all of the neurons within a volume.

Hence whilst potentially useful in fields studying specific areas of the brain or individual cells, this method of imaging the brain does not scale up to the volumes of tissue that we

are concerned with and so is not useful to us.

3.3.1.3 Brainbow

Similar to expansion microscopy, Brainbow[96] makes it much easier to trace neuronal circuits in dense neuropil. By labelling individuals cells with different combinations of colours, a large number of hues can be expressed that allow for individual cells and their processes to be identified from the surrounding neuropil. The colours are expressed by the insertion of different combinations of spectrally distinct fluorescent proteins (XFPs) into the cells. These XFPs combine in different quantities to form a variety of colours (> 100, ≈ 160 in Figure(27a)[96]). A simple example is shown in Figure(27b) of how 10 colours can be made by combining three different coloured XFPs

The XFPs are delivered into the cells using transgenics, and hence our problem. The process requires that the genes coding for the fluorescent proteins are present in the cells from birth, which whilst possible and ethical in mice, is not possible or ethical for human subjects. As well, is not possible to determine the relative strengths of neurons as the colouring is not a staining die, *i.e.* ultrastructural details such as vesicles and post synaptic densities are not highlighted in the process.

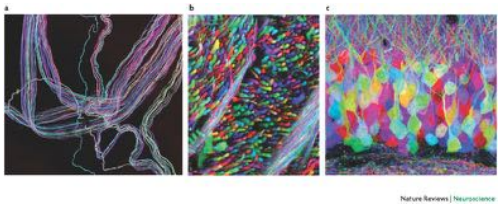

(a) Brainbow images[96]

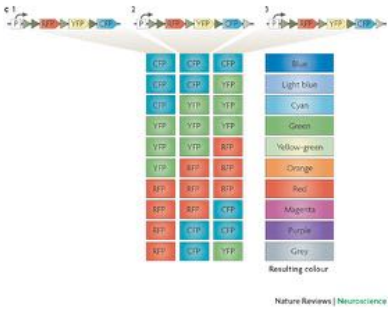

(b) The colors that can result from mixing three different XFPs[96]

This process is very useful for studying and developing models of the connectome. However it is not very helpful to us. Firstly we cannot use it on patients due to the transgenic requirements, although, in the future, it may be possible to introduce the transgenes later in life using a virus[97]. But also we are not able to gain some of the information that we desire, such as synaptic density or other ultrastructural details such as vesicle density.

3.3.1.4 μCT

The last of the light based methods considered is μCT, which is functionally identical to CT scans done in hospitals. The key difference is the energy of the X-rays used in the imaging. Conventional CT uses relatively low energy photons, so as to limit the radiation exposure of the patient. As μCT is typically not used on live samples, the permitted dose can be much much higher. It is worth noting, that in our case, the use of resin to embed the sample significantly increases the resistance of the sample to radiative damage. The higher energies of the photons allows for greater penetration of samples and thus shorter exposure times are needed to capture the images. Using a synchrotron source allowed a 1mm^3 volume to be imaged in 6 minutes, compared to 13 hours using a 'benchtop' X-ray source[95].

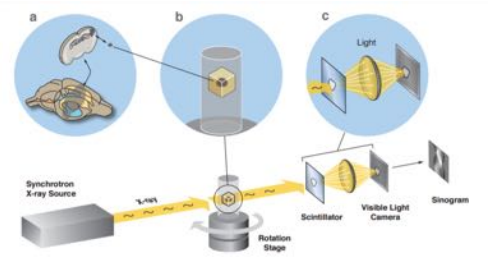

Figure 28: Diagram showing use of μCT on a sample of mouse brain[95].

The process works by firing X-rays at a sample, stained with heavy elements like osmium, on a rotating stage. The photos pass through the stage and onto a scintillating plate, then through a lens and onto a CCD (Figure(28)). The resulting image is called a 'sinogram', and can be thought of as a frequency representation of the object. To obtain the image, an inverse Radon transformation is needed to compute the image. As a result a 3D model with isotropic voxels is generated.

The current achieveable resolution of the technology is $\approx 1\text{mm}^3$, low compared to electron based methods that will be considered next. However the limitation on the resolution is not the technique itself, but instead the solution of the inverse Radon transformation. As such it is possible that the achievable resolution of μCT will increase over time, to the necessary resolutions to compete with SEM (3.3.2.2). If the resolution were to increase, this technology would become the clear winner in the decision over which imaging technology to use, from those shown in 3.3.3 as, assuming the imaging time is linear with volume, it would take less than 100 years to image the whole brain with only one machine (assuming only one detector per synchrotron, which may be extremely conservative). Which, despite the high cost of the synchrotron, is much smaller than the costs associated with other machines.

3.3.2 Electron Based Methods

To improve on the resolution of the light based methods, we turn to electron microscopy. Invented in 1931, electron microscopy, and its two main variants, currently, have much higher resolving power than any of the light based methods shown above. The two differing approaches center on the relative orientations of the electron source and the detector, *i.e.* different or the same side of the sample. Both methods require the sample to be in vacuum, which due to the fragility of biological matter, requires samples to be properly embedded in a hard resin to prevent damage. Further, the samples need to be coated in a conductive material to minimise the build up of charge on the surface of the sample, due to the injection of relatively large numbers of electrons onto the sample surfaces.

3.3.2.1 TEM - Transmission Electron Microscopy

Transmission electron microscopy (TEM), is the first of the two approaches that we will consider. In TEM, electrons are fired at ultra-thin samples. Electrons that don't encounter heavy elements from the staining pass through the sample. Those electrons that pass through the sample are then magnified using magnetic lenses onto an imaging device. Traditionally, this was some kind of chemical plate, but later this was replaced with CCDs.

It is possible to get 50pm resolution from TEMs (sufficient to resolve atoms in a crystal lattice). In this regard the TEM vastly exceeds our resolution requirements.

The issue with TEMs for our purposes are the ultrathin sample requirements. The kapton tape used by ATUM (3.2.3.2) is too thick to allow for the proper transmission of electrons, as a result, the samples would have to be prepared manually, an incredibly expensive and slow process. For smaller experiments this is typically not a problem, but given the number of images we plan to take this is not acceptable.

3.3.2.2 SEM - Scanning Electron Microscopy

Unlike TEM, SEM, does not have the same sample requirements. This is because SEM relies on the scattering of electrons upon collision with the heavy elements. The electrons that are scattered backwards from the sample are detected, and the intensity of the detected electrons is converted to a pixel value. Unlike TEM where each pixel is recorded at the same

time, in SEM each pixel of the image is recorded sequentially, a process called rastering. Obviously this makes the SEM slower than the TEM to take an image of a particular size.

The benefit of the SEM however is that the image is taken from the face of the sample. Hence not only is this imaging compatible with ATUM, as the electrons don't have to pass through the kapton tape, but also with a several other sectioning methods.

The resolution of SEM is of the order $0.5\,\text{nm} - 5\,\text{nm}$, depending on the model of the machine, which just meets our requirements on resolution on higher end models.

Unfortunately the imaging time of SEMs is governed by several factors including: beam current, detector sensitivity, and sample properties determined by the stains used. Because biological samples require lower beam currents, so as not to damage the samples during imaging, there are limits on the required 'dwell time' (the time spent imaging each pixel in the image) imposed by the quality of the detector in the machine. For some of the more common models of SEM, the dwell time is around 100ns to achieve the desired resolution. Given voxel dimensions of $4 \times 4 \times 29\text{nm}$ the time taken on a single SEM machine to image the whole human brain is $\approx 83.8 \cdot 10^9\,\text{h}$ or around 9 million years. As well as the imaging time it is worth noting that as the samples have to be in vacuum, extra time is added to the process when the chamber has to be cycled to insert new samples, although some of the SEMs are sold with optional attachments, that allow the samples to be changed using an airlock, that reduces the time needed to change samples down to $\approx 45\text{s}$[98].

3.3.2.3 MultiSEM

Recently Zeiss, a German instrument manufacturer, started manufacturing the MultiSEM. The MultiSEM[99] is a novel type of SEM employing multiple beams and detectors, in the same device, to drastically speed up the imaging of large samples. The beams work in parallel to image different areas of the sample at the same time, so whilst the individual beam/sensor pair is not significantly faster than others, the overall imaging time for a sample is drastically lowered.

There are two models available, the 505 (61 beams) and the 506 (91 beams), with the cheaper of the two (505) costing $4-6 million (Priv. Comm. Zeiss customer service) depending on the add-ons, *e.g.* airlock to speed up sample change times. The models have a few

important differences, the most important for our purposes, is that the 505 has a minimum resolution of 3.5nm whereas the 506 has minimum resolution of 8nm. For our purposes this places the faster 506 outside of our minimum resolution requirements, however the 505 does just meet our requirements.

The imaging speed is blindingly fast, imaging 1cm^2 at 4nm resolution in under 3 hours. Given a human brain size of 1400cm^3 this would mean one machine could image the human brain in $165,000$ years, a significant improvement on ordinary SEM devices. However the documentation[100] states that the machines require a maximum of 1hr per day for beam alignment and calibration so a more realistic estimate of imaging time is close to $172,000$ years.

3.3.3 Comparison and Costs

A Multi criteria analysis of the different options is shown in Table 9. Where the technology does not meet our resolution requirements, a score of $-\infty$ is awarded, to represent an infeasibility of the technology for our purposes. The resolution scores were given as a metric of how much the technology surpasses the minimum requirement. The weight of this category was chosen to reflect the relative importance of this criteria.

Time scores were ranked in accordance with whole brain imaging time, in a roughly logarithmic sense, *i.e.* a score of 5, implies it is 10 times faster than a score of 4. This category's weight was lower, to reflect the relative flexibility possible within our design. Due to the inability to process the TEM samples using ATUM, it is given a very low time score. The results show that as expected the MultiSEM is the best of the available choices.

The costs were scored, as the expected whole brain in ten years or less. It is again worth noting, that μCT may in the future be able to achieve the necessary resolution for the task. At which point it would become a clear winner, as the most expensive part required, is a synchrotron, costing $\$467.2$ million[101] in 1996 ($\$740$ million today). This is much cheaper than the cost of MultiSEMs needed to meet the same time frame.

It is worth noting, that even at the more expensive end of its price cost, the MultiSEM ($6 million), is much less than 61 times more expensive than ordinary SEM machines ($200,000-$500,000 [price range found from variety of sites selling second hand SEM machines with

resolutions sufficient for our purposes]). Making it much more cost efficient when compared to SEM machines.

Table 9: MCA of Imaging Technologies

Type	Time		Cost		Resolution		Total Score
	Weight	Score	Weight	Score	Weight	Score	
fMRI	3	5	2	4	5	$-\infty$	$-\infty$
Expansion Microscopy	3	2	2	5	5	$-\infty$	$-\infty$
Brainbow	3	2	2	5	5	$-\infty$	$-\infty$
μCT	3	4	2	4	5	$-\infty$	$-\infty$
TEM	3	-2	2	2	5	5	23
SEM	3	1	2	2	5	4	27
MultiSEM	3	3	2	3	5	3	30

The result of this analysis is the choice of MultiSEM as our imaging technology. Given that as stated in 3.3.2.3, the time taken to image a brain with one machine is around 165,000 years, to completely image a brain in 10 years we would need to purchase 16,500 machines. This, assuming that some of the accessories are needed, would cost approximately $99 billion, although it may be reasonable to assume that a bulk discount would be offered, reducing the total cost considerably.

Also as stated in Eberle and Schalek's paper[102], we would need to spend some money, likely covered by the bulk discount, to improve the speed of the machines so that we can approach the $100\text{TB}\,\text{d}^{-1}$ maximum.

The power costs here have been neglected as we will have to build a power station for the data centre regardless, and the associated costs of that are covered in that section.

The company that manufactures the MultuSEM, Zeiss, is wholly owned by 'Carl-Zeiss-Stiftung' (Carl Zeiss Foundation). As a result it is not possible to purchase the company outright. However the IP covering the MultiSEM may possibly be purchased from the company for significantly less than the bulk purchase allowing the machines to be made at cost, potentially vastly reducing the total cost of the microscopes.

3.3.3.1 Facility

The MuliSEM consists of three main parts: The microscope itself, the PSU rack, and the IA rack. The recommended space needed from the documentation is $4.6\text{m} \times 4.2\text{m}$. This gives a total land area for all of the machines of 31.8ha or nearly 32 rugby pitches.

When designing the imaging facility, several factors must be taken into account. Given the length of time required to image even a small number of brains, it is extremely important that the facility is viable over the long term, *i.e.* low risk of natural disasters such as floods and earthquakes, or long term political stability. Further, electron microscopes are extremely sensitive to a variety of factors including electro magnetic interference (EMI), vibrations, and temperature[103]. To this end we seek to find regions significantly inland, no less than 20km (twice the inland distance of the 2011 tsunami in Japan[104]), with minimal earthquake risk, in a geopolitically stable region, far from large forests prone to fires, and maximally distant from any sources of EMI. We would also seek to limit exposure to governmental interference from state agents, *i.e.* dictatorial regimes or oppressive governments.

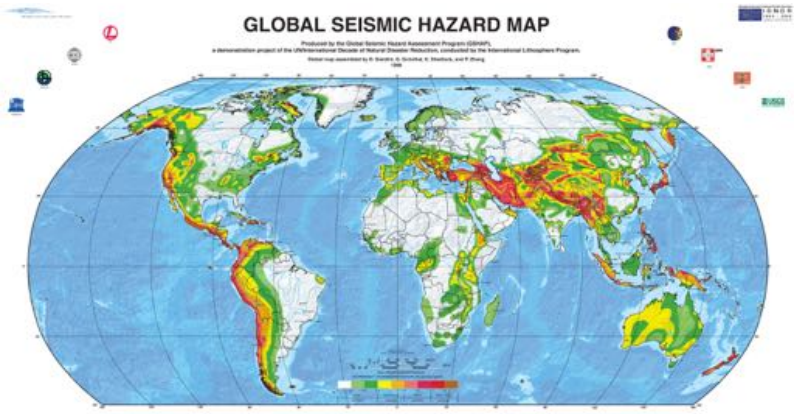

Figure 29: Global Seismic Hazard Assessment Program - Global Map

Looking at Figure 29, we can see that the areas of interest to mitigate seismic hazards are: much of Africa, Siberia, south west China, the Arabian Peninsula, Brazil, central North America, and Greenland. Political stability rules out Africa and the Arabian Peninsula. Greenland may not be geologically stable due to climate change, so it is excluded from consideration. State interference concerns rule out China. That leaves Brazil, Siberia, and North America.

Land in Brazil would likely require large amounts of deforestation, and the poor infrastructure would make construction and maintenance difficult. Further the temperature and humidity would necessitate the use of expensive HVAC systems.

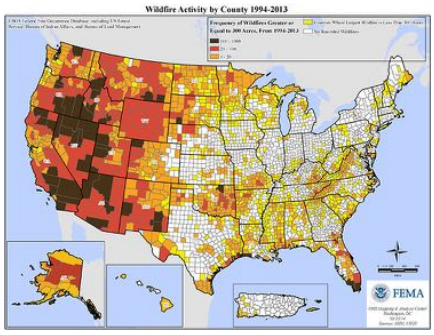

(a) Forest Fires In U.S.[105]

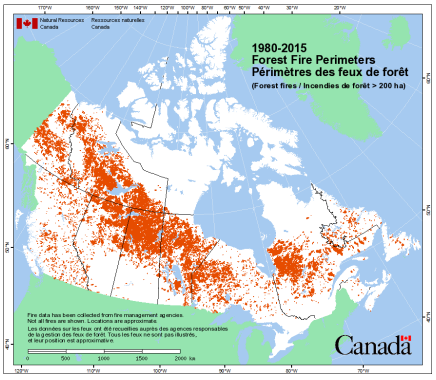

(b) Forest Fires in Canada[106]

Figure 30: Forest Fire Risk in North America

Siberia may present a better option as the trans-Siberian Railway would make delivery of goods and materials relatively easy, if the site is built near enough to the tracks. However again the extreme temperatures would require the need for expensive HVAC systems to maintain reasonable temperatures, although this could be mitigated through heavy insulation of the facility. Further given the land has little other use the land may be sold for a very low price. However, it may be hard to recruit the skilled technicians needed to operate that machines. So we find that this option may be possible but may prove very difficult.

North America provides ample space. Ideal locations would include north east Montana, North Dakota, Minnesota, Iowa, Wisconsin, Texas and, Michigan (Although we would avoid Texas due to high temperatures) in the U.S. And in Canada, much of Alberta, Saskatchewan, Manitoba, and Ontario would be acceptable. Here, the infrastructure would be more than capable, as well as the availability of a highly skilled workforce. Looking at locations of past forest fires in North America (Figure 30), shows southern Saskatchewan and Alberta as well as Wisconsin and Michigan as low risk.

Using land price data, we find that the cheapest land is in Saskatchewan, with land priced at $\$870\text{acre}^{-1}$[108]. However it may be necessary to locate the facility nearer to a larger population centre in order to have access to the nec-

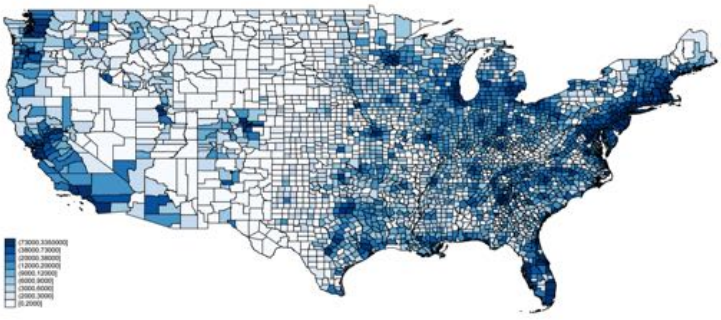

Figure 31: US Land Values, Dollars per Acre[107]

essary skilled labour, as such we may seek to purchase land in Alberta ($\$1,712$acre^{-1}[108]) or in Wisconsin ($\$3,000 - 12000$acre^{-1}[107]) near to Minneapolis. The cost to purchase the land is likely to be more than double the value of the land, due to the amount of contiguous land we seek to purchase. As a result we increase the cost of the land 3x, to account for likely increased costs of acquisition. Despite the increased costs of land, given that the land cost is a one time purchase, locating the facility nearer to a large population centre (Minneapolis), should reduce the long term running costs of the facility, given it should be easier to persuade the specialist labourers needed to live in a relatively large city like Minneapolis over Edmonton, Calgary, or rural Saskatchewan. Thus we hope to locate the facility in north west Wisconsin. Further, the reasonable climate will limit HVAC costs compared to Saskatchewan or Alberta, where temperatures can drop as low as $-45°$C[2]

Table 10: Differing Land Purchase Total Costs

Location	Cost
Saskatchewan	$205,170
Alberta	$404,200
Wisconsin	$2.8 mil

The cost of a basic warehouse is around $\$100 - 200/\text{m}^2$. However we require the microscopes to be vibration isolated[103]. Hence they need to rest on free standing concrete slabs, and be separated from the pumps and power supplies, by some acoustic isolation. This likely increases the cost of construction by several orders of magnitude. To estimate these costs, we sate the these specialised facilities will be 10x more expensive than ordinary conventional warehousing. Thus for the required 32ha, the cost would be, at $\$200/\text{m}^2$, $\$638$ million. Also needed, but not included directly are the HVAC, power, fire suppression, and transport infrastructure needed.

Hence the Expected start up costs for the imaging alone, at the worst case, are $\$99$Bn $+$ $\$638$M $+$ $\$2.8$M $+$ misc. unforseen ≈ 100Bn. The majority of the cost clearly comes from the MultiSEMs, which most likely will cost less than the stated amount due to bulk discounts. On top of this, there will be some cost associated with the operating of the facility, however, again this cost is trivial compared to the cost of the microscopes.

[2] http://climate.weather.gc.ca/climate_normals/results_1981_2010_e.html?stnID=2205&lang=e&dCode=1&province=ALTA&provBut=Go&month1=0&month2=12

3.3.4 Summary

The total estimated costs are shown in Table 11. Despite the wide array of neuroscience and connectomics research happening today, there are still few technologies capable of recording significant volumes of tissue in reasonable time frames. Above, we've suggested the path that, we currently feel is best. MultiSEM meets our resolution requirement and is compatible with our chosen sectioning method, unlike TEM. It provides cost and time savings, when compared to ordinary SEM devices.

Due to the long term nature of our imaging process, we were limited in choosing locations of the facility to minimise the long term risk associated with the large infrastructure and equipment investment. Wisconsin provides us with good seismic and fire safety, as well as geopolitical stability and a reasonable climate (average temp: 7.9°C[3]).

Table 11: Total Costs for Imaging

Part	Cost
Microscopes	$99,000,000,000
Land	$2,800,000
Building	$638,000,000
Total	$99,640,800,000

3.4 Introduction to data processing

NIHAAR SHAH

All the previous physical processes of chemical treatment, cutting and scanning that we have seen so far culminate in this stage of processing the data to obtain something meaningful out of a mere spaghetti of tissue and neurons.

It must be noted that without the significant advances in the technology behind data processing in the past decade this entire project would have been just a dream. The field of high performance computing with its introduction of highly parallelisable and specialised GPUs has made possible implementing algorithms in machine learning that were theoretical

[3] http://www.usclimatedata.com/climate/minneapolis/minnesota/united-states/usmn0503/2017/1 Accessed April 2017

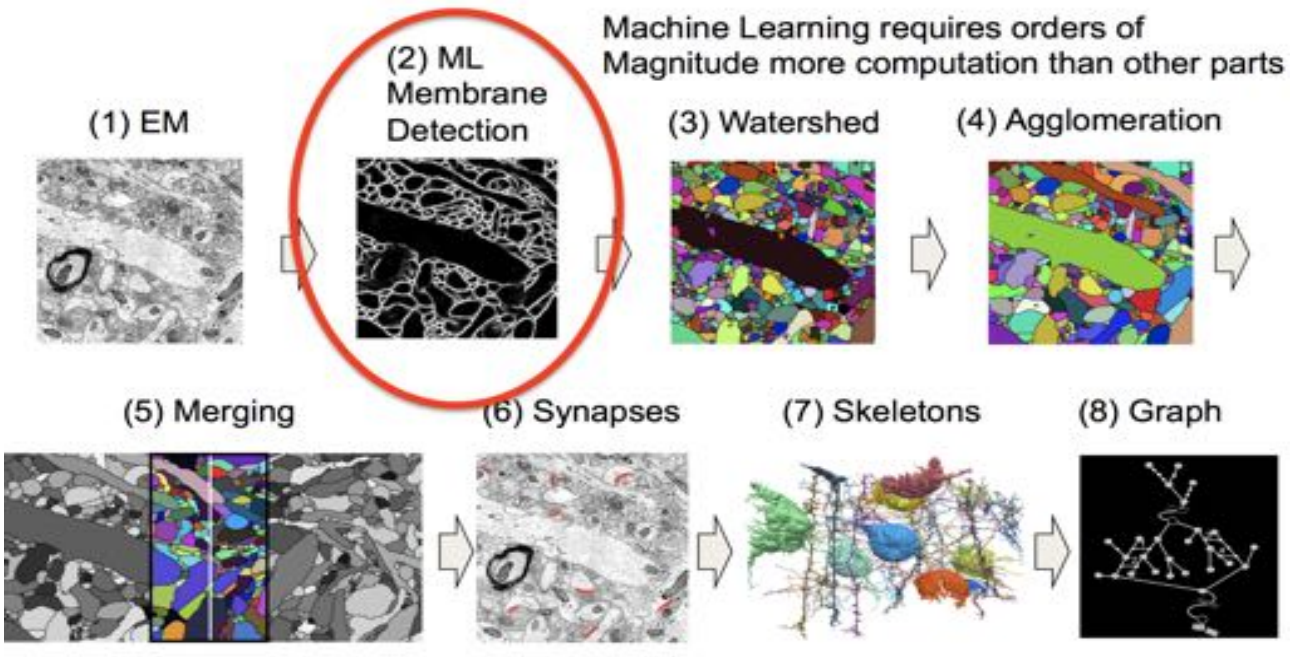

Figure 32: Stages of a data processing algorithm applied on raw image slices to obtain a meaningful 3d neuronal circuit[110]

when they were conceived. Even in the field of big-data, the scale of this project is unprecedented. The entire internet data was approximated to be around 1.2 zettabytes in 2016.[109] This project has a sum total of 343 zettabytes before compression.

Image 32 illustrates the various stages of processing that the brain images will pass through in order to finally reach the design goal of extracting all neuronal connections and their synaptic strength as well as to upload and save an entire human brain for possible future reanimation. The above image is an overview of the main steps in one possible algorithm to segment synapses and extract a 3d neuronal circuit in the form of a graph. The graph should be able to capture the synaptic strength in the form of a relative number at its nodes based on the thickness of the post synaptic density from the skeletonised form of the neurons.

In this section of the report we shall first present our proposed architecture for the big-data pipeline and later elaborate on the rationale and nitty-gritty behind each of the design choices.

3.4.1 Overview of major steps

- **Create cluster** : The first step is creating the cluster, this can be done using public clouds like those available at Amazon AWS, Google Compute Engine, Databricks Cloud or even own our own cluster. Apache Spark is an open-source cluster computing framework. The cluster typically consists of several nodes each with its own memory and processor (CPU and GPU) connected in a network and controlled by a master. We will build our own cluster and use Apache Spark to manage it.

- **Distributed file system** : Image data from the SEMs coming in at 1.65 Exabytes (EB)/day will be stored in directories on the file system and we will store references to the images i.e. path to the image,the image name, etc. in a database like mySQL. We shall use Solid State Drives (SSD) as temporary storage at this stage specially due to their low latency in I/O operations.

- **Load the data in**: Once the Spark Cluster has been created, the data can be loaded into the slave nodes via the master node using the Spark Image Layer. Spark can easily read petabytes of data from Amazons S3, Hadoop Filesystem (HDFS) or any shared / network filesystem that was used to store image data. In this project we use HDFS due to its support of the Map and Reduce algorithm.

- **Map and Reduce** Thousands of images will come in concurrently every second as input to the pipeline, and we may want to prcess them in the cluster asequentially i.e. images belonging to a stack being sent to various nodes depending on where there is vacancy. Yet we want to retrieve and store them in the same sequence in which they exist in the brain. The Map and Reduce algorithm 3.7.2 allows us to not lose this sequence even though we will be doing parallel processing of all of these images agnostic of their order. The Map function can be used to send images to GPUs after deploying Machine-learning algorithms and are returned in order at the end of the processing using the Reduce function.

- **Extract Neuronal Circuit** We now have all the images back in the same sequence where they were found in the original image volume. The penultimate step is to convert

these segmented images into a more useful neural circuit. This is done using Knossos, a tool built for this purpose by the Max Planck institute.

- **Store for future re-animation** The 3d neuronal circuit can now be tucked away for long-term storage until we process the rest of the brain. This will take around 140 years at present rates of processing taking into consideration an reasonable cost. We shall rely on magnetic tapes to be our storage medium of choice. Magnetic tapes only support sequential retrieval and are slow to access but that is perfectly fine since we have the images already in order (thanks to Map and Reduce) and we plan to access multiple tapes concurrently therefore reducing the overall latency.

- **Time and Cost** We have decided to trade-off more time for lower cost of data processing. The rationale being that investing money in buying large quantities of present state-of-the-art infrastructure (mainy GPUs) is not as cost effective as starting modest but waiting for developing technology (i.e. faster GPUs and algorithms) so as to gradually ramp up our full-scale infrastructure. With this in mind we have set a GPU cost of about 10 billion $ and time frame for entire brain processing to 140 years at current speeds of GPUs available (about 100 TFLOP/s)[111].

3.4.2 The Pipeline Architecture

Figure 33 shows our design for whole pipeline as a schematic. Figure 34 shows costings and some of our major design choices.

3.5 Algorithms

Synapses are particularly difficult to detect automatically due to their small size and limited contrast. Humans are too time consuming at this task while most algorithms are too erroneous. Machine learning tools have shown promise due to their ability to scale immensely and their growing accuracy. Here we shall discuss Convolutional Neural Networks (CNNs) and Random Forests (RFs). Both algorithms perform pixel operations on features selected from previously annotated set of images to generate a model that can then predict the category of similar but un-annotated pixels.

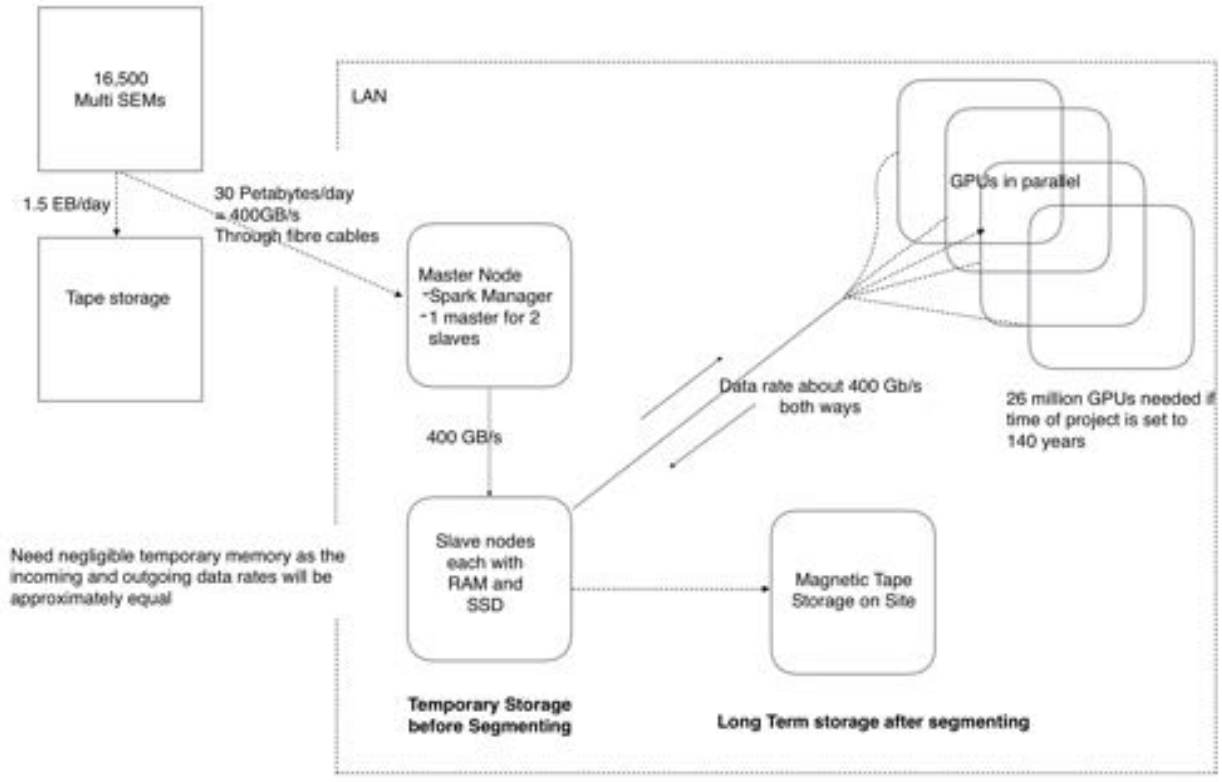

Figure 33: Schematic of the flow of data through various stages with proposed data rates.

Component	Choice of product	Number	Cost
GPU	Custom built e.g. TPU	26.2 million	$ 400 Total = $ 10.5 billion
Magnetic Tapes	Sony 185 TB	43 million EB = 232 million tapes	Total ~ 10 billion $ spread over 150 years
SSD	PM863 Series Data Center SSDs; 4TB	200 (Buffer storage only)	2000 $; Total = $400,000
Algorithm	Google Flood Filling Networks	N/A	N/A
RAID level	RAID 5	N/A	N/A
Distributed File System Software	Apache Hadoop	N/A	Open source
Cluster Node computers	Dell R310s; four 2.4GHz cores	1 million (4 GPUs per node)	100 $ per server; Total = $ 100 million
Network Bandwidth	6 fiber pair cable; 60 (Tbps)	Distance ~ 2 km	1000 $
3D circuit from Images software	Knossos tool	N/A	Open source

Figure 34: Table summarizing major design components and their numerical details.

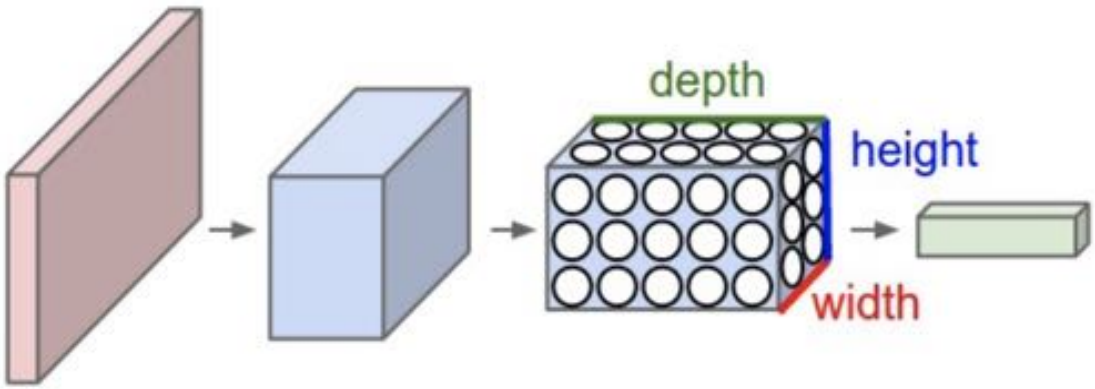

Figure 35: Every layer transforms the 3D input volume to a 3D output volume with some differentiable function[112].

3.5.1 CNN

The principle is to let the algorithm work-out the appropriate features by itself based on back-propagation of errors found after each iteration of the models prediction. The model is said to be trained when this error is minimised using stochastic gradient descent. Each layer outputs a tensor which becomes an input to the next layer. Typical architectures have convolutional layers, ReLu layers (to make all negative weights positive), Pool layer (to down-sample) and fully connected layer (to compute class score). Primary design choices in the CNN architecture are in: Convolution layer: Number of features and Size of features; Pooling: Window size and Window stride (how many pixels to jump while sliding the kernel/filter); Fully Connected layer: Number of neurons. There are no hard and fast rules on how to select these hyper-parameters and it is often determined by trial-and-error. Some experience based combinations are known to yield effective results. We shall discuss two state-of-the-art architectures specialised for dense semantic classification of synapses, vesicles and membranes.

3.5.1.1 'VESICLE' CNN

For each tile the classification problem is to determine the class label of the centre pixel as a synapse or not. It is crucial to note that the spread of synapses is very sparse amid the remaining brain tissue and using brute force to categorise every pixel as synapse or not-synapse would be wasteful because clearly some portions of the image can be assumed

to have lower probability of containing synapses. Using a Bayesian approach we can use prior information about the correlation between membrane and vesicle positions with the synapses.

Synapses occur along cell membrane boundaries between at least two neuronal processes. Thus, an important design aspect used was to leverage the prior information about membrane probability of a pixel while training the model to detect neurones. This meant membrane classification has to be done first which is computationally expensive.[113] Vesicles are also of biological interest for the estimation of synapse strength which is part of our design expectation. Thus, vesicle clusters are identified which help localise regions containing synapses, at a negligible time cost relative to the synapse detection. Some details of this architecture are tabulated later.

3.5.1.2 Flood Filling Networks

Flood filling network (FFN) is a newer architecture by Google which has attracted interest due to its superior performance than previous CNNs. This is a fully convolutional network which makes it less complex than the VESICLE CNN architecture. Thus it drastically reduces the hyper parameter tuning. FFNs outperform CNN+watershed architectures in Edge accuracy and in error performance measures such as merge edges, split edges and omitted edges. A drawback of this architecture is its significantly increased computational cost due to the sheer depth of the network.

3.5.2 Random forest classifier

This method is about estimating a function f : f(X) = Y where X are the features and Y is called the target. Decision trees are predictive models that impose sequential divisions (splits) of an input space. The splitting is decided based on maximising Entropy before and after a split (or information gain). It exhaustively searches all possible splits and chooses the best to create two new child nodes. The limitation of using decision trees alone is that they are prone to over-fitting the data (fits the training data perfectly but does terribly on the test data). Random Forest is an ensemble method i.e. it combines the results from several trees. This approach reduces the variance on prediction / less overfitting as not all trees will

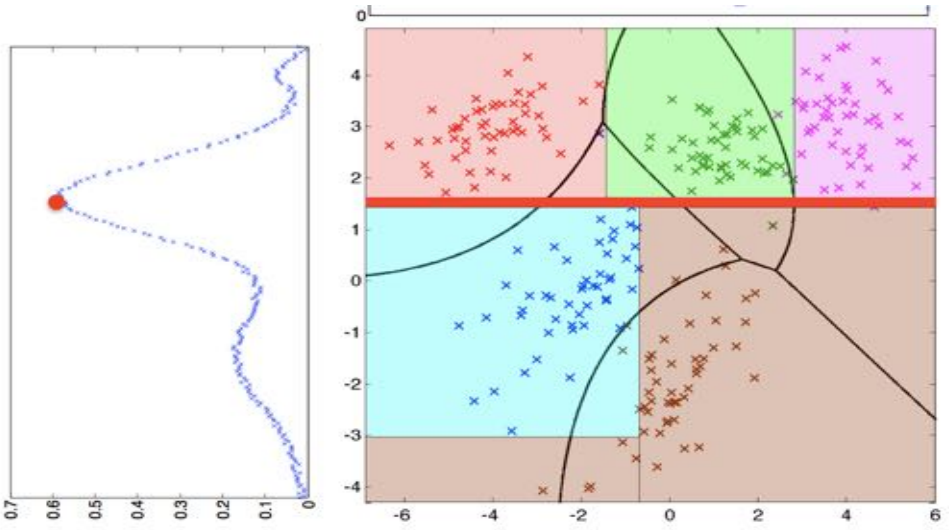

Figure 36: Illustration of how Random Forest splits features to maximise information gain (entropy)[114]

make the same mistakes. It allows us to have more complex decision boundaries and yields massive performance improvements.[114] We train each tree using a slightly different dataset. The data sets are generated by taking bootstrap sampling - i.e. sample with replacement a dataset of the same size. At each node randomly select some subspace of features to search over. This forces different trees to split along different dimensions at each node. Predict by aggregating (by voting) the predictions of the different trees. This algorithm called Bootstrap Aggregating (or Bagging). The random forest architecture in the VESICLE paper was found to be 200 times faster on the same data set than the CNN architecture. Some of the advantages of RF are: It is non-parametric, capable of using continuous and categorical data sets, easy to parametrize, not sensitive to over-fitting, good at dealing with outliers in training data, and it calculates ancillary information such as classification error and variable importance[115]. One of the challenges of using RF is that one must manually select the features that need to be used in the classification. This feature engineering is often very difficult to get exactly correct, especially in the case of image segmentation. Raw pixel values as features are highly inefficient (we verified this by implementing an RF with just pixel values). Usually we can derive some summary statistics from a subvolume of pixels such as mean, variance, median and so on. CNNs on the other hand choose their own features using back-propagation.

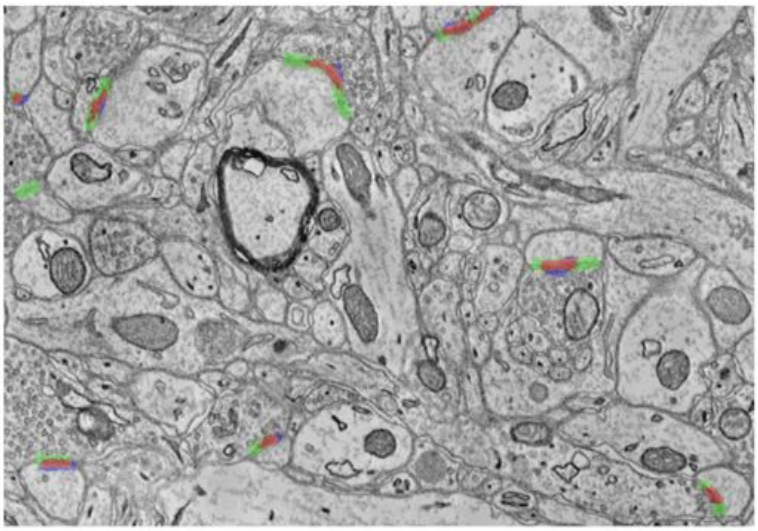

Figure 37: Example RF result. Gold standard labels are shown in green, and VESICLE-RF detections are shown in blue. Red pixels represent True Positives (TP). Objects that are only green are False Negatives (FN) and objects that are only blue are False Positives (FP). Object detection results are analyzed in 3D and so single slices may be misleading[113]

3.5.3 Experiment

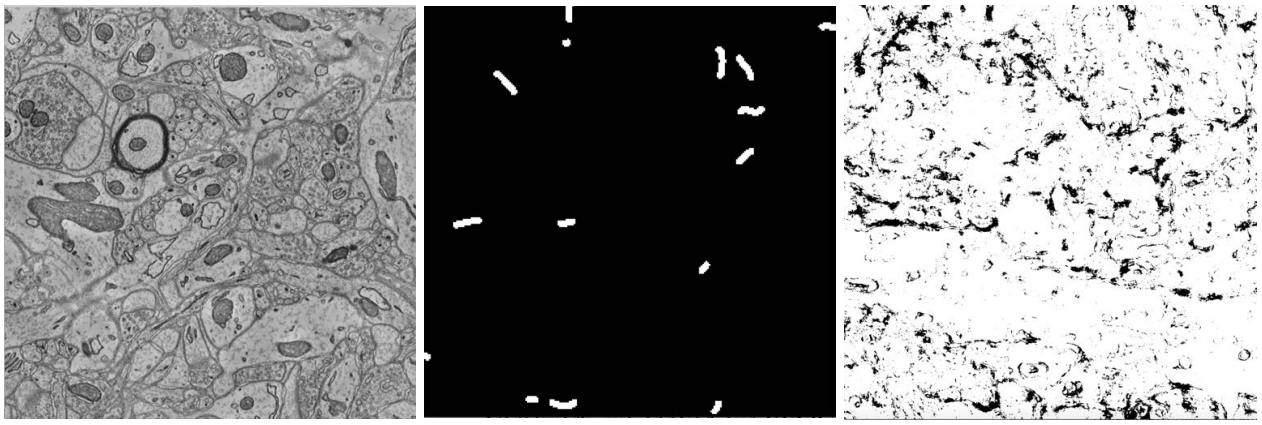

(a) Test Image (b) Validation image (c) Prediction

Figure 38: Result from the experiment

To understand the various aspects of implementing such algorithms, we implemented three different architectures on a stack of 125 training images on a high performance cluster. Whilst obtaining a high F1 score was one of the aims, we also wanted to understand first hand, the time complexity and the difficulty involved in feature engineering. We chose a 5 x 5 x 128 voxel sub-volume (because synapses are within this size) around every single pixel with the following features: Mean of pixels in the sub-volume, standard deviation, median, number of vesicle pixels and proximity to a membrane pixel. The F1 score was 0.065 and the time taken to train on 5 images was 30 min. We then replicated the VESICLE RF architecture

Segmentation	Edge accuracy [%]	Merged edges [%]	Split edges [%]	Omitted edges (adjusted) [%]	Omitted edges (raw) [%]
CNN + Watershed	87.7	1.0	10.6	0.7	1.1
CNN + Watershed + GALA	96.3	1.7	1.4	0.6	1.1
CNN + Watershed + CELIS	93.2	5.4	0.7	0.7	1.1
Flood-Filling Network	98.5	0.0	0.7	0.8	2.4

Figure 39: Table showing the superior accuracy of Google's FFN over current methods. Accuracy is the priority over costs for our project making it our choice of algorithm.[117]

and obtained an F1 score of 0.0117 for the same time. The CNN architecture though took significantly longer- 30 hours for 5 images but a similar F1 score. The number of epochs in the CNN was reduced from the original 200,000 to just 200 for the sake of the experiment. Clearly the observations confirmed the relatively immense time complexity of the CNN when compared to Random Forest. Note the F1 scores are not representative of what is expected from these architectures in reality because our training size was smaller due to time and computational constraints.

3.5.4 Evaluation Metrics

Type I error is to detect an effect that is not present, while a type II error is the inability to detect an effect that is present. The F1 score can be interpreted as a weighted average of the precision and recall, where an F1 score reaches its best value at 1 and worst at 0. It considers both the precision p and the recall r of the test to compute the score: p is the number of correct positive results divided by the number of all positive results, and r is the number of correct positive results divided by the number of positive results that should have been returned.[116]

To evaluate the segmentation performance of algorithms we need a reference ground truth image. An efficient method to generate ground truth representations of large-scale neuron topology is to skeletonize neurons into a collection of points that typically constitute an undirected tree. The edge accuracy is therefore defined as the percentage of correctly reconstructed edges over all the ground truth skeletons. Incorrect edges can be further subdivided into the percentage of edges which have a merge, split, or omitted error.[117]

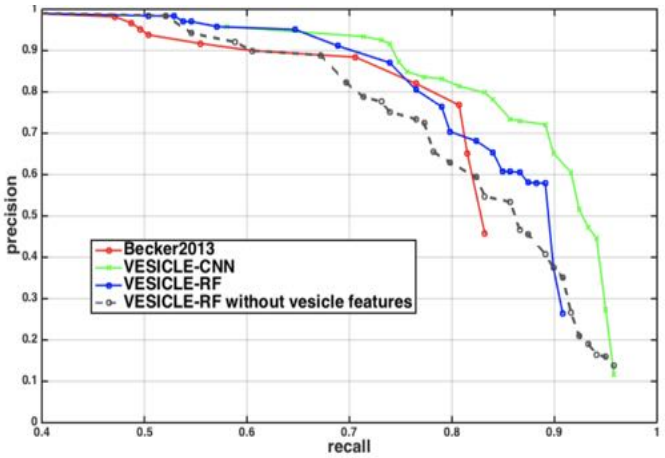

Figure 40: Precision vs Recall performance of RF vs CNN indicates the marginally better performance of CNN[113]

3.5.5 Discussion on choice of algorithm

It is clear that Random Forests are extremely fast relative to CNNs. Their training time complexity is $O(NL\lambda(\log(N))^2)$ while for testing it is $O(\log(N))$. For CNN it is $O(M*N*m*n)$ much larger.

CNNs in general showed marginally better F1 score performance than RF. However, the FFN even significantly outperformed previous CNNs followed by watershed methods as shown in Table 39. They are also significantly easier to implement due to there being less need to tune hyper-parameters in a fully-convolutional architecture. Secondly, feature engineering which is the hardest part of RF is altogether eliminated using a CNN. For different parts of the brain there may be variations and we may have to continually alter some features if we go ahead with RF.

These reasons have led us in favour of FFNs, although at the cost of immense computational cost of 4.6 PFLOPs when tested on a tiny sub-volume. It must be noted that FFN was proposed by Google in Nov 2016 and the VESICLE paper proposed the CNN and RF in Nov 2015. Clearly, this field of making faster, more accurate and less costly algorithms is bleeding edge with significantly newer approaches surfacing rapidly.

It would be an omission to not keep a provision to update our algorithmic approaches in the course of the project especially because this is a long term project. We can nonetheless make an initial choice based on the priorities of the sought design. Let us attempt to score the 3 approaches (higher the better) using Multi-Criteria Decision Analysis. The weights

	Accuracy * Weight	Computationally economical * Weight	Ease of implementing * Weight	Total Score
CNN (VESICLE)	7*1	5*.8	5*.7	10.5
RF (VESICLE)	6*1	8*.8	8*.7	18.0
FFN	9*1	3*0.8	7*.7	19.3

applied indicate the parameters importance in the context of this design project according to us. Given the significant superiority of FFNs accuracy, ease of deploying and our financial ability to provide high end parallel computing hardware architecture, we have decided to employ FFNs in the future discussion. We are aware that during the course of the execution of this project there may be newer more efficient algorithms and so since we will be over-providing the hardware infrastructure for FFNs there won't need to be many additions to be made in the hardware pipeline. Future, more efficient algorithms will simply be deployed on this pipeline.

3.6 Processing Hardware

To process immense quantities of image data (1.5 EB/day) needs robust, efficient and enormous scale of hardware infrastructure to take care of each stage in the data processing pipeline. This starts with high-throughput and secure data transmission lines, buffer storage for short term use, CPUs to coordinate the various jobs, GPUs to do the number crunching and long term storage. The huge scale of data means we need to employ parallel computing. The following sections will elaborate on these themes.

3.6.1 Role of GPU

The back propagation step in the CNN algorithm involves minimizing the error between ground truth and the model for every iteration. This minimisation uses Stochastic Gradient Descent (SGD) which is mainly matrix multiplication: perfect task for GPU. SGD is sequential, so multiple GPUs can help. GPUs are highly parallel making them useful for algorithms where processing of large blocks of data is done in parallel.

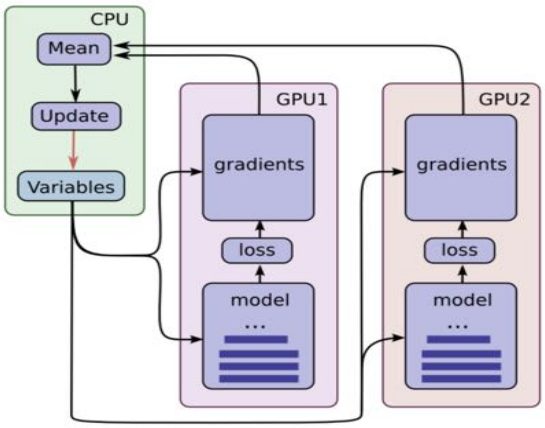

Figure 41: GPU parallelisation shown schematically[118]

3.6.2 Role of CPU

- Writing and reading variables in code
- Executing instructions such as function calls.
- Initiating function calls on our GPUs

3.6.3 How Parallelization is achieved

Needed number of CPU cores: Most deep learning libraries and in fact most software applications in general use a single thread. This means a multi-core CPU is rather useless. If we use multiple GPUs however and use a parallelisation framework like MPI then we can run multiple programs at once and we will need multiple threads also. Our choice of distributed file system, Apache Spark will manage the distribution of data into blocks and split them into various GPUs in the cluster.[118]

Training a CNN model can be done concurrently on multiple GPU cards using parallel computing to reduce time. To do this we can place an individual model replica on each GPU. Then update the model parameters synchronously by waiting for all the GPUs to finish processing a batch of data.[118] Note that each GPU computes inferences as well as the gradients for a unique batch of data. This setup effectively permits dividing up a larger batch of data across GPUs. The Map and Reduce algorithm ensures that the data can still be retrieved in original sequence they were imaged.

The setup requires that all the GPUs share model parameters. Transferring data to and

from GPUs is quite slow. Therefore we decide to store and update all model parameters on the CPU. A fresh set of model parameters is transferred to the GPU when a new batch of data is processed by all the GPUs.[118]

3.6.4 Concluding design decision on GPU and CPU

GPUs are optimized for memory bandwidth while sacrificing for memory access time (latency). CPUs are designed to do the opposite: CPUs can do quick computations if small amounts of memory are involved for example multiplying a few numbers (5*2*7), but for operations on large amounts of memory like matrix multiplication (A*B*C) they are slow. GPUs excel at problems that involve large amounts of memory due to their memory bandwidth. NVIDIA released Titan Xp in April 2017 which provides the highest memory bandwidth of 547.7 Gb/s and processing power of 12.15 TFLOP/s[119].

However, as GPUs are general purpose their performance both in terms of power (by a factor of 10x), speed(factor of 4x) and market-price (factor of 5x)[111] [120] can be significantly optimised (roughly by 10 * 4 * 5 = 200 times) using custom built GPUs for e.g. Google Tensor Processing Unit (TPU). Of course, the downside is that if we update our algorithms (which is inevitable), our TPUs shall gradually become inefficient for the new software thus adding a recurring cost of replacing the TPUs. From the above discussion we see that TPUs on the whole could be 200 times cheaper than GP-GPUs and quite likely the number of times we would expect to replace our TPUs is much less than 200 times over the span of 140 years.

It must also be noted that the gold standard GPU speed increased 5 fold in a span of a year[120] which clearly hints that the field of GPU design is rapidly flourishing. This is a further argument for replacing our ensemble of cheaper TPUs to keep up with the updating state of the technology rather than invest significant amounts in the status-quo.

3.6.4.1 Number of Custom GPUs needed

$$\text{number of voxels in brain} = \frac{\text{brain volume}}{\text{3D resolution of the Microscope}}$$

$$\text{nGPUs} \times \text{Calculation Speed of GPU} \times \text{Time duration} =$$
$$\text{number of voxels in brain} \times \frac{\text{FLOP/s FFN took on sub volume}}{\text{number of voxels in that sub volume}}$$

$$\text{nGPUs} = 26\text{million (if the processing time is set at 140 years)}$$

$$\text{Cost} = \$10.5bn, \quad \$400/\text{TPU}.$$

The FFN requires 4.6 PFLOP/sec to process a sub volume of 520 x 520 x 256 voxels. Our resolution of imaging is 3 x 3 x 29 nm and the volume of the brain for this calculation was taken to be 1500 cubic centimetres.

3.7 Distributed File Management System (for the Data cluster)

Apache Spark is an open source big data processing framework built around speed, ease of use, and sophisticated analytics. Spark enables applications in Hadoop clusters to run up to 100 times faster in memory and 10 times faster even when running on disk. In addition to Map and Reduce operations, it supports SQL queries, streaming data, machine learning and graph data processing. We want to use these capabilities and combine them to run in a single data pipeline use case which makes Spark a good choice.[121]

3.7.1 Hadoop File Storage System

Spark uses HDFS file system for data storage purposes. HDFS has a master/slave architecture. An HDFS cluster consists of a single NameNode, a master server that manages the file system namespace and regulates access to files by clients as seen in Figure 42. In addition, there are a number of DataNodes, usually one per node in the cluster, which manage storage attached to the nodes that they run on.[121]

HDFS exposes a file system namespace and allows user data to be stored in files. Internally, a file is split into one or more blocks and these blocks are stored in a set of DataNodes. The NameNode executes file system namespace operations like opening, closing, and renaming files and directories. It also determines the mapping of blocks to DataNodes. The DataNodes are responsible for serving read and write requests from the file systems clients. The DataNodes also perform block creation, deletion, and replication upon instruction from

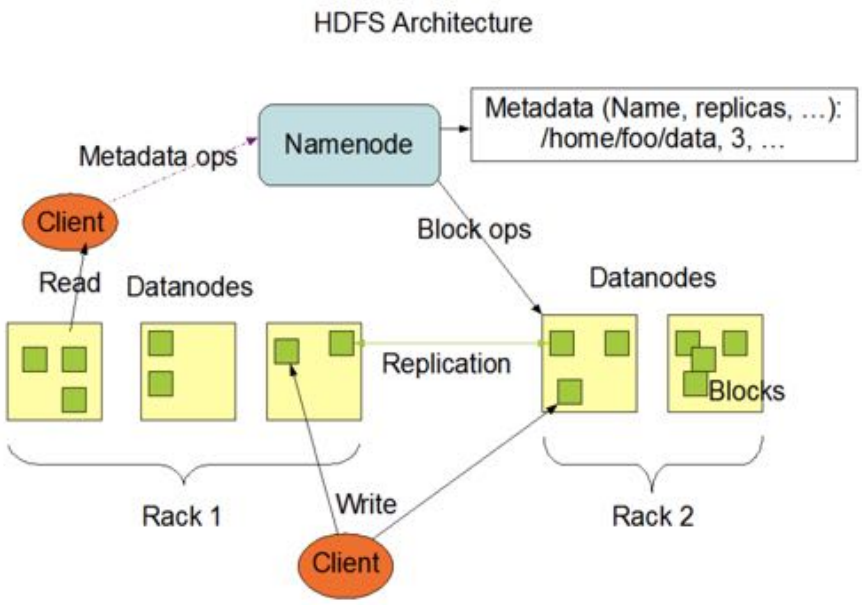

Figure 42: Arcitecture of the Hadoop File System which we shall use to store image data in a distributed fashion for rapid querying and parallel deployment[122]

the NameNode.[122]

3.7.2 Map and Reduce algorithm

In our architecture we receive an image stream from 16,500 SEM machines concurrently. Obviously, it would be inefficient to process all the images in sequence i.e. one GPU caters to only one stack of images that too in order.

Instead, we want to access the images and distribute the processing to any custom GPU that is currently vacant. The figure 44 shows our design to enable this.

3.7.3 Resilient Distributed Datasets

Resilient Distributed Dataset or RDD is the core concept in Spark framework. RDD is like a table in a database. It can hold any type of data. Spark stores data in RDD on different partitions. They help with rearranging the computations and optimizing the data processing. They are also fault tolerant because an RDD knows how to recreate and recompute the datasets - something that is very important for our design because we shall expect some of the 26 million GPUs and over 1 million nodes to fail occasionally.

RDD supports in-memory processing computation. This means, it stores the state of memory as an object across the jobs and the object is shareable between those jobs. RDDs are immutable. We can modify an RDD with a transformation but the transformation returns

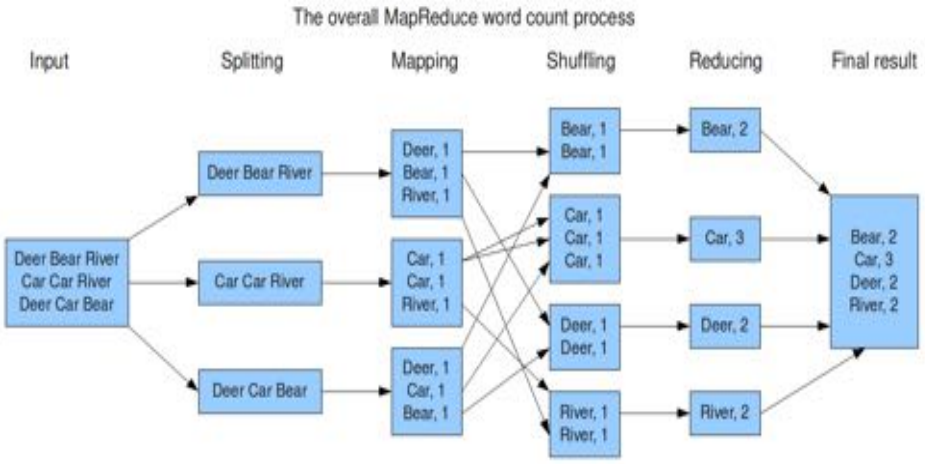

Figure 43: Map and Reduce steps of the algorithms shown as applied to word counting[123]

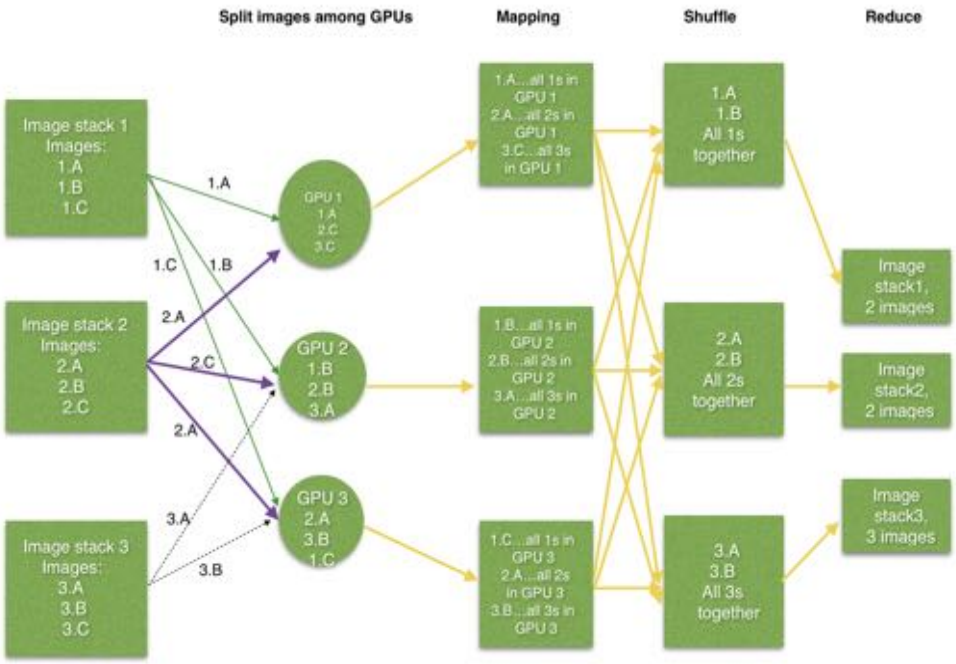

Figure 44: How we apply M&R to our design: Each image is mapped to a stack of subvolume and has numberings to show the sequence e.g. Stack A, sequence no. 7. We can retrieve original positions at the end of processing with this algorithm

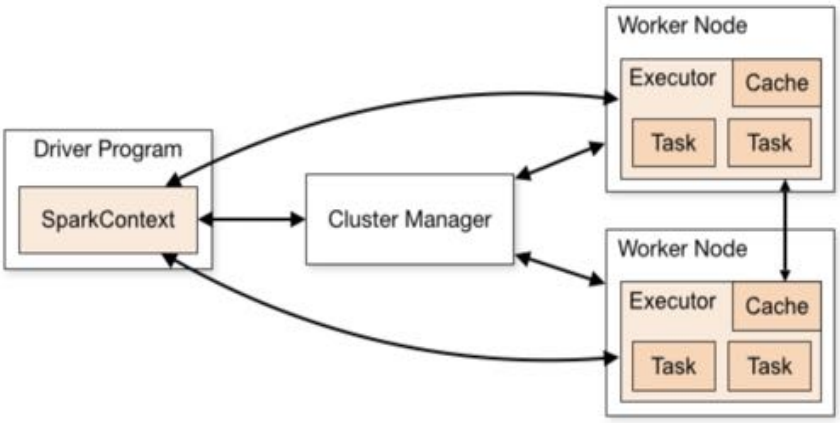

Figure 45: Schematic of a Spark cluster[124]

us a new RDD whereas the original RDD remains the same. Spark can be deployed as a Stand-alone server or it can be on a distributed computing framework like Mesos or YARN.

3.8 Storage hardware

Storing around 1.5 EB/day continuously for 140 years is an unprecedented task for any single oganization. Naturally any design decisions made initially will have huge repercussions in the cost and preservation of the data. Our design choices will include the medium of storage to be chosen, steps to ensure reliability of this stored data and any optimisations to be done to ensure maximum efficiency.

3.8.1 Medium

First let us define the parameters by which we shall judge our storage medium.

- Areal density: Measure of the quantity of information bits that can be stored on a given area of track of the storage medium.
- Latency: Measure of delay in the system. The time taken to respond to an Input-Output (I/O) request.
- IOPS (I/O per second): Number of individual input-output operations taking place per second. Often useful if we also know the nature of I/O such as the size and its randomness.

- Bandwidth (throughput): Measure of the data volume over time - the amount of data that can be pushed or pulled through a system per second (usually Gb/s).
- Throughput = IOPS x I/O size

3.8.1.1 Tapes

Magnetic tape plays a crucial role in assuring data integrity and is the lowest cost form of data storage. While tape still is the low-cost form of magnetic storage, the large disparity in recording areal densities between hard-disk drives and tape threatens this key distinction of digital tape storage. There has however been recent progress in the field of tape storage which has put tapes on level field with hard-disks.

Sony Corporation in 2015 announced that by independently developing a soft magnetic underlayer with a smooth interface using sputter deposition, it has succeeded in creating a nano-grained magnetic layer with fine magnetic particles and uniform crystalline orientation. This areal recording density is equivalent to approximately 74 times the capacity of current mainstream coated magnetic tape storage media, and makes it possible to record more than 185 TB (terabytes) of data per data cartridge.[125] Fujifilm followed Sony and made an announcement that it will develop a 154 TB tape cartridge by the end of 2015. Given this breakthrough let us do a cost-benefit analysis of various storage media.

- **Advantages**
  - Power Consumption: Tape really steals the show when it comes to calculating the energy that each medium uses once our enterprise stores its data for the long term, it no longer requires electricity. Disk systems, on the other hand, are always power-on and require constant cooling. Considering our time-scale this simply is not feasible
  - Cost: For very similar areal density (148 Gb/square inch) as hard disks, Tapes cost 5 times less ($ 9 per TB Vs. 45 $ per TB for HD).
  - Recent improvements in Latency: Backup tape's seek time improved greatly with the introduction of LTO-5's LTFS (linear tape file system). LTFS makes tapes more

like disks. This technology doesn't need to search through all of a tape's contents to find what you're looking for; rather, it goes right to it.

- **Challenges**
  - Maintenance: Tape requires attention to keep them durable. This media must be kept in a pristine environment to prevent error-causing dust or dirt from getting into those cartridges.
  - Physical labelling: Tape cartridges will need to be labelled, logged or tested using some robotic intervention (since manually is too time consuming). This will be an added cost.[126]
- **Best Practices for Tape Backup and Recovery** Tapes are sturdy, but they still need care for dependable results.
  - Testing: Regularly and vigorously test our tape data backup system to ensure it works correctly and that we can restore critical data.
  - Replacing: Retire a tape that is past its prime. A little dust where it shouldn't be can cause the occasional error. But if a tape begins having errors daily, it's time to retire it. We estimate replacing our tapes every 30 years which means around 4 times overall at current time estimates.
  - Upgrade: to newer tape systems as technology advances. While it might seem a burden to go from an older LTO-4 system to a new LTO-6, the improved features and capacity of newer tapes will deliver real productivity savings. We can combine this with each cycle of replacement of our tapes.

3.8.1.2 Disks

Disks are more expensive bot the hardware and the energy consumption (100 W just to keep them on). Yet they provide rapid I/O access and ability to use fault tolerant systems (see the discussion on RAID).

- **Advantages:**

  - Rapid recovery: Finding a particular file with a disk system is faster than with a tape data backup system.
  - Efficiency: from de-duplication. This process removes duplicate copies of saved data to free up space. Deduplication means we can store data more quickly and perform full backups less often.

- **Challenges:**
  - Cost: Disk systems are constantly onand constantly on the verge of running hot. That means we not only have to power them, you also have to power cooling systems to keep them from overheating. If we are thinking of investing in a disk-based data storage system we must be sure to total all the costs.
  - In-house storage comes with compromises. An onsite disk system eats up a great deal of space and energy. Being able to dedicate that real estate to other needs by sending less-used data to offsite vaulting for long-term storage is a big plus for tape data backup systems. Plus, it's good to have critical data stored offsite in case of a fire, flood or other disaster.
  - Overwriting comes with perils. Newer LTO tapes use WORM (write once, read many) security that prevents accidental overwriting from ever occurring. Overwriting is more of a risk with disk systems, since the entire disk could be accidentally reformatted. When that happens, we better have a redundant disk on hand.

- **Best practices:** Test: When it comes to restoring all our data, one test isn't enough. We need to test our data backup system regularly throughout the year.

3.8.1.3 Table of comparison

Storage Medium	Pros	Cons	Cost
Optical Storage	• Rapid access (high IOPS) • Un-sequentially accessible • Less bulky to store	• Low areal density (inefficient)	40 $/Tb
Magnetic Tape	• High areal density (148 Gb/ in^2) but much more area of tape per volume than HDD • Robust and long-lifespan • Energy efficient • Space efficient	• Slow to access data (3 orders of magnitude slow than hard drive) • Less scope of redundant storage	9 $ / Tb
Hard Drive	• High areal density (1.34 Tb/ in^2) • Rapid access • Random access of data possible	• Susceptible to data loss • Energy inefficient as the disks keep spinning at all times • Space inefficient • Accidental overwrite is perilous	40 $ / Tb

3.8.2 Solid State Drives

DESANKA MARKOVIC

3.8.3 Alternative Temporary Storage

We require temporary storage of the SEM image data both prior to and post segmentation. Currently there are two options suited to this task - SSD (Solid State Drives) and HDD (Hard Disk Drives). As already mentioned, performance can be assessed using a number of characteristics - we will be focusing on throughput, latency and IOPS to compare the performance of both forms of storage 12 along with power usage and Form Factor.

Table 12: Comparison of SSD and HDD Data Transfer characteristics

	Throughput (MB/s)	IOPS (Random 4KB Read/Write)	Latency	Form Factor (mm)	Power (Active) (W)	Power (Idle) (W)	Cost ($/GB)
SSD[4]	430	110,000	20 µs	15 x 69.85 x 100.45	7.5	4	0.97
HDD[5]	25	26000	2 ms	15 x 69.85 x 100.45	7.6	5.7	0.62

[5]Statistics for SSD's are based on the Intel SSD DC P3600 series - an SSD optimised for continuous data centre use and mixed (read and write) performance.

[5]Statistics for HDD's are based on the Seagate Enterprise Performance 15K.6 HDD 900 GB 512e/4Kn ST900MP0146, an SSD designed for continuous Data Centre Use

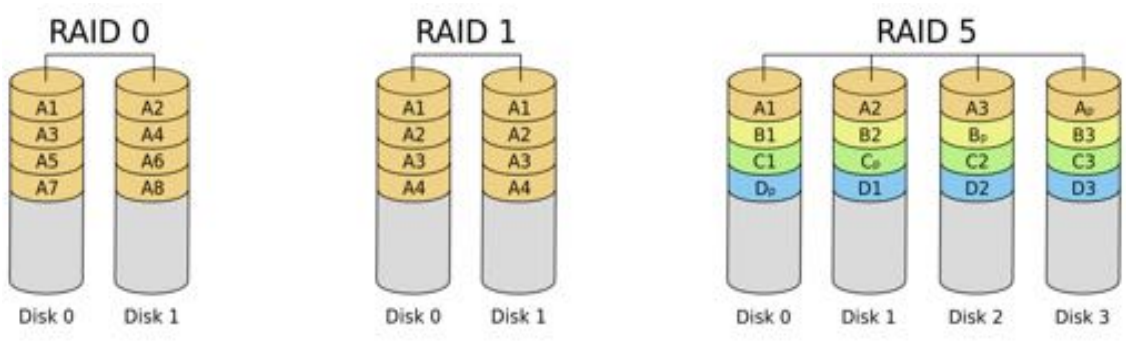

Figure 46: Redundant array of independent disks to create large reliable data stores from multiple general-purpose computer hard disk drives (HDDs)

Based on the characteristics discussed above, it is clear that SSD's are the preffered choice for fast, high throughput data storage. It is also worth noting that SSD storage is experiencing continual development - we expect to see a marked improvement in the cost per GB, along with other characteristics, by the time we have finished the earlier stages of our procedure. Consequently, the cost of temporary storage calculated with these numbers is a conservative, upper limit.

3.8.4 Reliability: RAID

NIHAAR SHAH

3.8.4.1 RAID level 0

RAID 0 uses disk striping stores bits of the same data spread over multiple disks which makes accessing the data very rapid. However, if one of the disks fails which hard drives are known to do, the entire data chunk is lost. Hence, RAID 0 requires the user to have sufficient redundant back up to ensure that the data isn't lost.

3.8.4.2 RAID level 1

RAID 1 uses disk mirroring and keeps an exact copy of data in parallel. If one disk fails, then the data isn't lost, the operation doesn't need to pause and the disk can be replaced (hot swappable) to automatically mirror the other disk. It is as fast as a normal hard drive but the memory requirement clearly doubles.

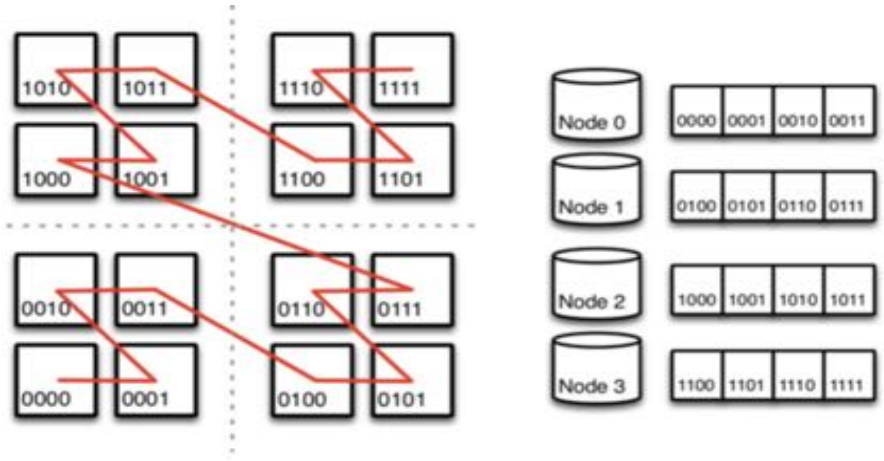

Figure 47: Schematic of an efficient way of storing image data[127]

3.8.4.3 RAID level 5

RAID 5 uses 1 parity bit giving us one degree of redundancy so that if out of n hard disks 1 is lost then the data of that one can be re-created by doing the XOR operation of the remaining discs data bits. This will be our choice of RAID for short term hard-disk/SSD storage.

3.8.5 Efficiency of storage

3.8.5.1 Morton order

With our kind of scale of storage, even small efficiency boosts could have major cost benefits. Morton order is a function which maps multidimensional data to one dimension while preserving locality of the data points. The z-value of a point in multi-dimensions is simply calculated by interleaving the binary representations of its coordinate values. Once the data are sorted into this ordering, any one-dimensional data structure. Some GPUs store texture maps in Z-order to increase spatial locality of reference during texture mapped rasterization. This allows cache lines to represent square tiles, increasing the probability that nearby accesses are in the cache. This is important because 3d rendering involves arbitrary transformations (rotations, scaling, perspective, and distortion by animated surfaces). These are referred to as swizzled textures or twidled textures. Other tiled formats may also be used.[128]

3.8.5.2 Image compression

THEO W. COSTAIN

The micrographs that come out of the microscopes have particular properties that are incredibly helpful for compression. Namely, each pixel has a very strong correlation with the same pixel in subsequent images. Thus, the images are particularly susceptible to video compression. So by storing the images sequentially we can benefit from the data savings that result. However, we require the compression to be lossless, as we are not certain of the effects of compression on the accuracy of the algorithms we intend to use. The key feature of video compression that we seek to exploit is that of keyframing. This is where pixels that do not change from frame to frame are replaced with filler data, pointing to the pixel of a previous frame, so the more pixels that do not change between images the better the compression can be.

There are various standards for video compression. Of particular note is the H.26x line of algorithms and specifically H.265 (HEVC). Developed by JCT in collaboration with ISO and ITU-T, it has several advantages over other competing algorithms.

Unlike its predecessor, H.264, H.265 has a much higher maximum permitted resolution of 81924320 pixels (H.264 only goes to 4096x2304 pixels), which, given the size of the stiched images that result from the MultiSEM, is very helpful. H.625 also significantly outperforms other compression and archiving compression algorithms for video data[129]. A royalty free alternative to H.265 is AV1, designed by the Alliance for Open Media based on VP9(which was developed by Google). It is one of the common codecs used for video compression online. Sadly however it has been shown to be less effective at compression than H.265[130], although it is faster in encoding data.

As a result we plan to purchase hardware H.265 encoders, such that even in lossless mode we can achieve compression ratios in the range $5\% - 25\%$, at rapid speed, allowing for the fast and simple compression of the images to be stored. Although, depending on the load on the image acquisition servers of the MultiSEMs, the hardware encoders may not be needed, if the rate of acquisition is slower than the encoding time. It is of note that most CPUs currently possess hardware decoders for H.265 meaning that the clusters used to extract the images should not become a bottleneck.

3.8.6 Discussion on storage

NIHAAR SHAH

For the design sought in this project, ideal characteristics include low cost, less energy consumption (and carbon footprint), high fault tolerance (through redundancy and distribution of data among different storage units) and space efficiency. Short term storage would need to be randomly accessible with a low latency before we can send it to the GPUs. The long term storage need should have high areal density due to the immense size of data that would need to be stored. The sheer time of operation means we must account for the possibility of a disaster (natural or otherwise). Let us attempt to cost the magnetic tape storage after compressing the 343 zettabytes to about 5 zettabytes at a rough cost of 2 $ per TB.[131]

$$\text{Cost of Tape storage} = 2\$/TB \times 5ZB = \$10\text{Bn}$$

Note this cost is not all up front but spread over 140 years so again can factor in the Net present value.

3.9 The final pipeline

3.9.0.1 Diagram

Figure 48 shows a chronological sequence of the various aspects of the data pipeline and the cluster operation.

3.9.1 Incoming data from SEMs

We plan to use 16,500 SEM machines each with a throughput of 100TB/s. Thus totally, the Multi-SEMs will churn out data at a remarkable rate of 1.65 EB/day. Apache Spark is a distributed file management system which has the capability to manage storage and processing of large scale parallel computing in a cluster that we propose to build.

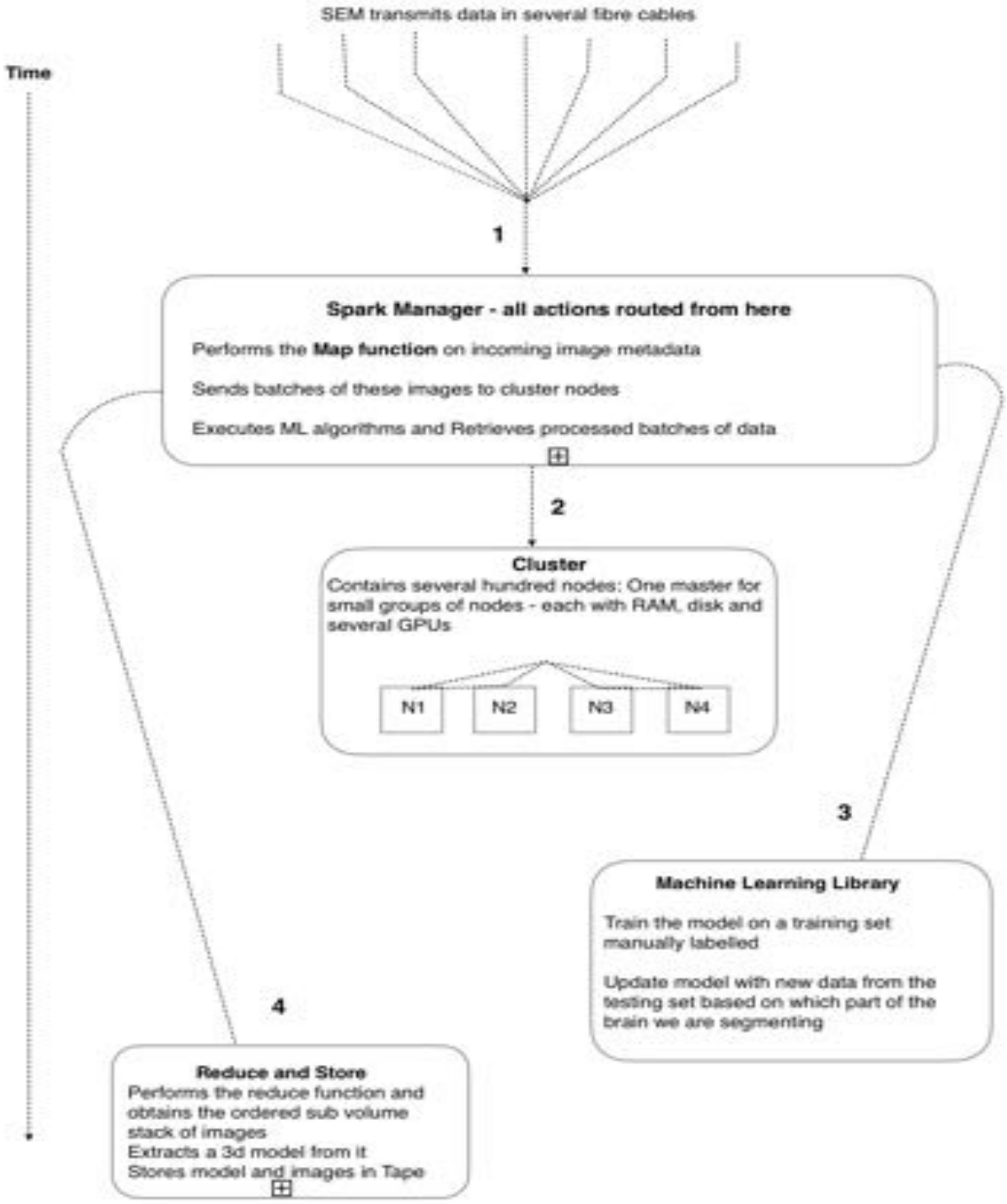

Figure 48: Schematic of the flow of data through various stages with proposed data rates.

3.9.2 Controlling the data rate

We plan to reduce the data rate by storing off part of this data to tapes so as to deal with a more manageable data rate from the point of view of hardware.

3.9.3 Map function

The Spark architecture is centered around the master node which is in charge of the control of data flow. The master performs the Map function on the data. This helps us to collate and structure all the images into manageable chunks and in the correct order as seen in a previous section.

3.9.4 Data transfer

The data rate incoming to the Spark layer is maintained equal to the data rate coming out of the spark layer and going into the nodes of the clusters. This is done to have minimal buffer storage to house this data temporarily. We plan to use multiple fibre-optic cables in a network to parallelise the data flow from any one component to the other. Spark provides APIs that let us do 'health monitoring' of these cables.

3.9.5 Buffer Storage

The latter features make it especially suitable if we wish to divide the data into batches and randomly access them based on the availability of the GPUs and send it in parallel format to the GPUs. A schematic of this batch parallelisation is shown in Fig. 44. As discussed in the section on data storage, however, Hard disks or SSDs are not the most reliable medium because they are known to have random faults and data can be lost. To minimise the chances of data loss, we employ RAID (redundant array of independent disks) method of data storage which is specifically suited to hard disks. RAID ensures data redundancy using certain encryption methods as elaborated before. Then how should we store the processed data in the long term? Magnetic tapes provide cost-effective, energy-efficient, space-efficient and reliable storage for the long term. Let us consider the usage of the data that will be stored after processing. Processed data will be segmented images with each pixel labelled as synapse, membrane, vesicle or none of these. There may also be metadata associated with each im-

age for instance a labelling scheme to identify the index of the image from the volume stack or information about number of synapses in that image slice etc. The rationale for storing metadata is that it could be later used to get some context about the image and even detect any anomalies based on the metadata from the neighbouring images.[132] Importantly the data retrieval will be done in bulk after we have processed image data from a huge chunk of or the entire brain volume. Moreover, the access of this data will be sequential because we would most likely wish to recreate a part of or the entire brain circuit at the time of access. Magnetic tapes are suited for sequential access. The final design goal of this project is to upload and save the connectome thus storing the neural circuit These qualities help us to cut-down overheads of energy required to keep hard-disks spinning and keeping the storage environment cool.

3.9.5.1 Data center feasibility

Table 49 tabulates various factors considered for building a data-centre along with a cost breakdown. Figure 34 should be viewed as well to get a picture of more factors that we have considered to build this pipeline.

3.10 Post processing

This step requires inference in the z direction. The Max Planck Institute made a software tool named Knossos (http://knossostool.org/) that provides a means to go from segmented synapses in a 3d volume into a reconstruction of the skeleton of the 3d neural circuit of the brain (i.e. step 6 to step 7 in the image). This method is fast and accurate but it must be noted that any such technique to merge annotations in a 2d slice into a 3d reconstruction asks for a certain degree of extrapolation in the out-of-image-plane dimension. This is because the resolution is much lower in that direction than it is in the image plane.[134]

3.10.1 How to capture synaptic strength

The process of creating a skeleton of axons and dendrites from the segmented volume of images will record data regarding the length and width of sections. This snapshot is from the knossos software showing the skeleton along with the widths indicating synaptic strength.

Figure 49: Data centre costs

Data Center Summary	Numerical Values	Rationale	Cost
Space to house tapes	20m x 20m x 20 m building with sealed interior to prevent dust and heat to corrupt tapes	Calculated from 1.7 bn 185 TB tapes of dimensions 6 x 8 x 15 cm plus buffer space	50 million $
Average power for GPU?	800 MW	Taking 200 W average power spec of Titan GPU Cost: $0.12 per kWh for 30 years	80 billion $ for 140 years (it is therefore suggested to build a power plant to get this cost down by an order of magnitude) Thus ~ 8 Billion $
Evaluation period (in years)	140 years for data processing	This is chosen keeping in mind the exorbitant cost of GPUs if time is reduced.	N/A
Average power for SSD	4W x no. of SSDs No. of HD is likely to be around the same as the number of nodes in the cluster - 1 million	We have minimised number of SSDs by matching the incoming data rate and outgoing data rate to the cluster.	US$200,000
Network connection (Gb/s)	400 Gb/s Using 6 fibre-optic cables	This is done to minimise the need for buffer memory	US$100,000
Construction cost			2.5 million $
Staff (number and wages)	40 skilled humans to update the training data from time to time 10 semi-skilled humans permanently to maintain the data centre operations	Different parts of the brain may need an updated model Operations such as safety, alerting of any mishaps etc.	20 million $

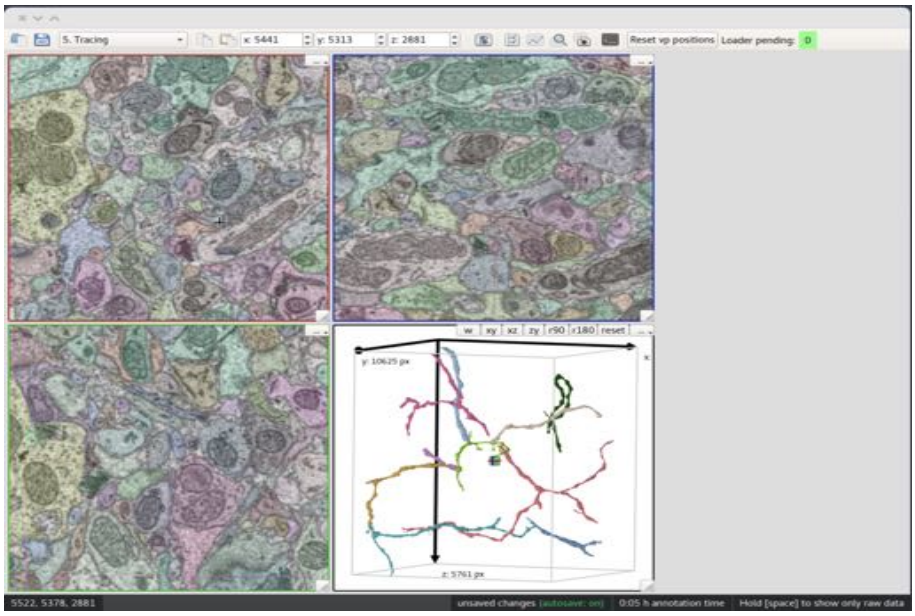

Figure 50: A snapshot of the tool shows how it converts from segmented stack of images into a 3d circuit[133]

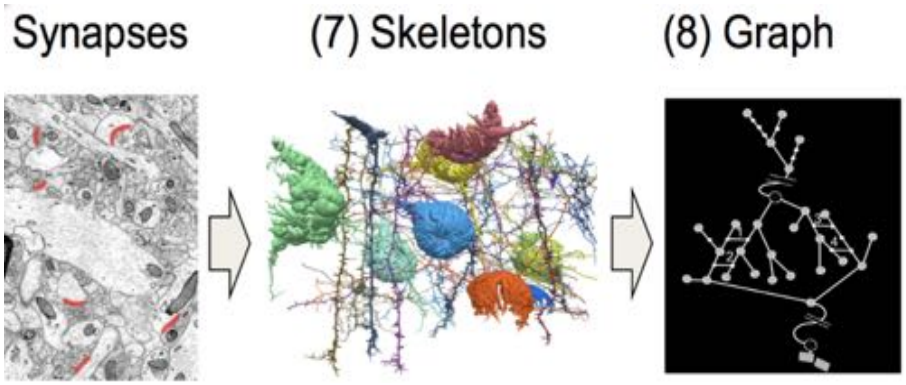

Figure 51: Final steps of converting synapses into a 3d neuronal circuit and graph capturing synaptic strength for future re-animation.

This could be then converted into a 3d graph of the neural circuit. Each node being a synapse and the edges being the axons. Depending on the strength of synaptic connection, the node could be assigned numerical values too. We aim to store multi-dimensional information about the neural circuitry for instance at eac synapse there could be a flag that encodes whether it is an inhibitory or excitatory synapse. Similarly, the node could contain a number indicating the synaptic strength based on its dimensions or the post synaptic density in the form of a numerical value. It could also store information on how many organelles such as vesicles are in close proximity to the synapse.

3.11 Conclusion of Data Processing

This project, as we have seen, significantly raises the bar of what ”big” could really mean when we talk about big-data these days. Building the processing infrastructure at this scale is akin to, if not more ambitious than, building a modern technological wonder of the world.

26 million interconnected custom GPUs, 1 million server nodes of the distributed computing system, 250 million highly dense tape cartridges, a data centre of the size of Oxford’s town centre and the power consumption of a small city. These are just some of the highlights of the data pipeline. All along the design route, we have considered alternatives for various components such as comparing custom GPUs with General-Purpose GPUs, evaluating the short and long term benefits of using magnetic tape over HD for storage or SSDs vs HDDs for buffer storage. Various parameters were considered which we believe to be crucial to this design such as fault-tolerance, redundancy of storage, low-latency read/write, image compression and power consumption. We have also shown what tools are to be used to transform segmented images into a more suitable graph data-structire for the purpose of re-animation. Finally, we have shown that despite being ambitious, brain uplodaing is achievable and within the affordability of the world’s financial elite.

One might wonder is this investment worth for simply extracting the whole map of someone’s brain? Whilst this aim is quite a noble and worthy one, one can also view this magnitude of computing infrastructure as a major asset for the people or organizations that fund it. Artifical intelligence is driven by Data centers that house the most powerful electronics mankind has ever invented. In the future there is certainly going to be a pressing demand

for such hardware. Our project may not be the only use of this enormous data pipeline but it could be subsequently used for several other noble ventures. With this hope we conclude the data processing section.

4 Reanimation

DESANKA MARKOVIC

The entire point of our procedure as discussed so far is reanimation from the connectome recorded. Broadly speaking resurrection requires two things. One, the simulation of a neural circuits with the capacity for plasticity (the ability of synapses to change strength and form new connections) in real-time and two, the means for this simulated consciousness to interact with and experience the world - a 'body'. Full detail on simulating a human consciousness and body is outside the scope of this project. Furthermore, currently, there are no practical examples of a successfully simulated consciousness, human or other, or a fully functioning artificial body. What follows are some thoughts on what we believe the requirements for these two things will be, and how we anticipate them being solved, based on the current state of research and technology.

4.0.0.1 Simulating the Brain

As discussed, the first step in resurrecting a person is simulating a brain in its entirety. We believe the connectome provides the fundamental 'road-map' describing an individuals consciouness. However, this roadmap needs to be filled with working neurons, synapses and the singals they emit. Improved computing power has caused the field of computational neuroscience to flourish in recent years. The neural circuits for functions like touch sensitivity, or specific memories, have already been sequenced in small animals[135] and there are a number of cognitive architectures being explored. One particularly promising project is Markram's Blue Brain, which has the eventual aim of simulating an entire human cortex (around 80% of the brain's total volume[136]).

At it's lowest level, this kind of framework (see figure 52) uses mathematical models alongside experimental data to build neurons in terms of ion channels, morphology and

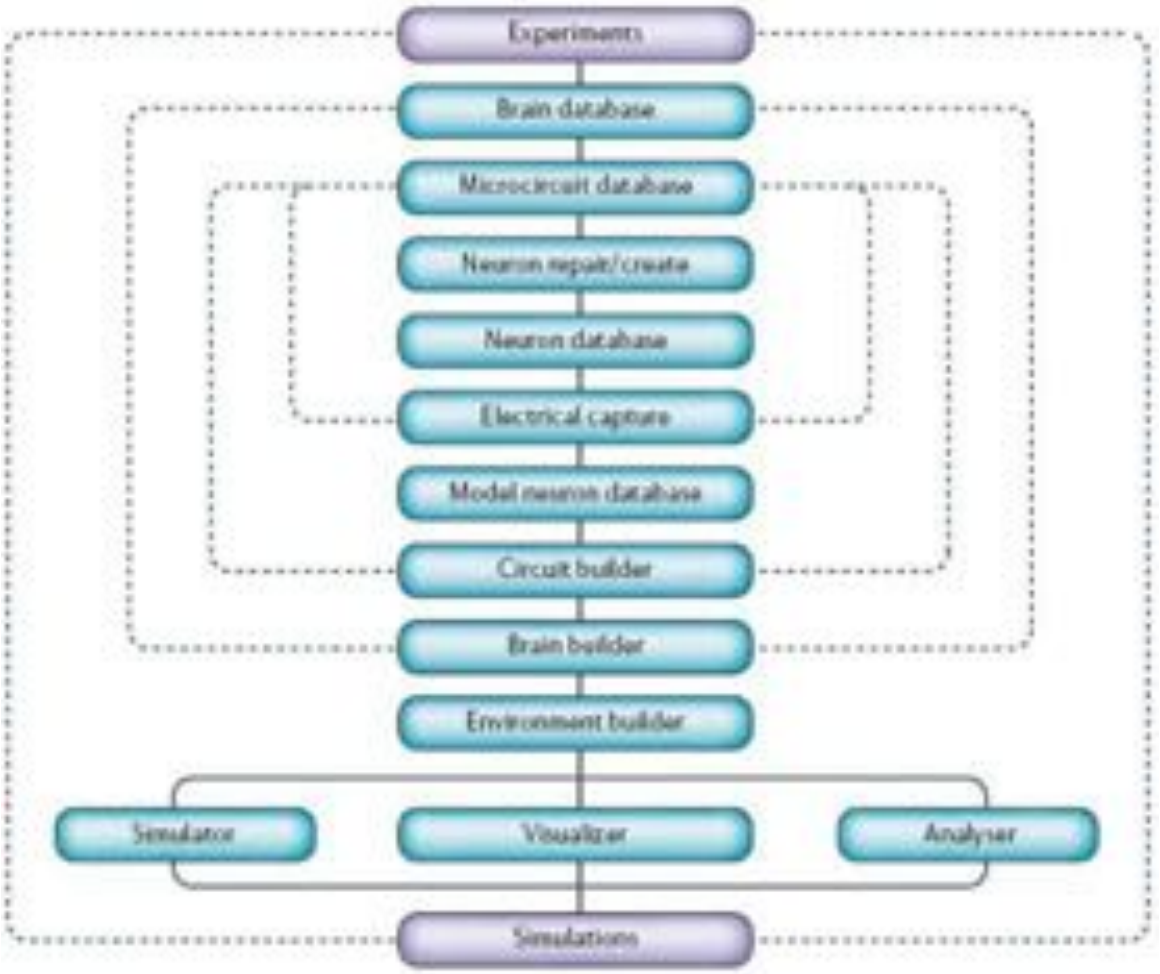

Figure 52: Cascade Code Structure[137]

other key characteristics. A Circuit Builder then groups these neurons into blocks (in the case of the cortex, columns) that are inserted into the correct section of the brain at the Brain Builder level[137]. Our connectome, supplemented by other data, would be used at all levels to guide the specific positioning of neurons and their relative strengths and types.

The benefit of such a framework is twofold. Firstly, the abstraction allows will allow us to create a database of neurons and microcircuits (small collections of neurons) that can be used 'off the shelf'. Secondly, it allows for the creation of high level models that capture the characteristics of lower level processes[137], reducing the computational and temporal cost of full scale brain simulation. Despite this, the level of complexity involved in simulating an entire brain is still beyond the reach of modern computers. The Blue Brain project currently models a single Cortical Column, in order to model an entire brain 'computational power needs to increase about 1-million-fold'[137].

Clearly the technology required to simulate an entire brain still has a long way to go.

As an intermediate, or even alternative step, the connectomes saved using our procedure could be used to recover memories without the reanimation of a consciousness. There is a strong argument to suggest that individual memories may be collected by sequencing small sections of the connectome - the neurons involved in certain memories have already been identified in rodents[138] [139].

4.0.0.2 Creating the Body

As discussed, simulating the human consciousness is only part of the problem and any true attempt at reanimation should include the capacity for interacting with the world. To that end we propose the creation of a fully functioning synthetic body for each brain, with the capacity for all the key senses - taste, touch, hearing, sight, smell - and the ability to move. The technology involved in hearing aids has been around for decades, and there are already examples of basic artificial retinas[140] and 'mind controlled' limbs[141] among other things. Although some of these technologies are still in their relative infancy, it is not unreasonable to imagine that we will develop the technology to build an entire body within the timescale of our brain uploading protocol.

The second part of the puzzle will be how our newly resurrected person can use this new body. Interfaces between 'normal' brains and machines have been developed[142] and the communication between simplified brain models and robotic bodies has already been simulated[143]. However the ability of our client to interface with their new body is highly dependent on the artificial brain effectively simulating plasticity. Without this, the new neural pathways required simply cannot be built. Building or rebuilding these neural pathways is also a time consuming process - functional recovery of stroke victims (performance of activities comparative to pre-stroke ability) can take up to 12.5 weeks on average[144]. It is however, worth noting that most recovery occurs in a relatively small window of increased plasticity post injury[145] - it may be possible to enhance and extend this window in our simulated brains, with increased understanding of the process. In addition to this, we propose that clients undertake a period of training with existing prosthetics technology prior to the procedure, in an attempt to decrease rehabilitation time.

5 Legal and Ethical Considerations

DESANKA MARKOVIC

A key barrier to our procedure is the requirement that patients be euthanized onsite. This severely limits countries where our facility can be built - see table 13. Furthermore, the list of countries where non-residents may undertake euthanasia is smaller still, essentially Switzerland and Colombia are our only options. As a consequence onsequently it will be necessary to split our facility into two with one facility dedicated to patient preparation and chemical processing based in a euthanasia-friendly country.

Table 13: Countries where Euthanasia is Legal

Country	**Type of Euthanasia**	**Conditions**	**Non-Residents/Nationals**
Belgium	Voluntary Active & Physician Assisted Suicide	Patient must be terminal and suffering, and undergoing regular treatment in Belgium for the illness	yes (conditonal)
Canada	Physician Assisted Suicide	Grevious and irremedial medical condition required, Advance requests are not allowed and patient must be an adult of sound mind	no
Colombia	Voluntary Active & Physician Assisted Suicide	Patient must be an adult of sound mind, terminal and suffering or able to provide proof (writter,video or audio)	yes
Germany	Physician Assisted Suicide	Assistance must not be conducted on a business basis (but no a comprehensive legal framework)	no
Japan	Voluntary Active & Physician Assisted Suicide	Patients must be terminal and suffering	no
Netherlands	Voluntary Active & Physician Assisted Suicide	Suffering must be lasting and unbearable, parental consent is equired for minors over 12	no
Switzerland	Physician Assisted Suicide	Does not require the involvement of a physician be involved or that one be a Swiss national.	yes
USA (California, Oregon, Vermont, Montana, Colorado)	Physician Assisted Suicide	Patient must be an adult of sound mind, terminal and with 6 months or less to live	no

However, finding a country where euthanasia is legal is only part of the problem - another huge ethical consideration of our protocol is the perfusion of solutions into a living humans brain. Without perfusion, it is impossible to obtain the level of ultrastructural preservation

we require. Even in countries where euthanasia is legal, we may have to lobby for separate legislature to cover this situation.

Finally, the entire procedure as it stands is purely theoretical has never been tested on a human, or even an animal of greater size than a pig. Moreover, the protocol described assumes that the human mind is completely encoded in the connectome, and optimised to preserve that in as great detail as possible. This claim has never been verified and future developments in the field of neuroscience may reveal that other aspects of the brain are also required for viable resurrection of the consciousness. As such, we cannot guarantee that reanimation of the person will in fact be possible.

6 Business Proposal

THEO COSTAIN

We see this project as two linked but separate businesses. The first business is that of preserving the human brain. Second, is the business of imaging, mapping, and recovering the patients connectome, for potential future reanimation. The advantage of splitting the business in this way, is that the more conventional side, preserving intact brains, which has existing market presence, can be built separately to the much more experimental business of imaging and recreating the human connectome. The total costings for both of these are shown in Table 14.

We seek two different sectors of the market for the businesses. The first business of merely preserving the brain is aimed at those individuals of reasonable but not vast wealth, *i.e.* low figure millionaires. The second business, seeks investment from billionaires who have access to the capital required. As of the 31st edition of the Forbes billionaires list, there are 2,043 billionaires, with a total net worth of $7.67 trillion[6]. The top ten alone are worth more than half a

Table 14: Total Costings

Division	Cost
Fixing	$2,462,531
Sectioning	$20,000,000
Imaging	$99,640,800,000
Processing	$8,072,800,000
Total	$107,736,062,531

[6] https://www.forbes.com/sites/kerryadolan/2017/03/20/forbes%2D2017%2Dbillionaires%2Dlist%2Dmeet%2Dthe%2Drichest%2Dpeople%2Don%2Dthe%2Dplanet/ Accessed April 2017

trillion dollars.

Our initial plan is to seek investments to meet the large upfront expenditures of the project. Particularly the facilities required, including the imaging facility, data centre, and the power plant required to operate the data centre, although some of the cost for the Swiss facility may be sourced from lower net worth investors.

We plan to start slow, with a smaller amount of the total machines needed, around 1,000-5,000. Although this increases the time for imaging, it allows us more time to both prove ourselves and our technology, as well as to gather more investment, and allow better technologies to mature, *e.g.* μCT.

The initial expenditures will be in three main areas. Firstly, the facilities, namely the patient processing facility in Switzerland, where patients brains are fixed and prepared for transport to the US facility, where sectioning and imaging will take place. Secondly, equipment. We require a large number of a few types of equipment, MultiSEM microscopes, GPUs, and magnetic tape. Once we have a fraction of the equipment that we will eventually require we can then start to demonstrate our functioning business model with which we can seek further investment from other individuals, to eventually scale to our planned size.

There is another crucial aspect to our business plan, investment. Given the large amounts of capital we hope to have access to, there are several things that are necessary. As part of our slow ramp up in purchases, much of the capital should be invested in long term, low risk assets. The subsequent interest from these assets should be used for two main purposes.

First, investment into technological research and developments. As stated earlier, μCT could provide great cost savings to us. To this end investment should be made in developing nano-scale μCT, as this would have massive ROI. If one synchrotron takes 95 years and costs around $1Bn, then 10 of them would take 9 and a half years and still be 10 times cheaper than an equivalent number of MultiSEMs, even ignoring the probable scaling that can be achieved. That is to say, a synchrotron twice as big may be more than twice as powerful, and hence be able to image more samples in a given time.

Second, there is much research needed to be done before full reanimation can be considered possible. So investment would have to be made into researching this field. Even a small fraction of our avaliable funds would make a huge difference to the field. The NIH

recently (2010) made available $40 million over 5 years, through the Human Connectome Project[146]. We could easily donate hundreds of millions each year from interest on assets alone. This would hopefully spur the field into breakthroughs, that could both reduce the costs of our process, as well as further the end goals of the business.

To meet our spending desires as outlined above, we would seek to raise as much of the $110 billion as possible, however we would only need $10-20 billion to start the construction and begin purchasing equipment. A strategy to generate this capital would be to approach wealthy and elderly persons, with an offer to manage their assets after their death, taking an upfront sum to go towards business costs, and offering to manage the rest, for a small but considerable amount of the returns generated from investment, preserving their assets until they are revived at a future date. Not only would this give us access to upfront capital, but it would also lend itself towards meeting our desires for research investment.

6.1 Risks

Due to the scope of this project there are several risks. Foremost among these is that there is a qualia to human experience, beyond that which can be captured with even the highest resolution microscopy. If Roger Penrose is to be believed[147], it may never be possible to recreate conciousness, as it has an inherent quantum nature. Obviously there is nothing that can be done by us to mitigate this, money will not change the nature of the universe.

However, there are several problems that might arise, that careful planing, and the deliberate and considered use of capital, can mitigate.

As with any business venture there is always the risk that competitors will steal our business. This can, in part, be mitigated by the nature of any business that seeks to enter this field. The process, or any others similar to ours, will likely incur similar costs. So whoever is first to raise the capital, will likely have a large advantage, as they will already have existing agreements with those persons able to foot the bill of the enterprise. Thus the risk of competitors is limited by the nature of the problem.

Given that we are storing individuals, there is a serious concern over losing data. Especially, given that this loss may constitute murder or manslaughter. We have mitigated this in two distinct ways.

Firstly, we have chosen a storage process, that allows for the brains to be preserved for extended periods, with no damage to cellular structure, and a non-destructive sectioning process, that allows the samples to be preserved indefinitely. Thus if data is lost at any point in the process, barring physical damage to the samples themselves, which itself can be mitigated by storing the samples in a high security facility, the data can be generated again, with ease.

Second we have chosen an architecture for storing the data on disk (Section 3.8.4, that preserves the data in case of corruption. This combined with the presence of 'hard copies' ensures that the likelihood of data loss is low.

7 Conclusion

THEO COSTAIN

In 1962 JFK, speaking about the Apollo space program, said "We choose to go to the Moon in this decade and do the other things, not because they are easy, but because they are hard;". This same sentiment rings true here.

The scale of this endeavour is similar to that of the Apollo space program. It will require armies of engineers and technicians, require breakthroughs in a wide variety of fields, cost exorbitant amounts of money, and may never be successful. The technologies we plan to use are new, and in some cases unproven, and it is for us to show that they are up to the task. The work we do may benefit other endeavours in myriad fields and if we are successful, we will change the nature of humanity. Much like the Apollo program made us a space faring species, this may make us immortal.

Our final design is as follows. We will start by perfusing the brain with washout solution followed by a fixative agent, at our Swiss facility. The brain is then impregnated with crypro-tectants and frozen for transport to the imaging facility in the US. Once there it is stained using the BROPA protocol before ultra-thick sections of the brain are taken. The ultra-thick sections are then further sectioned on multiple ATUM devices in parallel. The tape is then placed into MultiSEM microscopes to be imaged, after imaging the tape is kept as a physical backup. The resulting data is then fed into long term magnetic tape storage and a small

amount is siphoned of to be processed at a slower rate. The data is then processed to extract relevant information about the connectome using flood filling networks, and the information will then converted into a graph like data structure for long term storage. Finally, we hope that at an unknown point in the future, the connectomes will be reanimated, allowing those preserved individuals to live again.

Despite the many philosophical questions that this endeavour poses, there can be little doubt that the preservation of human life, beyond its natural span, is a noble aim. And though there are many barriers in the way, it is only human nature “to strive, to seek, to find, and not to yield.”

References

[1] Narayanan Kasthuri, Kenneth Jeffrey Hayworth, Daniel Raimund Berger, Richard Lee Schalek, José Angel Conchello, Seymour Knowles-Barley, Dongil Lee, Amelio Vázquez-Reina, Verena Kaynig, Thouis Raymond Jones, et al. Saturated reconstruction of a volume of neocortex. *Cell*, 162(3):648–661, 2015.

[2] Eileen Lüders, Helmuth Steinmetz, and Lutz Jäncke. Brain size and grey matter volume in the healthy human brain. *Neuroreport*, 13(17):2371–2374, 2002.

[3] John Lackie. *A Dictionary of Biomedicine*. Oxford University Press, 2010.

[4] R Thavarajah, V.K Mudimbaimannar, J Elizabeth, U.K Rao, and K. Ranganathan. Chemical and physical basics of routine formaldehyde fixation. *Journal of Oral and Maxillofacial Pathology*, 16(3):400–405, 2012.

[5] Robert L. McIntyre and Gregory M. Fahy. Aldehyde-stabilized cryopreservation. *Cryobiology*, 71(3):448 – 458, 2015. ISSN 0011-2240. doi: http://dx.doi.org/10.1016/j.cryobiol.2015.09.003. URL http://www.sciencedirect.com/science/article/pii/S001122401500245X.

[6] Hayworth Kenneth J. Electron imaging technology for whole brain neural circuit mapping. *International Journal of Machine Consciousness*, 4(1), 2012.

[7] Preparing samples for the electron microscope. https://www.sciencelearn.org.nz/resources/500-preparing-samples-for-the-electron-microscope. (Accessed: 04/04/2017).

[8] Robert McIntyre. Lecture 1 - aldehyde stabilised cryopreservation. https://www.robots.ox.ac.uk/ fwood/teaching/3YP_2016/vids/McIntyre-2016.mp4, October 2016.

[9] Introduction to aldehyde stabilised cryopreservation. http://aurellem.org/ASC/html/ASC-introduction.html. (Accessed: 06/04/2017).

[10] Office for National Statistics. average briton highlighted on un world statistics day - press release. (Accessed: 20/04/2017).

[11] Ciara Donohue, Ben Hobson, and Robert C. M. Stephens. An introduction to anaesthesia. *British Journal of Hospital Medicine*, 74(5), May 2013.

[12] General anaesthesia. https://www.evidence.nhs.uk/formulary/bnf/current/15-anaesthesia/151-general-anaesthesia. (Accessed: 18/04/2017).

[13] Patterson Scientific. http://pattersonscientific.com/files/2013/05/Principals_of_Anesthetic.pdf. (Accessed: 26/04/2017).

[14] Encyclopaedia brittanica: Physiology - human respiratory system. https://www.britannica.com/science/human-respiratory-system/The-respiratory-pump-and-its-performance#ref537226. (Acessed: 26/04/2017).

[15] What is blood pressure? http://www.nhs.uk/chq/Pages/what-is-blood-pressure.aspx. (Accessed: 14/04/2017).

[16] Brain facts and figures. https://faculty.washington.edu/chudler/facts.html. (Accessed: 14/04/2017).

[17] Bing Quan Huang and Edward C. Yeung. *Plant Microtechniques and Protocols*, chapter 2) Chemical and Physical Fixation of Cells and Tissues: An Overview, pages 23–43. Springer, September 2015.

[18] John A. Kiernan. Formaldehyde, formalin, paraformaldehyde and glutaraldehyde: What they are and what they do. *Microscopy Today*, 0(1):8–12, 2000.

[19] Olavi Eranko, editor. *Histochemistry of Nervous Transmission, Volume 34*. Elsevier Science, January 1971.

[20] Shawn Mikula and Winfried Denk. High-resolution whole-brain staining for electron microscopic circuit reconstruction. *Nature methods*, 12(6):541, 2015.

[21] G. Fahy, D. MacFarland, C. Angell, and H. Meryman. Vitrification as an approach to cryopreservation. *Cryobiology*, 21:407426, 1984.

[22] P. Clark, G. Fahy, and J.A.M Karrow. Factors influencing renal cryopreservation. ii. toxic effects of three cryoprotectants in combination with three vehicle solutions in nonfrozen rabbit cortical slices. *Cryobiology*, 21:274284, 1984.

[23] Pig model of neural injury. http://www.westlaboratory.org/pig-model-of-neural-injury. (Accessed: 20/04/2017).

[24] The Miriam Hospital Department of Pathology and Brown University Rhode Island Hospital. Autopsy procedure manual.

[25] Shrimpton P, C. Electron density values of various human tissues: in vitro compton scatter measurements and calculated ranges. *Phys. Med. Biol.*, 26(5):907 – 911, 1981.

[26] Michael J. Dykstra and Laura E. Reuss. *Biological Electron Microscopy: Theory, Techniques, and Troubleshooting*, chapter 1. Springer, 2003.

[27] EL Scheller, N Troiano, JN VanHoutan, and et al. Use of osmium tetroxide staining with microcomputerized tomography to visualize and quantify bone marrow adipose tissue in vivo. *Methods in enzymology*, 537:123–139, 2014.

[28] JC Tapia, N Kasthuri, K Hayworth, and et al. High contrast en bloc staining of neuronal tissue for field emission scanning electron microscopy. *Nature protocols*, 7(2), 2012.

[29] Brief introduction to contrasting for em sample preparation. http://www.leica-microsystems.com/science-lab/brief-introduction-to-contrasting-for-em-sample-preparation/. (accessed 07/04/2017).

[30] Shawn Mikula, Jonas Binding, and Winfried Denk. Staining and embedding the whole mouse brain for electron microscopy. *Nat. Meth.*, 9(12):1198 – 1201, 2012.

[31] M.C. Willingham and A.V Rutherford. The use of osmium-thiocarbohydrazide-osmium (oto) and ferrocyanide-reduced osmium methods to enhance membrane contrast and preservation in cultured cells. *J. Histochem. Cytochem.*, 32:455460, 1984.

[32] Patricia K. Rivlin and Pamela A. Raymond. Use of osmium tetroxide-potassium ferricyanide in reconstructing cells from serial ultrathin sections. *Journal of Neuroscience Methods*, 20(1):23 – 33, 1987.

[33] Biological sample preparation for the sem. https://research.jcu.edu.au/archive/enabling/aac/cairns-aac/biological-sample-preparation-for-the-sem. (Accessed: 05/04/2017).

[34] B.G. Nordestgaard and J. Rostgaard. Critical-point drying versus freeze drying for scanning electron microscopy: a quantitative and qualitative study on isolated hepatocytes. *Journal of Microscopy*, 137(2):189–207, 1985.

[35] Susan Billings-Gagliardi, Shirwin M. Pockwinse, and Gary B. Schneider. Morphological changes in isolated lymphocytes during preparation for sem: freeze drying versus critical-point drying. *Developmental Dynamics*, 152(3):383–389, 1978.

[36] Fixation, tissue processing, histology and immunohistochemistry procedures for diagnosis of animal tse (bse, scrapie, atypical scrapie). https://science.vla.gov.uk/tse-labnet/documents/tse-oie-rl-prp.pdf, Nov 2016.

[37] Jos Guillermo Frontera. The effects of some dehydrating techniques on the measurements of the brain of macaques. *The Anatomical Record*, 135(2):83–91, 1959.

[38] A. Grace and R. Llinas. Morphological artifacts induced in intracellularly stained neurons by dehydration: circumvention using rapid dimethyl sulfoxide clearing. *Neuroscience*, 16(2):461475, 1985.

[39] Robert W. Henry. Principles of plastination: dehydration of specimens. *Journal of Plastination*, 10:27, 1996.

[40] K.J Hayworth and et al. Ultrastructurally smooth thick partitioning and volume stitching for large-scale connectomics. *Nat. Methods*, 12:319322, 2015.

[41] Geoff R. Newman and Jan A. Hobot. Resins for combined light and electron microscopy: A half century of development. *The Histochemical Journal*, 31:495 505, 1999.

[42] Arthur R. Spurr. A low-viscosity epoxy resin embedding medium for electron microscopy. *Journal of Ultrastructure Research*, 26:31–43, January 1969.

[43] Polysciences Inc. Unicryl. http://www.polysciences.com/skin/frontend/default/polysciences/pdf/Ur

[44] Electron Microscopy Sciences. Technical data sheets - unicryl. https://www.emsdiasum.com/microscopy/technical/datasheet/14660.aspx.

[45] Zhongqin Yang, Bihe Hu, Yuhui Zhang, Qingming Luo, and Hui Gong. Development of a plastic embedding method for large-volume and fluorescent-protein-expressing tissues. 8(4), April 5 2013.

[46] Kenneth J Hayworth, C Shan Xu, Zhiyuan Lu, Graham W Knott, Richard D Fetter, Juan Carlos Tapia, Jeff W Lichtman, and Harald F Hess. Ultrastructurally smooth thick partitioning and volume stitching for large-scale connectomics. *Nature methods*, 12(4):319–322, 2015.

[47] R Schalek, N Kasthuri, K Hayworth, D Berger, J Tapia, J Morgan, S Turaga, E Fagerholm, H Seung, and J Lichtman. Development of high-throughput, high-resolution 3d reconstruction of large-volume biological tissue using automated tape collection ultramicrotomy and scanning electron microscopy. *Microscopy and Microanalysis*, 17(S2): 966–967, 2011.

[48] Werner Villiger and Andreas Bremer. Ultramicrotomy of biological objects: from the beginning to the present. *Journal of structural biology*, 104(1-3):178–188, 1990.

[49] TF Malis and D Steele. Ultramicrotomy for materials science. *MRS Online Proceedings Library Archive*, 199, 1990.

[50] Leica-microsystems. URL http://www.leica-microsystems.com.

[51] Lennart Heimer. *Dissection of the human brain*. Sinauer, 2007.

[52] Thomas Schuelke and Timothy A Grotjohn. Diamond polishing. *Diamond and Related Materials*, 32:17–26, 2013.

[53] F.M.V. Hum. Diamond cutting tool having an edge thickness of 0.001 to 0.01 micron, October 30 1962. URL https://www.google.com/patents/US3060781. US Patent 3,060,781.

[54] Ted Pella Inc. Pelco diamond knives. URL https://www.tedpella.com/diamond_html/diamondk.htm.

[55] H.F.M. Villalobos. Ultrasharp diamond edges and points and method of making, April 18 1978. URL https://www.google.com/patents/US4084942. US Patent 4,084,942.

[56] Clague P Hodgson and William P Cunningham. A synthetic corundum knife for ultrathin sectioning. *Journal of Microscopy*, 146(1):103–107, 1987.

[57] Michael Schwander and Knut Partes. A review of diamond synthesis by cvd processes. *Diamond and related materials*, 20(9):1287–1301, 2011.

[58] RS Balmer, JR Brandon, SL Clewes, HK Dhillon, JM Dodson, I Friel, PN Inglis, TD Madgwick, ML Markham, TP Mollart, et al. Chemical vapour deposition synthetic diamond: materials, technology and applications. *Journal of Physics: Condensed Matter*, 21(36):364221, 2009.

[59] H Sumiya and S Satoh. High-pressure synthesis of high-purity diamond crystal. *Diamond and Related Materials*, 5(11):1359–1365, 1996.

[60] Kamal Ahmed. Lesedi la rona diamond fails to sell in london auction. URL http://www.bbc.co.uk/news/uk-england-london-36660076. (Accessed: 21/04/2017).

[61] Mark S Akselrod and Frank J Bruni. Modern trends in crystal growth and new applications of sapphire. *Journal of Crystal Growth*, 360:134–145, 2012.

[62] MonoCrystal. Worlds first 350 kg ky sapphire crystal. URL http://www.monocrystal.com/en/news/photos. (Accessed: 21/04/2017).

[63] SE Demina, EN Bystrova, M Af Lukanina, VM Mamedov, VS Yuferev, EV Eskov, MV Nikolenko, VS Postolov, and VV Kalaev. Numerical analysis of sapphire crystal growth by the kyropoulos technique. *Optical Materials*, 30(1):62–65, 2007.

[64] Kenneth J Hayworth. Electron imaging technology for whole brain neural circuit mapping. *International Journal of Machine Consciousness*, 4(01):87–108, 2012.

[65] Huckfinne. Wikimedia. URL https://commons.wikimedia.org/wiki/File:Vibratome.jpg. (Accessed: 21/04/2017).

[66] Steve Gentleman. Wellcome collection. URL https://wellcomecollection.org/. (Accessed: 21/04/2017).

[67] Robbin Gibb and Bryan Kolb. A method for vibratome sectioning of golgi–cox stained whole rat brain. *Journal of neuroscience methods*, 79(1):1–4, 1998.

[68] Hadia M Abdelaal, Hyeon O Kim, Reece Wagstaff, Ryoko Sawahata, Peter J Southern, and Pamela J Skinner. Comparison of vibratome and compresstome sectioning of fresh primate lymphoid and genital tissues for in situ mhc-tetramer and immunofluorescence staining. *Biological procedures online*, 17(1):2, 2015.

[69] Hans-Ulrich Dodt, Ulrich Leischner, Anja Schierloh, Nina Jährling, Christoph Peter Mauch, Katrin Deininger, Jan Michael Deussing, Matthias Eder, Walter Zieglgänsberger, and Klaus Becker. Ultramicroscopy: three-dimensional visualization of neuronal networks in the whole mouse brain. *Nature methods*, 4(4):331–336, 2007.

[70] Daniel C Pease and Keith R Porter. Electron microscopy and ultrarnicrotomy. *The Journal of cell biology*, 91(3 PT 2):287s–292s, 1981.

[71] John D Verhoeven, Alfred H Pendray, and Howard F Clark. Wear tests of steel knife blades. *Wear*, 265(7):1093–1099, 2008.

[72] Harrison Latta and J Francis Hartmann. Use of a glass edge in thin sectioning for electron microscopy.. *Proceedings of the Society for Experimental Biology and Medicine*, 74(2):436–439, 1950.

[73] TR Matzelle, Helmut Gnaegi, Andrea Ricker, and Rudolf Reichelt. Characterization of the cutting edge of glass and diamond knives for ultramicrotomy by scanning force microscopy using cantilevers with a defined tip geometry. part ii. *Journal of microscopy*, 209(2):113–117, 2003.

[74] Hilton H Mollenhauer and OE Bradfute. Comparison of surface roughness of sections cut by diamond, sapphire, and glass knives. *Journal of electron microscopy technique*, 6(1):81–85, 1987.

[75] IM Roberts. Tungsten coatinga method of improving glass microtome knives for cutting ultrathin sections. *Journal of microscopy*, 103(1):113–119, 1975.

[76] Bruce A Buck. Ancient technology in contemporary surgery. *Western Journal of Medicine*, 136(3):265, 1982.

[77] H Fernandez-Moran. A diamond knife for ultrathin sectioning. *Experimental cell research*, 5(1):255–256, 1953.

[78] LEED PEACHEY. I. a study of section thickness and physical distortion produced during microtomy. *The Journal of Biophysical and Biochemical Cytology*, 4(1):233–42, 1958.

[79] JC Jésior. Use of low-angle diamond knives leads to improved ultrastructural preservation of ultrathin sections. *Scanning microscopy. Supplement*, 3:147–52, 1988.

[80] D Studer and H Gnaegi. Minimal compression of ultrathin sections with use of an oscillating diamond knife. *Journal of microscopy*, 197(1):94–100, 2000.

[81] Arvid B Maunsbach and Björn A Afzelius. *Biomedical electron microscopy: Illustrated methods and interpretations*. Academic Press, 1998.

[82] Winfried Denk and Heinz Horstmann. Serial block-face scanning electron microscopy to reconstruct three-dimensional tissue nanostructure. *PLoS Biol*, 2(11):e329, 2004.

[83] Inc Gatan. Gatan 3view system. URL http://www.gatan.com/products/sem-imaging-spectroscopy/3view-system. (Accessed: 21/04/2017).

[84] Real-time 3d analytical fib-sem composite instrument nx9000 released. http://www.hitachi-hightech.com/global/about/news/2015/nr20150730.html. (Accessed: 10/05/2017).

[85] G. Knott, H. Marchman, D. Wall, and B. Lich. Serial section scanning electron microscopy of adult brain tissue using focused ion beam milling. *The Journal of Neuroscience*, 28(12):2959–2964, 2008.

[86] Kedar Narayan and Sriram Subramaniam. Focused ion beams in biology. *Nature methods*, 12(11):1021–1031, 2015.

[87] Heinz Horstmann, Christoph Körber, Kurt Sätzler, Daniel Aydin, and Thomas Kuner. Serial section scanning electron microscopy (s 3 em) on silicon wafers for ultrastructural volume imaging of cells and tissues (serial section scanning electron microscopy). *PLoS ONE*, 7(4):e35172, 2012.

[88] Kenneth J. Hayworth. Electron imaging technology for whole brain neural circuit mapping. *International Journal Of Machine Consciousness*, 04(01):87–108, 2012. doi: 10.1142/s1793843012400057. URL http://www.worldscientific.com/doi/abs/10.1142/s1793843012400057.

[89] Gregory McCarthy Scott A. Huttel, Allen W. Song. *Functional Magnetic Resonance Imaging 2nd Ed.* Sinauer, 2009. ISBN 978-0-87893-286-3.

[90] Fei Chen, Paul W. Tillberg, and Edward S. Boyden. Expansion microscopy. *Science*, 347(6221):543–548, 2015. ISSN 0036-8075. doi: 10.1126/science.1260088. URL http://science.sciencemag.org/content/347/6221/543.

[91] Paul W. Tillberg, Fei Chen, Kiryl D. Piatkevich, Yongxin Zhao, Chih-Chieh (Jay) Yu, Brian P. English, Linyi Gao, Anthony Martorell, Ho-Jun Suk, Fumiaki Yoshida, Ellen M. DeGennaro, Douglas H. Roossien, Guanyu Gong, Uthpala Seneviratne, Steven R. Tannenbaum, Robert Desimone, Dawen Cai, and Edward S. Boyden. Protein-retention expansion microscopy of cells and tissues labeled using standard fluorescent proteins and antibodies. *Nat Biotech*, 34(9):987–992, Sep 2016. ISSN 1087-0156. URL http://dx.doi.org/10.1038/nbt.3625. Research.

[92] Fei Chen, Asmamaw T. Wassie, Allison J. Cote, Anubhav Sinha, Shahar Alon, Shoh Asano, Evan R. Daugharthy, Jae-Byum Chang, Adam Marblestone, George M.

Church, Arjun Raj, and Edward S. Boyden. Nanoscale imaging of rna with expansion microscopy. *Nat Meth*, 13(8):679–684, Aug 2016. ISSN 1548-7091. URL http://dx.doi.org/10.1038/nmeth.3899. Article.

[93] Daniel Evanko. Hybridization chain reaction. *Nat Meth*, 1(3):186–187, Dec 2004. ISSN 1548-7091. doi: 10.1038/nmeth1204-186a. URL http://dx.doi.org/10.1038/nmeth1204-186a.

[94] Jae-Byum Chang, Fei Chen, Young-Gyu Yoon, Erica E Jung, Hazen Babcock, Jeong Seuk Kang, Shoh Asano, Ho-Jun Suk, Nikita Pak, Paul W Tillberg, et al. Iterative expansion microscopy. *Nature Methods*, 2017.

[95] Eva L. Dyer, William Gray Roncal, Hugo L. Fernandes, Doga Grsoy, Vincent De Andrade, Rafael Vescovi, Kamel Fezzaa, Xianghui Xiao, Joshua T. Vogelstein, Chris Jacobsen, Konrad P. Krding, and Narayanan Kasthuri. Quantifying mesoscale neuroanatomy using x-ray microtomography, 2016. URL https://arxiv.org/abs/1604.03629.

[96] J. W. Lichtman, J. Livet, and J. R. Sanes. A technicolour approach to the connectome. *Nature Reviews Neuroscience*, 9(6):417–422, 2008.

[97] Guo rong Zhang, Hua Zhao, P.M. Abdul-Muneer, Haiyan Cao, Xu Li, and Alfred I. Geller. Neurons can be labeled with unique hues by helper virus-free hsv-1 vectors expressing brainbow. *Journal of Neuroscience Methods*, 240:77 – 88, 2015. ISSN 0165-0270. doi: http://doi.org/10.1016/j.jneumeth.2014.11.009. URL http://www.sciencedirect.com/science/article/pii/S0165027014004014.

[98] Carl Zeiss AG. Zeiss GeminiSEM family product information, 2017. URL https://applications.zeiss.com/C125792900358A3F/0/8AA75F6A864B2BBAC1257E180037CCA0/$FILE/EN_40_011_095_GeminiSEM_rel_2_0.pdf.

[99] A.l. Eberle, S. Mikula, R. Schalek, J. Lichtman, M.l. Knothe Tate, and D. Zeidler. High-resolution, high-throughput imaging with a multibeam scanning electron microscope.

Journal of Microscopy, 259(2):114–120, 2015. ISSN 1365-2818. doi: 10.1111/jmi.12224. URL http://dx.doi.org/10.1111/jmi.12224.

[100] Carl Zeiss AG. Zeiss MultiSEM research partner program product information, 2017. URL https://applications.zeiss.com/C125792900358A3F/0/E22B336878B463FCC1257EDC004FFFF1/$FILE/EN_41_011_078_MultiSEM_rel2_2.pdf.

[101] John N Galayda. The advanced photon source. In *Particle Accelerator Conference, 1995., Proceedings of the 1995*, volume 1, pages 4–8. IEEE, 1995.

[102] Anna Lena Eberle, Richard Schalek, Jeff W. Lichtman, Matt Malloy, Brad Thiel, and Dirk Zeidler. Multiple-beam scanning electron microscopy. *Micros. Today*, 23(02): 12–19, 2015. ISSN 1551-9295. doi: 10.1017/S1551929515000012.

[103] Michael A. O'Keefe, John H. Turner, Crispin J. D. Hetherington, A. G. Cullis, Bridget Carragher, Ron Jenkins, Julie Milgrim, Ronald A. Milligan, Clinton S. Potter, Lawrence F. Allard, Douglas A. Blom, Lynn Degenhardt, and William H. Sides. Laboratory design for high-performance electron microscopy. *Lawrence Berkeley National Laboratory*, 2004.

[104] Becky Oskin. Japan earthquake & tsunami of 2011: Facts and information, May 2015. URL http://www.livescience.com/39110-japan-2011-earthquake-tsunami-facts.html.

[105] April 2017. URL https://community.fema.gov/hazard/wildfire-en_us/be-smart?lang=en_US.

[106] April 2017. URL http://cwfis.cfs.nrcan.gc.ca/ha/nfdb.

[107] William Larson. New estimates of value of land of united states. Technical report, Bureau of Economic Analysis, April 2015. URL https://www.bea.gov/papers/pdf/new-estimates-of-value-of-land-of-the-united-states-larson.pdf.

[108] Table 002-0003 1, value per acre of farm land and buildings, at july 1, November 2016. URL http://www5.statcan.gc.ca/cansim/a26?lang=eng&retrLang=eng&id=0020003&pattern=&csid=.

[109] ScienceFocus. *Internet Size*, 2017 (accessed March 16, 2017). URL http://www.sciencefocus.com/qa/how-many-terabytes-data-are-internet.

[110] MIT. *Stages of the image for the data pipeline*, 2017 (accessed April 9, 2017). URL http://www.rle.mit.edu/eems/wp-content/uploads/2016/11/Tutorial-on-DNN-1-of-9-Background-of-DNNs.pdf.

[111] Google. *Google-Tpu performance specs*, 2017 (accessed April 12, 2017). URL https://cloudplatform.googleblog.com/2017/04/quantifying-the-performance-of-the-TPU-our-first-machine-learning-chip.html.

[112] Stanford. *CS231-stanford*, 2016 (accessed December 6, 2016). URL http://cs231n.github.io/convolutional-networks/.

[113] William Gray Roncal, Verena Kaynig-Fittkau, Narayanan Kasthuri, Daniel R. Berger, Joshua T. Vogelstein, Lindsey R. Fernandez, Jeff W. Lichtman, R. Jacob Vogelstein, Hanspeter Pfister, and Gregory D. Hager. Volumetric exploitation of synaptic information using context localization and evaluation. *CoRR*, abs/1403.3724, 2014. URL http://arxiv.org/abs/1403.3724.

[114] Beatrix-Matthews. *Random-forests illustration*, 2017 (accessed April 3, 2017). URL http://www.robots.ox.ac.uk/~fwood/teaching/3YP_2016/lectures/forests/random_forests_lecture.pdf.

[115] Ned Horning. Random forests : An algorithm for image classification and generation of continuous fields data sets. URL http://wgrass.media.osaka-cu.ac.jp/gisideas10/viewpaper.php?id=342.

[116] Wikimedia. *precision-recall*, 2017 (accessed April 1, 2017). URL (https://en.wikipedia.org/wiki/Precision_and_recall).

[117] Michal Januszewski, Jeremy Maitin-Shepard, Peter Li, Jörgen Kornfeld, Winfried Denk, and Viren Jain. Flood-filling networks. *CoRR*, abs/1611.00421, 2016. URL http://arxiv.org/abs/1611.00421.

[118] Tensorflow. *Tensorflow-GPU-Parallel*, 2017 (accessed January 9, 2017). URL https://www.tensorflow.org/tutorials/deep_cnn.

[119] NVIDIA. *NVIDIA GPU*, 2017 (accessed April 23, 2017). URL http://www.geforce.co.uk/hardware/10series/titan-xp/#redirected.

[120] NVIDIA. *GPU-Specs*, 2017 (accessed April 9, 2017). URL http://www.geforce.com/hardware/desktop-gpus/geforce-gtx-titan-x/specifications.

[121] Apache Hadoop. *Spark Documentation*, 2017 (accessed March 26, 2017). URL http://spark.apache.org/docs/latest/programming-guide.html.

[122] NVIDIA. *HADOOP Guide*, 2017 (accessed April 12, 2017). URL https://hadoop.apache.org/docs/r1.2.1/hdfs_design.html.

[123] Xiaochong Zhang. *Map and Reduce graphic*, 2017 (accessed April 15, 2017). URL http://xiaochongzhang.me/blog/?p=334.

[124] Apache. *Spark-cluster*, 2017 (accessed April 12, 2017). URL http://spark.apache.org/docs/latest/cluster-overview.html.

[125] Sony. *Sony develops magnetic tape technology with the world's highest areal recording density*, 2017 (accessed February 18, 2017). URL https://www.sony.net/SonyInfo/News/Press/201404/14-044E/.

[126] IronMountain. *ironmountain*, 2017 (accessed April 2, 2017). URL http://www.ironmountain.com/Knowledge-Center/Reference-Library/View-by-Document-Type/General-Articles/D/Disk-vs-Tape-Which-Ones-Game-for-the-Long-Term.aspx.

[127] Randal C. Burns, William Gray Roncal, Dean Kleissas, Kunal Lillaney, Priya Manavalan, Eric A. Perlman, Daniel R. Berger, Davi Bock, Kwanghun Chung, Logan Grosenick, Narayanan Kasthuri, Nicholas C. Weiler, Karl Deisseroth, Michael M. Kazhdan, Jeff Lichtman, R. Clay Reid, Stephen J. Smith, Alexander S. Szalay, Joshua T. Vogelstein, and R. Jacob Vogelstein. The open connectome project data cluster: Scal-

able analysis and vision for high-throughput neuroscience. *CoRR*, abs/1306.3543, 2013. URL http://arxiv.org/abs/1306.3543.

[128] Yunfeng Gu and Azzedine Boukerche. Hd tree: A novel data structure to support multi-dimensional range query for p2p networks. *J. Parallel Distrib. Comput.*, 71(8): 1111–1124, August 2011. ISSN 0743-7315. doi: 10.1016/j.jpdc.2011.04.003. URL http://dx.doi.org/10.1016/j.jpdc.2011.04.003.

[129] M. Zhou, W. Gao, M. Jiang, and H. Yu. Hevc lossless coding and improvements. *IEEE Transactions on Circuits and Systems for Video Technology*, 22(12):1839–1843, Dec 2012. ISSN 1051-8215. doi: 10.1109/TCSVT.2012.2221524.

[130] Dan Grois, Tung Nguyen, and Detlev Marpe. Coding efficiency comparison of av1/vp9, h. 265/mpeg-hevc, and h. 264/mpeg-avc encoders. 2016.

[131] tapeandmedia.com. *Tape Storage Details*, 2017 (accessed April 5, 2017). URL https://www.tapeandmedia.com/lto-6-tape-media-tapes.asp.

[132] Stanford. *Metadata and buffer*, 2017 (accessed April 15, 2017). URL https://cs.stanford.edu/people/jcjohns/papers/iccv15/JohnsonICCV2015.pdf.

[133] Max Planck Institute. *Knossos*, 2017 (accessed April 15, 2017). URL http://knossostool.org/.

[134] NCBI. *2D slice to 3D*, 2017 (accessed April 15, 2017). URL https://www.ncbi.nlm.nih.gov/pmc/articles/PMC3406305/.

[135] M Chalfie, JE Sulston, JG White, E Southgate, JN Thomson, and S Brenner. The neural circuit for touch sensitivity in caenorhabditis elegans. *Journal of Neuroscience*, 5(4):956–964, 1985.

[136] Hugo de Garis, Chen Shuo, Ben Goertzel, and Lian Ruiting. A world survey of artificial brain projects, part i: Large-scale brain simulations. *Neurocomputing*, 74(13):3 – 29, 2010. Artificial Brains.

[137] Akanksha V. Patil, Ruchita R. Kesarkar, Sapana G. Buwa, Jyotsna T. Kumbhar, and Vijay U. Patil. Blue brain. *International Journal of Computer Science and Information Technology & Security*, 2(6), Dec 2012.

[138] Josselyn SA. Continuing the search for the engram: examining the mechanism of fear memories. *Journal of Psychiatry & Neuroscience*, 35(4), 2010.

[139] Xu Liu, Steve Ramirez, Petti T. Pang, Corey B. Puryear, Arvind Govindarajan, Karl Deisseroth, and Susumu Tonegawa. Optogenetic stimulation of a hippocampal engram activates fear memory recall. *Nature*, 484(7394), 2012.

[140] Chow AY, Chow VY, Packo KH, Pollack JS, Peyman GA, and Schuchard R. The artificial silicon retina microchip for the treatment of vision loss from retinitis pigmentosa. *Archives of Ophthalmology*, 122(4):460–9, 2004.

[141] Guy Hotson et al. Individual finger control of a modular prosthetic limb using high-density electrocorticography in a human subject. *Journal of Neural Engineering*, 13 (2), Feb 2016.

[142] Tomislav Milekovic et al. An online brainmachine interface using decoding of movement direction from the human electrocorticogram. *Journal of Neural Engineering*, 9 (4), June 2012.

[143] Egidio Falotico et al. Connecting artificial brains to robots in a comprehensive simulation framework: The neurorobotics platform. *Frontiers in Neurorobotics*, 11:2, 2017.

[144] Jorgensen HS, Nakayama H, Raaschou HO, Vive-Larsen J, Stoier M, and Olsen TS. Outcome and time course of recovery in stroke. part ii: Time course of recovery. the copenhagen stroke study. *Archives of Physical Medicine and Rehabilitation*, 76(5): 406–12, May 1995.

[145] Dancause N and Nudo RJ. Shaping plasticity to enhance recovery after injury. *Progress in brain research*, 192:273–295, 2011.

[146] Anon. A critical look at connectomics. *Nat Neurosci*, 13(12):1441–1441, December 2010. ISSN 1097-6256. URL http://dx.doi.org/10.1038/nn1210-1441.

[147] Roger Penrose. *The Emperor's New Mind : Concerning Computers, Minds And The Laws Of Physics*. Vintage, 1990. ISBN 0-09-977170-5.